INFORMATION TO USERS

This manuscript has been reproduced from the microfilm master. UMI films the text directly from the original or copy submitted. Thus, some thesis and dissertation copies are in typewriter face, while others may be from any type of computer printer.

The quality of this reproduction is dependent upon the quality of the copy submitted. Broken or indistinct print, colored or poor quality illustrations and photographs, print bleedthrough, substandard margins, and improper alignment can adversely affect reproduction.

In the unlikely event that the author did not send UMI a complete manuscript and there are missing pages, these will be noted. Also, if unauthorized copyright material had to be removed, a note will indicate the deletion.

Oversize materials (e.g., maps, drawings, charts) are reproduced by sectioning the original, beginning at the upper left-hand corner and continuing from left to right in equal sections with small overlaps.

Photographs included in the original manuscript have been reproduced xerographically in this copy. Higher quality 6" x 9" black and white photographic prints are available for any photographs or illustrations appearing in this copy for an additional charge. Contact UMI directly to order.

Bell & Howell Information and Learning
300 North Zeeb Road, Ann Arbor, MI 48106-1346 USA
800-521-0600

Environmental Control of Stable Carbon Isotope Systematics in Emiliania huxleyi

by

Magnus Eek
B.Sc.-Chemical Engineering, Chalmers University of Technology, 1987
M.Sc.-Chemical Reaction Engineering, Chalmers University of Technology, 1991

A Thesis submitted in Partial Fulfillment of the
Requirements for the Degree of

DOCTOR OF PHILOSOPHY

in the

SCHOOL OF EARTH AND OCEAN SCIENCES

We accept this thesis as conforming
to the required standard

Dr. Michael J. Whiticar, Supervisor (School of Earth and Ocean Sciences)

Dr. Andrew Weaver, Departmental Member (School of Earth and Ocean Sciences)

Dr. Louis. A. Hobson, Outside Member (Department of Biology)

Dr. Chi Shing Wong, Additional Outside Member (Institute of Ocean Sciences, Sidney, B.C.)

Dr. John P. Jasper, External Examiner (Molecular Isotope Technologies, LLC.)

Supervisor: Dr. Michael J. Whiticar

Abstract

The carbon isotope fractionation in the coccolithophore Emiliania huxleyi constitutes the basis for the paleo-pCO_2 barometry. Under the premise that the carbon isotope fractionation is dependent on the availability of dissolved CO_2, measurements of the carbon isotope ratio of sedimentary alkenones can potentially produce a proxy record of ancient atmospheric CO_2 levels. However, recent studies, including this thesis have suggested that other factors than CO_2 may influence the carbon isotope fractionation in Emiliania huxleyi and hence the validity of the proxy.

In this thesis work the effects of irradiance on carbon isotope fractionation were studied in batch cultures of non-calcifying Emiliania huxleyi. It was found that the biomass becomes more ^{13}C depleted as the light intensity decreases. This is in agreement with utilization of CO_2 via passive diffusion where fractionation is a function of the rate of diffusion of CO_2 into the cell relative to the rate of carbon utilization. However, results reported in the literature for a calcifying strain show the opposite trend with a ^{13}C

enrichment of the biomass. These results suggest that the carbon utilization of the calcifying strain of Emiliania huxleyi differ from that of the non-calcifying strain. This is supported by observations in the literature, which indicates a connection between the process of calcification and the supply of carbon for photosynthesis.

A mechanism for the effect of calcification on carbon isotope fractionation in light limited cells is presented here. The mechanism is based on the fact that the calcification and photosynthesis respond differently to light limitation. This difference leads to an imbalance in the rate of calcification to the rate of photosynthesis ratio (C/P), which ultimately affects the availability of CO_2 inside the cell. Apart from light, the availability of nutrients has also been shown to affect calcification. Nutrient starved cells will enhance calcification to the degree that the C/P ratio changes, thus affecting the internal concentration of CO_2.

To study the effect of these environmental parameters on carbon isotope fractionation, $C_{37:2}$-alkenones were extracted from samples of marine particulate organic matter. The particulate organic matter was collected together with information of the environmental conditions during three cruises in the North-East Pacific and during a Pacific transect from Victoria B.C. to Guam. Results from the NE Pacific show a lower carbon

isotope fractionation in samples collected at the bottom of the euphotic zone compared to samples collected in the mixed layer. This may be an expression of the effect of light limitation.

In this work carbon isotope fractionation shows no correlation with dissolved CO_2. Instead, a correlation with the ratio of phosphate concentration to concentration of dissolved CO_2 ($[PO_4^{3-}]/[CO_2]_{aq.}$) was observed. Nitrate availability appears to play an important role in maintaining this relationship as in the absence of nitrate the carbon isotope fractionation is lower than can be predicted from the relationship relating carbon isotope fractionation to $[PO_4^{3-}]/[CO_2]_{aq.}$.

The $C_{37:2}$-alkenone based results from the Pacific transect shows a strong correlation between carbon isotope fractionation and phosphate. This correlation is independent of the concentration of dissolved CO_2, implying a nutrient dominated control of isotope fractionation. However, this control may not be typical as the transect passed through waters with very low nutrient levels. Therefore, the results seen here may be a consequence of extreme nutrient conditions.

In conclusion, the results presented in this thesis challenge the classical belief that the carbon isotope fractionation in Emiliania huxleyi is a direct function of the availability of dissolved CO_2 by suggesting that the

observed isotope fractionation is a result of a complex interaction between environmental factors such as irradiance and the availability of nutrients. In particular, a correlation between phosphate concentration and carbon isotope fractionation has been found.

Examiners:

Dr. Michael J. Whiticar, Supervisor (School of Earth and Ocean Sciences)

Dr. Andrew Weaver , Departmental Member (School of Earth and Ocean Sciences)

Dr. Louis. A. Hobson , Outside Member (Department of Biology)

Dr. Chi Shing Wong, Additional Outside Member(Institute of Ocean Sciences, Sidney, B.C.)

Dr. John P. Jasper, External Examiner (Molecular Isotope Technologies, LLC,)

Table of Contents

List of Tables

List of Figures

Acknowledgments

I'd like to thank my supervisor, Michael Whiticar, for giving me the opportunity to work with him in the Biogeochemistry Facility at the University of Victoria, and allowing me the freedom to learn from my own mistakes. I also want to thank him for providing financial support for my studies. None of this would have been possible without him.

Colleagues, past and present, have been a valuable source of inspiration and motivation. Paul Eby, Scott Harris, Lisa Kadonaga, Mike Kory and Hinrich Schaefer have all been there for useful conversation and distraction. Nick Grant and Ruben Veefkind deserves a special mention as they listened patiently to my ideas and participated in endless discussions about the inner workings of *Emiliania huxleyi*. Thank You, Nick and Ruben.

For help with the culture work and general support I wish to thank Lou Hobson and Melissa McQuoid.

I also want to express my gratitude to the people at the Institute of Ocean Sciences, Sidney B.C. Especially to CS Wong, who was my first contact in Canada and therefore partly responsible for bringing me here, and to Keith Johnson, who's patience seems infinite as he never fails to lend a helping hand.

Most of all, I'd like to thank my friends and family for supporting me through both the successes and the failures of the past few years.

Chapter 1

Statement of Problem

For the last 30 years there has been an increased interest in the natural abundance of stable carbon isotopes in the marine environment. The driving force behind this intensified attention is the potential use of stable carbon isotopes as a tool to study different aspects of the marine carbon cycle. Stable carbon isotopes can be used to quantify fluxes of carbon between different trophic levels, to identify food sources of animals, and also to estimate primary production via the fractionation that occurs during carbon uptake by marine phytoplankton. The apparent relationship between the availability of carbon for photosynthesis and the resulting isotope composition of the produced photosynthate in phytoplankton has prompted many investigations aiming at a proxy for ancient atmospheric pCO_2-levels. The premise for such a proxy is an interpretable relationship between the isotope fractionation and the concentration of dissolved CO_2 in the surface ocean. However, since the isotope signal is produced by a biological system such a understanding is difficult to obtain. The carbon isotope fractionation is affected by the phytoplankton physiology, thus factors affecting the physiology may also have an effect on the carbon isotope fractionation.

This thesis focuses on the relationship between carbon isotope fractionation and the availablity of CO_2 and in particular on the influence environmental factors other

than CO_2 may have on the isotope fractionation in *Emiliania huxleyi*, a unicellular marine alga. The effects of varying concentrations of macro-nutrients on the isotopic composition of $C_{37:2}$-alkenone, a long chain ketone exclusively produced by a few prymnesiophyte algae, have been studied in samples collected during three CJGOFS cruises in the North East Pacific and during a Pacific transect from Vancouver Island to Guam. The field studies was complemented with an laboratory study, where batch cultures of a non-calcifying strain of *E. huxleyi* were grown according to a factorial design. This experiment was aimed at evaluating the effect of depth on carbon isotope fractionation by varying the intensity and spectral quality (white and blue) of the incident light.

Chapter 2

Introduction

2.1 Isotope Composition of Marine Organic Carbon

Variations in the isotope composition of marine Particulate Organic Carbon, $\delta^{13}C_{POC}$, have intrigued many investigators for the past three decades. The driving force behind this interest is the potential use of stable carbon isotopes as a tool to study different aspects of the marine carbon cycle.The fractionation of stable carbon isotopes can provide insight into biotic processes and their controlling factors. Factors that have been suggested to affect $\delta^{13}C_{POC}$ include a variety of physical and biological parameters, such as: sea surface temperature, water-mass, latitude, concentration of dissolved CO_2, phytoplankton physiology and species composition (Fry and Sherr 1984; Rau *et al.* 1989; Falkowski 1991; Rau *et al.* 1992; Goericke and Fry 1994; Bentaleb *et al.* 1996). The parameter that has received the most attention is the availability of inorganic carbon. This is partly due to the fact that dissolved inorganic carbon (DIC) is the source of carbon in auto-trophic biosynthesis and therefore plays a primary role in fractionation of carbon isotopes. In addition, a link between concentration of dissolved CO_2 and $\delta^{13}C_{POC}$ constitutes a potential proxy for DIC/CO_2 in past oceans via remains of phytoplankton found in marine sediments. Unfortunately, the relationship between a biological system and its environment is very complex and

full understanding of the controls of carbon isotope fractionation in phytoplankton is lacking.

Studies of large data sets have shown that $\delta^{13}C_{POC}$ covary with latitude, SST and dissolved CO_2 ($[CO_2]_{aq.}$) (Rau *et al.* 1989; Freeman and Hayes 1992; Goericke and Fry 1984). Since SST is linked to latitude and $[CO_2]_{aq}$ is, by thermodynamics, linked to SST it is very difficult to assess the significance of any individual parameter. However, Goericke and Fry, (1994) showed that even though $\delta^{13}C_{POC}$ does covary with the above mentioned parameters, variations of $\delta^{13}C_{POC}$ at a single latitude can be as high as latitudinal variations of $\delta^{13}C_{POC}$. This indicates that biological factors may have a larger effect on $\delta^{13}C_{POC}$ than $[CO_2]_{aq}$. Although some of these variations, especially at low and high latitudes, may be caused by variable $[CO_2]_{aq}$ in the mixed layer due to enhanced biological activity (Rau *et al.* 1992) it is clear that variations in $\delta^{13}C_{POC}$ cannot be explained by availability of carbon alone. A good example of this are the observations made by Francois *et al.*, (1993), which, in spite of a general agreement with $[CO_{2(aq)}]$ as the main control of carbon isotope fractionation, also show a 5 $^{\circ}/_{oo}$ variation in $\delta^{13}C_{POC}$ across the subtropical convergence in the Indian Ocean without concurrent variations in $[CO_2]_{aq}$(Fig.2.1). As suggested earlier the link between dissolved CO_2 (C_e) and carbon isotope composition of phytoplankton presents the possibility that estimates of C_e may be produced based on measurements

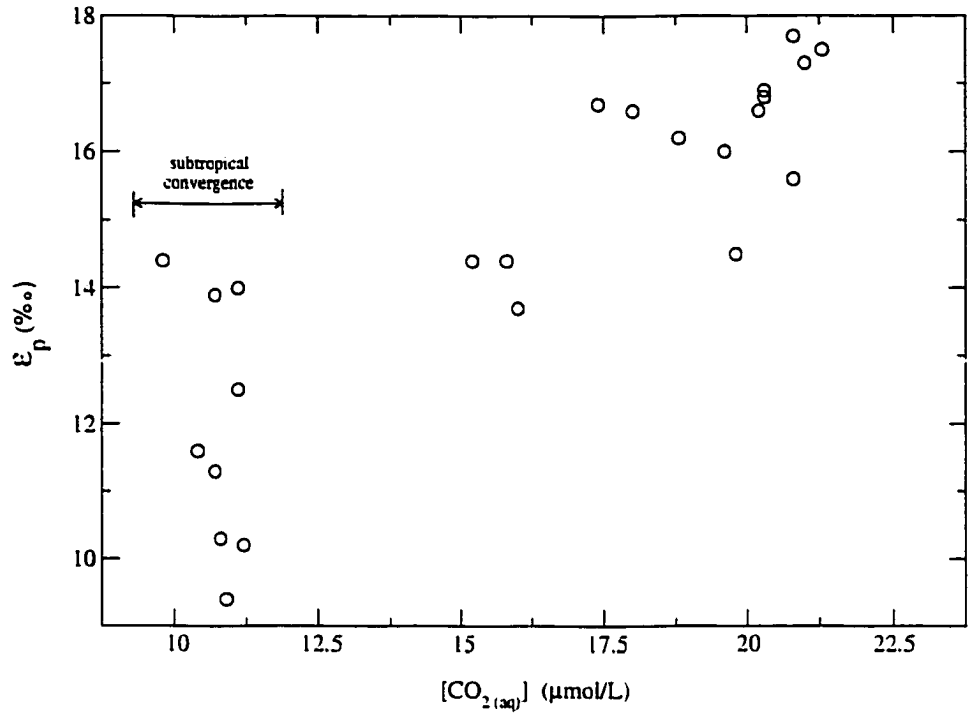

Figure 2.1: Observations of carbon isotope fractionation and $[CO_2]_{aq}$ in the SW Indian Ocean. Data from Francois *et al.*, (1993), table 1.

of $\delta^{13}C_{POC}$. The carbon isotope fractionation (ε_p) is defined as:

$$\varepsilon_p = \left(\frac{\delta_S + 1000}{\delta_P + 1000} - 1\right) \cdot 1000 \tag{2.1}$$

where δ_S and δ_P denote the carbon isotope composition of substrate and product respectively. Thus, ε_p can be determined by measuring the carbon isotope composition of CO_2 and the produced biomass. If then the relationship between dissolved CO_2 and ε_p is known, an estimate of CO_2 concentration can be made based on carbon isotope fractionation. Such a phenomenlogical relationship was demonstrated by McCabe, (1985) , who for fresh water phytoplankton described the relationship between

the concentration of CO_2 and carbon isotope fractionation as a linear function of $\log(C_e)$. Since then several authors have adopted a relationship of the form:

$$\varepsilon_p = A \cdot \log(d) + B \tag{2.2}$$

where d denotes the concentration of dissolved CO_2 and A and B are empirically determined parameters (Freeman and Hayes 1992; Popp *et al.* 1989; Jasper and Hayes 1990).

2.2 Paleo-pCO_2 barometry

Jasper and Hayes (1990) produced estimates of ancient CO_2 levels based on stable carbon isotopes. By comparing the stable carbon isotope composition of photosynthate with coeval foramniferal calcite, both extracted from a sediment core taken in the Gulf of Mexico, they produced estimates of atmospheric CO_2 concentrations by comparison of equilibrium concentrations calculaed from the pCO_2 of Antarctic ice-cores.

Organic carbon in marine POC may be derived from many different sources. The carbon may come from different trophic levels within the marine system or it can be terrigenous, introduced via river input and aeolian transport. To avoid contaminating the isotope signal in the phytosynthate with organic material from other sources, Jasper and Hayes (1990) measured the carbon isotope composition of specific organic compounds unique to a few phytoplankton species. These compounds,

the alkenones, are poly-unsaturated methyl- or ethyl-ketones with unusual characteristics. The molecules are large (C_{37} - C_{39}) and the double bonds are seven carbon apart instead of the more common 2-3. The configuration of the double bonds are *trans* as opposed to the more common *cis* (Rechka and Maxwell 1988). These unusual characteristics are most likely responsible for the stable nature of these molecules. The alkenones appear to be unaffected by food web processes since they remain unaltered after digestion by both copepods and mussels (Rowland and Volkman 1982). Oxidative degradation during sedimentation does affect the amount of alkenones being preserved in the sediments (Prahl *et al.* 1989). However, alkenones that survive the oxidative sedimentation processes will remain stable over geologic time scales. The combination of a known origin and the stability of the alkenones makes them very suitable as paleo-climatic proxies.

Since the effect of CO_2 concentration is manifested in the carbon isotope fractionation, i.e. the change in isotope composition between the substrate (CO_2) and the product (alkenone), the PCO_2 barometer must account for the isotope composition in the CO_2 that was utilized. Jasper and Hayes (1990) estimated the isotope composition of coeval CO_2 by measuring the carbon isotope composition of foramniferal tests found at the same depth in the sediment core as the alkenones. Tests from the planktonic foramnifera *Globigerinoides ruber* consists of calcite with a carbon isotope composition which is depleted in ^{13}C relative Dissolved Inorganic Carbon (DIC) by

0.5 °/$_{oo}$ (Fairbanks *et al.* 1982). Surface sea water DIC is in turn enriched in ^{13}C relative dissolved CO_2 by 8.8 °/$_{oo}$ (T=24 °C, pH=8.2). Measurement of the $\delta^{13}C_{G.ruber}$ therefore allows for estimation of $\delta^{13}C_{CO_2}$. Since both *Globigerinoides ruber* and the alkenone-producing phytoplankton live in the surface ocean where the dissolved CO_2 may be assumed to be in or near equilibrium with the atmosphere, the estimate of dissolved CO_2 can be used to calculate the atmospheric concentration of CO_2. To calibrate the relationship between ε_p and CO_2, (i.e. determine the values of the parameters A and B in equation 2.2). Jasper and Hayes, (1990) used data from the Vostok ice core and sediment core DSDP 619. By fitting the model to eight of their data points and applying the model to the rest of the data they produced a provisional record of atmospheric CO_2 concentrations for the last 100,000 yr.

2.3 *Emiliania huxleyi*

Emiliania huxleyi, a cosmopolitan alga abundant in all modern oceans, is commonly used as a model for the alkenone-producing species.

Morphology

Emiliania huxleyi is a unicellular planktonic marine alga, coccoid in shape with a diameter of 4-6 μm. Externally, the cell is covered with extracellular calcite plates or coccoliths. The coccoliths are formed internally in a specialized vesicle derived from the Golgi apparatus (Klaveness 1972). The cells have one chloroplast surrounded by

four membranes.

E. huxleyi occurs in three different cell-types: a coccolith forming cell-type (C-cells), the scaly motile cell with flagella (S-cells) and the completely naked cell-type, lacking both coccoliths and organic scales (N-cells). The different cell types are believed to represent different stages in their life cycle (Klaveness 1972).

2.3.1 Taxonomy

Emiliania huxleyi belongs to the phylum Prymnesiophyta, which include some 50 genera of living organisms with approximately 500 species. In early classification schemes (Lohmann 1902) the coccolithophores, which include *Emiliania huxleyi*, were placed together with the chrysomonads in a group possessing many flagellar types. Those chrysomonads which have two equal flagella were separated into the order Isochrysidales (Pascher 1910), whilst those possessing a "modified third flagellum" were later placed in the Prymnesiales (Pappenfuss 1955). On the basis of the unique third flagellum and the fact that species belonging to both orders bore smooth flagella, Christensen (1962) created a new class; the Haptophyceae, to contain the Isochrysidales and the Prymnisales. This classification was revised by Hibberd, who proposed that all taxa above the rank of family must be based on generic names. The class name was therefore changed to Prymnesiophyceae after the genus *Prymnesium* (Hibberd 1976). As haptophytes the coccolithophores were originally assigned to the Isochrysidales (Pappenfuss 1955) and later reassigned to the Prymnesiales (Round

1973). In 1980, Hibberd "re-separated" the coccolithophores into the Coccospherales (Haeckel 1894; Parke and Green 1976), giving the following classification of *Emiliania huxleyi*:

Kingdom: Protista (Haeckel, 1866)

Phylum: Prymnesiophyta (Hibberd, 1976)

Class: Prymnesiophyceae (Hibberd, 1976)

Order: Coccolithophorales (Schiller, 1926)

Family: Noelaerhabdaceae (Jerkovic, 1970)

Genus: Emiliania (Hay & Mohler, 1967)

E. huxleyi (Lohmann, 1902)

The family association for *E. huxleyi* is somewhat uncertain, Jercovic created this family in 1970 to include his new genus *Noelaerhabdus* and since then the genera *Emiliania, Gephyrocapsa* and *Reticulofenestra* have been added. However, more recent papers still include them in the Coccolithaceae (Okada and Mcintyre 1977), Gephyrocapaceae (Black 1971; Tappan 1980) or Prinsaceae (Haq 1978; Perch-Nielsen 1985).

2.3.2 Biogeography of E. huxleyi

The presence of coccolithophores in oceanic waters has been measured with a variety of techniques ranging from microscopic cell counts in water samples tosatellite imagery.

By utilizing thin layer chromatography (TLC) and high performance liquid chromatography (HPLC), unique pigments can be separated and identified. In the case of *E. huxleyi* the most abundant pigments are chlorophyll *a* and *c* along with 19'Hexanoyloxyfucoxanthin (Aprin *et al.* 1976). Unfortunately none of these pigments are particularly unique, the fucoxanthin has been detected in a few other prymnesiophyte species as well as in both chrysophyte and dinoflagellate species. Chlorophyll *a* and *c* are common to many phytoplankton groups, although some features of the chlorophyll *c* unit seems to be unique to *E. huxleyi* (Jeffrey and Wright 1987; Nelson and Wakeham 1989). These features are, however, too subtle to be detected by methods such as flurometry and satellite imagery.

Satellite imagery has been used to detect blooms of coccolithophores based on light scattering caused by abundant coccoliths in the surface water (Holligan *et al.* 1983; Groom and Holligan 1987). A limitation of this method is that it does not provide any information regarding speciation and it can only detect anomalies in the upper 15-30 m in clear waters and to even lesser depths in turbid waters (Holligan *et al.* 1989).

Extraction of alkenones from particulate matter have also been used to estimate vertical profiles of coccolithophore production (Ohkouchi *et al.* 1999), although this is not necessarily a species-specific method either since alkenones are also produced by other oceanic species such as *Gephyrocapsa Oceanica.* Due to the lack of specificity of available indirect methods, most of the data regarding the distribution of *E. huxleyi* has been acquired by collecting surface water samples (0-10 m) by slow-moving research vessels. This provides spatial coverage, but little information about the vertical distribution of the species. There are a few more extensive investigations which provide vertical profiles of coccolithophore abundances over larger areas, from which species distributions can be described according to depth and environmental preferences (McIntyre and Bé 1967; Okada and Honjo 1973; Marshall 1966).

From this kind of data, it is clear that *Emiliania huxleyi* is the most abundant and ubiquitous coccolithophore in today's ocean. A relative abundance of 60-80 % of the phytoplankton population is not uncommon. For example, *E. huxleyi* is one of the most euryhaline and eurythermal coccolithophore species. *E. huxleyi* has been found in the Red Sea with salinities as high as 41 ppt (Winter *et al.* 1979) and at salinities as low as 11 ppt and 17-18 ppt in the Sea of Azov and the Black Sea (Bukry 1974) respectively. It also has the largest temperature range (1-30°C) shown by any coccolithophore species (Okada and McIntyre 1979). It is very tolerant of nutrient levels, which is shown by its ability to grow in eutrophic Norwegian fjords (Van

Der Wal *et al.* 1994) and oligotrophic subtropical gyres. The fact that *E. huxleyi* is present throughout the top 200 m in coccolithophore communities indicates that it also has a wide tolerance for varying light conditions.

Evidence from the sedimentary record show that *Emiliania huxleyi* has been the dominant coccolithophore for the last 73,000 years and is likely to have evolved from a *Gephyrocapsa* species approximately 268,000 years ago (Thierstein *et al.* 1977). The ability to synthesize alkenones is most likely an inherited characteristic, since these compounds exist in sediments deposited long before the documented appearance of *E. huxleyi*. Due to the co-occurrence of both alkenones and nannofossils in these sediments it has been proposed that members of the Noelaerhabdaceae have been producing alkenones for at least 45 Ma (Marlowe *et al.* 1990).

2.4 Physiological Aspects of Inorganic Carbon Utilization in *E. huxleyi*

2.4.1 Inorganic Carbon Utilization by *E. huxleyi*

At sea water DIC and pH levels the concentration of dissolved CO_2 is significantly lower than the K_m (the CO_2 concentration at which CO_2 fixation occurs at maximum rate) for Rubisco suggesting that availability of CO_2 may under certain circumstances limit phytoplankton growth (Riebesell *et al.* 1993). As a response to this limitation, many phytoplankton species have developed a "CO_2 concentrating mechanism" by which the concentration of CO_2 at the site of Rubisco is increased

(Raven and Johnston 1991). Criteria for the presence of such a mechanism include saturation of photosynthesis at sea water concentrations of DIC and a $K_{0.5}$ (the CO_2 concentration providing half of the maximum photosynthetic rate) significantly lower than the K_m for Rubisco. *E. huxleyi* is unable to accumulate DIC significantly above external DIC, $[DIC]_{int} \approx 0.3$ mM (Nimer and Merrett 1992), and has been shown to have a $K_{0.5}$ of 10-50 μM which is similar to K_m ($\approx$30 μM) of Rubisco (Brownlee *et al.* 1995; Badger *et al.* 1998), indicating the lack of a CO_2 concentrating mechanism. Also, photosynthesis in *E. huxleyi* at saturating light conditions is not saturated at sea water CO_2 levels (Steeman-Nielsen 1966; Nimer and Merrett 1993).

The source of inorganic carbon for photosynthesis in *E. huxleyi* is clearly demonstrated by studies showing that low calcifying cells are unable to grow when the media is being bubbled with CO_2 free air (Dong *et al.* 1993) and photosynthetic oxygen evolution decreases with increasing external pH (Nimer *et al.* 1992). Both these findings indicate that CO_2 and not HCO_3^- is utilized for photosynthesis. However, high-calcifying cells can obtain carbon for growth from HCO_3^- via the calcification process used to produce coccoliths (Dong *et al.* 1993; Nimer and Merrett 1993). The concept of calcite formation as a photosynthetic adaptation for the use of bicarbonate has been thoroughly investigated (Sikes *et al.* 1980; Nimer and Merrett 1992; Nimer *et al.* 1992; Nimer *et al.* 1994a; Anning *et al.* 1996). *Sikes et al* (1980) suggested two routes for bicarbonate utilization in *E. huxleyi* which form the basis for a model of

the interaction between photosynthesis and calcification. Calcite is produced in the coccolith vesicle, i.e.:

$$HCO_3^- + Ca^{2+} \rightarrow CaCO_3 + H^+ \tag{2.3}$$

To favor the conversion of HCO_3^- to CO_3^{2-} within the vesicle, the proton must be extruded into the cytosol. The cytosol would then be acidified as a response to calcification, but since cytosolic pH is observed to be close to neutral (Nimer *et al.* 1994a; Dixon *et al.* 1989), a simultaneous alkalinization must occur. According to *Sikes et al* (1980) a second HCO_3^- produces CO_2 for photosynthesis:

$$HCO_3^- \rightarrow CO_2 + OH^- \tag{2.4}$$

If this occurs in the chloroplast, extrusion of OH^- to the cytosol would then neutralize the H^+ produced in the coccolith vesicle, and thus the interaction between calcification and photosynthesis would maintain the cytosol at neutrality. The observed stoichiometry between CO_2 fixation and oxygen evolution is 2:1 in high-calcifying cells (Nimer and Merrett 1993), which implies fixation of one additional carbon by a C_4-type reaction. *Nimer and Merrett* (1993) suggested that the C_4-mechanism would utilize HCO_3^- , i.e.:

$$C_3 + HCO_3^- \rightarrow C_4 \tag{2.5}$$

giving an overall process of:

$$3HCO_3^- + Ca^{2+} \rightarrow CaCO_3 + 2'CHOH' + O_2 \tag{2.6}$$

However, under conditions resulting in an excessive acidification of the cytosol some HCO_3^- would be expended to produce OH^- in order to maintain constant pH. The stoichiometry between CO_2 fixation and O_2 evolution would then be 1:1, and the overall reaction becomes:

$$3HCO_3^- + Ca^{2+} \rightarrow CaCO_3 +' CHOH' + CO_2 + O_2 + H_2O \qquad (2.7)$$

A schematic description of the model can be found in figure 2.2.

The carbon utilized for photosynthesis by *E. huxleyi* is thus CO_2 originating from either the external media or from dissociation of HCO_3^- in the cytosol/chloroplast with additional carbon fixed via a C_4-mechanism.

2.4.2 Calcification

The calcification process takes place in a vesicle closely associated with the Golgi body. In this coccolith vesicle, calcite is precipitated to form coccoliths which, when completed, are extruded to the exterior of the cell. *E. huxleyi* utilizes HCO_3^- as a source of carbon for calcification (Sikes *et al.* 1980; Dong *et al.* 1993; Buitenhuis *et al.* 1999). The rate at which carbon is fixed into $CaCO_3$ has been shown to be equivalent to, or even exceed, photosynthetic carbon fixation. These high rates can occur in both cultures (e.g Van Bleijswijk *et al.*, 1994) and in natural populations (e.g. Balch *et al.*, 1992). The calcification rate is dependent on the external DIC concentration, it is saturated at 1 mM DIC when measured at a light flux of 50 μmol

m^{-2} s^{-1}, but is not saturated at 2 mM DIC when the light flux is increased to 300 μmol m^{-2} s^{-1} (Nimer and Merrett 1993).

The calcification process is light dependent although its light saturating point is much lower than that of photosynthesis (Paasche 1964). The exact nature of the energy requiring processes involved in calcification is not known, however the transport of HCO_3^- and Ca^{2+}, and the extrusion of the completed coccolith likely require energy. Therefore, at low light levels the flux of HCO_3^- into the chloroplast is sufficiently high to saturate photosynthesis, such that the stoichiometry between calcification and photosynthesis is 1:1. At higher light levels the flux of HCO_3^- may not provide enough carbon to saturate photosynthesis. If available, exogenous CO_2 could then contribute to the photosynthetic carbon fixation (Nimer and Merrett 1993). A consequence of the lower light levels required for calcification relative to photosynthesis is an increasing ratio of carbon allocated to calcification relative to carbon utilized by photosynthesis with decreased light availability. This Calcification/Photosynthesis ratio (C/P) will then increase with depth as suggested by Balch *et al.*, (1992). In a model describing a coccolithophore bloom they showed an increase in C/P from 1 at the surface to over 30 at 20 m depth. Even though this model estimates a situation with extreme light attenuation, the principle could be extrapolated to non-bloom situations, especially considering the depth distribution of *E. huxleyi*. Thus, the C/P ratio could be expected to increase with depth in natural populations.

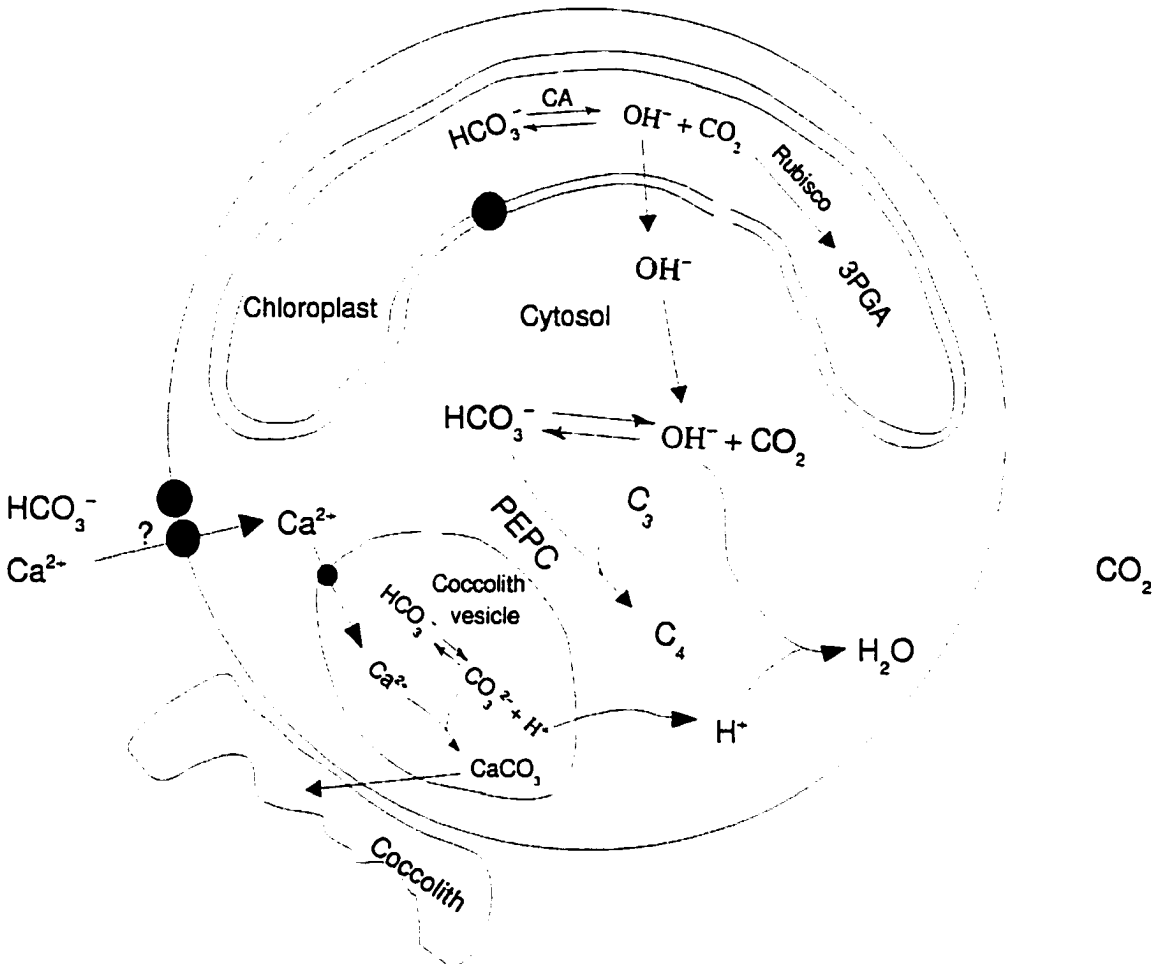

Figure 2.2: Schematic of carbon uptake in Emiliania huxleyi.

The model describes carbon uptake as suggested by (Sikes et al. *1980) where HCO_3^- is actively transported into the cytosol. Once inside the cell, the HCO_3^- ion can either dissociate into CO_2 and OH^- or be transported into the coccolith vesicle to form calcite. A third alternative is transport into the chloroplast where facilitated dissociation to CO_2 occurs via carbonic anhydrase. At alkaline pH, HCO_3^- can also react with PEP via a C_4 pathway. Meanwhile, CO_2 in the cytosol can diffuse into and out of the cell depending on the sign of the concentration gradient and also diffuse into the chloroplast to complement the transported HCO_3^-. (Filled circles depict active transport)*

Nitrogen availability may also affect calcification: an inverse relationship between calcification and nitrogen concentration was shown in a *Hymenomonas* spp. in culture (Baumann *et al.* 1978) and a naked strain of *E. huxleyi* developed coccoliths when the $NaNO_3$ concentration was decreased from 150 to 16.7 mg/l (Wilbur and Watabe 1963). More recently, Paasche, (1998) demonstrated a two-fold increase in the number of coccoliths per cell after the onset of N-limitation. The fact that N-limitation can induce a change in the C/P-ratio is of great interest since nitrogen is commonly quoted as the limiting nutrient in marine systems (Falkowski 1997).

Phosphate-limitation also causes an over-production of calcite (Van Bleijswijk *et al.* 1994; Paasche and Brubak 1994; Anning *et al.* 1996; Paasche 1998). The effect of P-limitation is more dramatic, resulting in three times more coccoliths produced (Paasche 1998). Paasche's data also showed an inverse relationship between calcification and growth rate for both N-limited and P-limited cultures, implying that nutrient induced calcification is a gradual phenomenon rather than a step response.

2.4.3 Diffusion of CO_2

Photosynthesis requires a net influx of inorganic carbon from the surrounding water into the cell. As in many other eukaryotic cells, the site of carbon fixation in *Emiliania huxleyi* is located in the chloroplast stroma and therefore this flux of carbon has first to pass through the plasmalemma and the associated endoplasmic reticulum (ER), then through the cytosol and finally through two membranes of

chloroplast ER. The flow of carbon is either maintained by diffusion of CO_2 along a concentration gradient into the cell or by active transport of CO_2 or HCO_3^- across the cell membrane.

Only CO_2 can freely pass through the plasmalemma and the chloroplast envelope membranes. The gas has to dissolve into the lipid membranes, diffuse across to the interior of the cell/chloroplast and there dissolve in the cytosol/stroma. The diffusion of CO_2 into the cell can be approximated as diffusion across a plane:

$$J_{bs} = -D\frac{\partial C}{\partial z} \tag{2.8}$$

where J is the flux of CO_2 through the plane $[mol\ m^{-2}s^{-1}]$ and C is the concentration of the solute and has the dimensions of $[mol\ m^{-3}]$. D is the diffusion coefficient with dimension $[m^{-2}s^{-1}]$ and z is the boundary layer thickness $[m]$. This differential equation can be solved using the finite difference form:

$$J_{bs} = \frac{D(C_b - C_s)}{z} \tag{2.9}$$

where C_b is the concentration of CO_2 in the bulk medium and C_s is the concentration of CO_2 at the surface of the plane. The boundary layer that surrounds the cell is a layer closest to the cell in which no turbulent mixing of media takes place. Transport of molecules across this layer is limited to diffusion. The thickness of this layer (z in Eq. 2.9) is a function of the object's size and the relative velocity of the surrounding media. However, for small objects like phytoplankton with a size less than the smallest

scale for turbulent/advective transport of 1mm, fluid flow can be considered viscous and the boundary layer thickness is only dependent on the size of the object. The thickness for phytoplankton can therefore be approximated by one cell radius (Wolf-Gladrow and Riebesell 1997). For *E. huxleyi*, with its small cell size, the boundary layer is approximately 3 μm thick. This is thin enough to prevent any conversion of HCO_3^- to CO_2 within the boundary layer (Wolf-Gladrow and Riebesell 1997). Therefore diffusion of CO_2 into an *E. huxleyi* cell can be approximated with Eq. 2.9.

The continued diffusion across the cell membranes can be treated in a similar manner if solubility of CO_2 in the lipid bilayer is taken into account. Consequently this can be accomplished by introducing the partition coefficient K for CO_2 in equilibrium with the membrane:

$$J_{si} = D\frac{K(C_s - C_i)}{z} = P(C_s - C_i) \tag{2.10}$$

where C_i is the concentration of CO_2 inside the cell and z is the distance across the membrane. The permeability coefficient (P), describes membrane diffusion and is defined from Eq. 2.10 as:

$$P = \frac{DK}{z} \tag{2.11}$$

By using an artificial lipid bilayer Gutknecht *et al.*, (1977) showed that as a result of the slow conversion of HCO_3^- to CO_2 the diffusion across the surface boundary layer is the rate limiting step in the diffusive transport of CO_2 into the cell (Gutknecht *et al.* 1977).

2.4.4 Carbonic anhydrase

The presence of carbonic anhydrase (CA), which catalyses the conversion of HCO_3^- to CO_2, on the exterior of the cell membrane steepens the concentration gradient and can speed up the diffusive transport of CO_2 by a factor of 10-100 (Gutknecht *et al.* 1977). *E. huxleyi* have been shown to produce external CA in batch cultures when the cultures reach stationary phase (Nimer *et al.* 1994b; Nimer and Merrett 1996). In contrast, exponentially-growing cells lack external CA indicating that the expression of external CA is a response to culture age. Data for nutrient-limited but not DIC-limited cells is not available, but it is likely that the expression of external CA is facilitated by low DIC concentrations. The eco-physiological significance of CA is therefore limited to bloom situations, where the oceanic DIC may be depleted to the extent observed in laboratory cultures.

While no external CA is found in nutrient and DIC replete cells, CA have been found in chloroplasts of exponentially growing cells of *E. huxleyi* (Nimer *et al.* 1995) and another coccolithophorid (Quiroga and Gonzalez 1993). The location of the intracellular CA in the chloroplast supports the model by *Sikes et al* (1980) where the CA catalyzed conversion of HCO_3^- to CO_2 and OH^- would result in the extrusion of OH^- to the cytosol, thus counteracting the acidification caused by calcification.

2.4.5 Bicarbonate uptake

In high-calcifying cells of *E. huxleyi*, most results suggest that HCO_3^- is the external carbon source for calcification (Sikes *et al.* 1980; Dong *et al.* 1993; Nimer *et al.* 1992; Buitenhuis *et al.* 1999). High-calcifying cells also have a high affinity for HCO_3^-; the concentration of dissolved DIC required for half-maximal rate of photosynthetic O_2 evolution ($K_{0.5}$[DIC]) is 200 μM at pH 8.3 (Nimer and Merrett 1992). The transport mechanism for HCO_3^- across the plasmalemma is not known. A passive uniport, HCO_3^-/Cl^- exchange, HCO_3^-/OH^- exchange or co-transport with a cation such as Na^+ have been suggested (Dixon and Merrett 1987; Katz *et al.* 1986; Rees 1984). HCO_3^-/OH^- exchange seems unlikely since calcifying cells do not increase pH while reducing external DIC (Dong *et al.* 1993; Merrett *et al.* 1993). The influx of HCO_3^- may be controlled by cytosolic Ca^{2+}. In the presence of the Ca^{2+}-channel blocker Gd^{3+}, the increase in intracellular pH observed upon re-addition of HCO_3^- to carbon starved cells is prevented. This indicates a calcium-controlled bicarbonate uptake mechanism (Nimer and Merrett 1996; Brownlee *et al.* 1995). Once inside the cell, there are three possible scenarios for the fate of the HCO_3^- ion. At the intracellular pH of 7 (Dixon *et al.* 1989), a significant proportion will dissociate and form CO_2($\approx$ 8% of available DIC, compared to $\approx$ 0.5% at pH=8.2). This may be the major source of carbon for photosynthesis in calcifying cells. An equivalent number of HCO_3^- ions will also be transported into the coccolith vesicle. Little is known about

the details of this mechanism. Knowledge of the intra-coccolith vesicle concentration of HCO_3^- would enable assessments regarding the direction of the concentration gradient. Finally, the third destination for the HCO_3^- ion is the chloroplast, where facilitated conversion to CO_2 occurs via carbonic anhydrase.

2.4.6 CO_2 efflux

The partial pressure of dissolved CO_2 in blooms of *E. huxleyi* have been shown by several studies to be substantially higher than that encountered in blooms of other phytoplankton species (Holligan *et al.* 1993; Robertson *et al.* ; Purdie and Finch 1994). To explain this several mechanisms have been suggested: (*i*) leakage of CO_2 from the cell due to elevated cytosolic CO_2 concentration caused by calcification (Paasche and Brubak 1994), (*ii*) temperature influence on CO_2 solubility caused by solar radiation trapped by detached coccoliths (Holligan *et al.* 1993), (*iii*) enhanced removal of HCO_3^- causing an equilibrium effect on the carbonate system (Holligan *et al.* 1993; Purdie and Finch 1994; Robertson *et al.*), and (*iv*) a lesser change in pCO_2 relative to the change in ΣCO_2 than expected due to preferential removal of HCO_3^- combined with nocturnal respiration of free CO_2 (Crawford and Purdie 1997)

.

The suggestion that the cells are leaking CO_2 into the external media is supported by the fact that the internal pH is close to 7 (Nimer *et al.* 1994a), and with an internal DIC concentration of 0.3 mM the internal concentration of CO_2 will be higher than

Cell Status	CO_2 flux[a]	C_i[b]	pH[c]	$[DIC]_{int}$[d]
Nutrient replete	$1.09 \cdot 10^{-6}$	12.21	7.318	159
Nitrate limited	$1.60 \cdot 10^{-6}$	12.31	7.316	160
Phosphate limited	$1.48 \cdot 10^{-6}$	12.29	7.316	160

[a]pmol C $cell^{-1}$ s^{-1}
[b]internal CO_2concentration (μM)
[c]assuming 0.3 mM internal DIC
[d]assuming internal pH of 7.0 (Nimer and Merrett 1992) (μM)

Table 2.1: Calculated values of C_i and pH_i based on measured CO_2 flux from (Nimer and Merrett 1995)

20 μM inside the cell. An actual efflux of CO_2 from *E. huxleyi* cells was measured by *Nimer and Merrett* (1995), who found that nutrient replete cells released CO_2 into the media corresponding to 10 % of total carbon fixed as organic carbon and as calcite. For nutrient limited cultures (NO_3^- and PO_4^{3-}) the release of CO_2 from the cells increased to 50 % of total carbon uptake.

An attempt to calculate the flux of carbon based on the measured $[DIC]_{int.}$ as well as the calculated $[DIC]_{int.}$ from the measured flux revels a paradox; 0.3 mM DIC at a cytosolic pH of 7.0 corresponds to a outward flow of carbon two orders of magnitude larger than that measured. Also, the both internal DIC concentration and pH as calculated from the measured efflux of CO_2 is very different from measured results as shown in Table 2.1. The diffusitivity constant D, is taken to be: $1.37 \cdot 10^{-9}$ $m^{-2}s^{-1}$ (Rau *et al.* 1996) and the boundary layer thickness is equal to the cell radius, r=3 μm. Permeability coefficient: $5 \cdot 10^{-5} ms^{-1}$ (Rau *et al.* 1997): Although the pH

values are higher than the measured, it is interesting to note that the change in pH needed to cause the CO_2 efflux to increase from 10 % to 50 % is very small, i.e. even the slightest change in pH will have an effect on the magnitude of CO_2 efflux (Table 2.1). This presents the possibility that a change in the balance between calcification and photosynthesis causing a change in cytosolic pH would affect the extent of CO_2 leakage. Support for this hypothesis is given by the fact that CO_2 efflux increases in nutrient limited cells which have an increased calcification rate relative to the photosynthetic rate.

The offset between the calculated and the measured pH in Table 2.1 may be explained by the permeability coefficient. The estimates are made by setting the permeability coefficient to a value commonly used for algae which rely on passive CO_2 uptake, i.e. the membrane is assumed to be permeable to the degree that it does not suppress CO_2 diffusion significantly. *E. huxleyi* have the ability to transport HCO_3^- across the membranes and therefore a high permeability is no longer advantageous. It is more likely that the permeability in *E. huxleyi* is lower, enabling the cells to maintain a higher cytosolic DIC concentration.

For example: assume a cell which is not carbon limited, chloroplast CO_2 concentration C_{cp} is saturating Rubisco at 30 μM, with an external CO_2 concentration of 12 μM, and that the chloroplast has a surface area corresponding to 10 % of the cell surface area. Then the flow of carbon from the chloroplast to the external media can

be described as in eq. 2.12, 2.13 and 2.14:

flow out of chloroplast:

$$F_{cp} = 0.1 \cdot A \cdot (30 \cdot 10^{-3} - C_{cytosol}) \cdot P \tag{2.12}$$

flow out of the cell:

$$F_{leak} = A \cdot (C_{cytosol} - C_{surf}) \cdot P \tag{2.13}$$

flow across the boundary layer:

$$F_{leak} = D \cdot \frac{C_{surf} - C_e}{r} \tag{2.14}$$

The concentration of CO_2 on the outside surface of the cell, C_{surf}, can be calculated by re-arranging Eq.2.14. Using F_{leak}=9.62 nmol C m^{-2} s^{-1} (*Brownlee et al* 1995), D=$1.37 \cdot 10^{-9}$, calculated for 15 °C (Rau *et al.* 1996) and a cell radius of 3 μm:

$$C_{surf} = \frac{F_{leak}}{D} \cdot r + C_e = \frac{9.62 \cdot 10^{-9}}{1.37 \cdot 10^{-9}} \cdot 3 \cdot 10^{-6} + 12 \cdot 10^{-3} = 12.02 \cdot 10^{-3} (\mu M) \tag{2.15}$$

Solving for $C_{cytosol}$ by setting $F_{cp} = F_{leak}$ and combining Eq. 2.12 and Eq. 2.13 gives:

$$C_{cytosol} = \frac{C_{surf} + 3 \cdot 10^{-3}}{1.1} = 13.65 \mu M \tag{2.16}$$

This can be used to calculate the permeability coefficient (P):

$$P = \frac{F_{leak}}{C_{cytosol} - C_{surf}} = \frac{9.62 \cdot 10^{-9}}{13.65 \cdot 10^{-3} - 12.02 \cdot 10^{-3}} = 5.9 \cdot 10^{-6} m s^{-1} \tag{2.17}$$

This suggests that it may be possible for the cells to maintain saturating conditions in the the chloroplast while not leaking more than that observed. However, the calculated cytosolic CO_2 concentration corresponds to about 0.17 mM DIC at pH 7.0. The measured value is slightly higher, thus requiring a lower permeability. The estimated value for permeability at the same efflux of CO_2 but with an internal DIC concentration of 0.3 mM is approximately $0.8 \cdot 10^{-6}$ which is somewhat lower than the interval of reported P values of 2 to $3500 \cdot 10^{-6}$ m s^{-1} (Raven 1993). A low permeability may therefore be the reason for *E. huxleyi*'s low affinity for CO_2.

2.4.7 β-carboxylation

As mentioned earlier the stoichiometry between carbon fixed as organic material and oxygen evolution is 2:1 in nutrient replete cells. This implies that carbon is being fixed via a β-carboxylase enzyme. Although the extent of β-carboxylation seems somewhat high, Beardall, (1989) estimated that β-carboxylation cannot account for more than 25% of the net carbon fixed in phytoplankton, assuming balanced growth and that all fixed carbon is shuttled through the TCA-cycle. High β-carboxylase activity has, however, been reported in nitrogen-starved cultures that were enriched with ammonia (Guy *et al.* 1989).

The type of β-carboxylase present in *E.huxleyi* is somewhat uncertain. Descolas-Gros and Oriol, (1992), tested for both phosphoenolpyruvate carboxylase (PEPC) and phosphoenolpyruvate carboxykinase (PEPCK) and found only PEPC. This concurs

with the activity of PEPC found in another coccolithophore, *Coccolithus pelagicus*, by Glover and Morris, (1979). However, Brownlee *et al.*, (1995) mention that PEP carboxykinase has been found in *E. huxleyi*, although no details were given. PEP carboxylase is an enzyme that uses HCO_3^- and PEP as substrates to form oxaloacetate, a precursor to amino acid synthesis via the TCA-cycle. On the other hand, PEP carboxykinase can function as both carboxylating and decarboxylating enzyme, although in algal cells the decarboxylating function is uncertain (Davies 1979). In contrast to PEP carboxylase the carboxylating function of PEP carboxykinase uses CO_2 as substrate to form oxaloacetate (Arnelle and O'Leary 1992).

When *E. huxleyi* cells are either phosphate- or nitrate-starved the ratio of CO_2 fixed as organic carbon and oxygen evolution becomes 1:1 (Nimer and Merrett 1995), indicating that the β-carboxylation is no longer active. This may be in response to cytosolic pH. Davies (1973) suggests a role of PEPC in the fine control of cytosolic pH, where the activity of carboxylating enzymes increases with increasing pH. Since cytosol pH may be linked to calcification rate, a decrease in the relative fraction of calcification would increase pH and thus promote β-carboxylation. Regulation of PEPC by the concentration of phosphate in the cytosol has also been reported for a number of PEP carboxylases (Tchen and Vennesland 1955; Wong and Davies 1973). In these cases, the activity of PEPC was stimulated by increased phosphate concentration.

2.4.8 Carbon isotope fractionation

Based on the information described above, a model for carbon isotope fractionation in *Emiliania huxleyi* can be proposed. The main control of the fractionation appears to be the availability of nutrients. Since *E. huxleyi* mainly utilize HCO_3^-, which is abundant in sea water, the availability of carbon is subordinate to the availability of both nitrate and phosphate. The nutrient control is manifested in two ways. Firstly, by turning off and on β-carboxylation, and secondly by affecting the relative rate of calcification. Calcification plays an important role in the fractionation. It regulates the availability of carbon within the cell by active transport of HCO_3^- into the cell and may also acidify the cytosol which controls the degree of CO_2 efflux from the cell. Partial uptake of external CO_2 via diffusion may only occur when high concentrations of nutrients and light cause photosynthesis to widely exceed calcification. This would result in an increase of the cytosolic pH, thus allowing for diffusion of external CO_2 into the cell by decreasing the internal CO_2 concentration. The fractionation associated with active HCO_3^- uptake and a subsequent leaky cell is described in Figure 2.3. A isotope mass balance for this system can be written as (Hayes 1993):

$$\phi_i(\delta_e - \varepsilon_{d/b} - \varepsilon_a) = \phi_o(\delta_i - \varepsilon_t) + \phi_f(\delta_i - \varepsilon_f) \tag{2.18}$$

where ϕ_i, ϕ_o are the fluxes of carbon in and out of the cell, ϕ_f is the flux of carbon into organic material. δ_e, δ_i are the isotope composition of dissolved CO_2 outside and

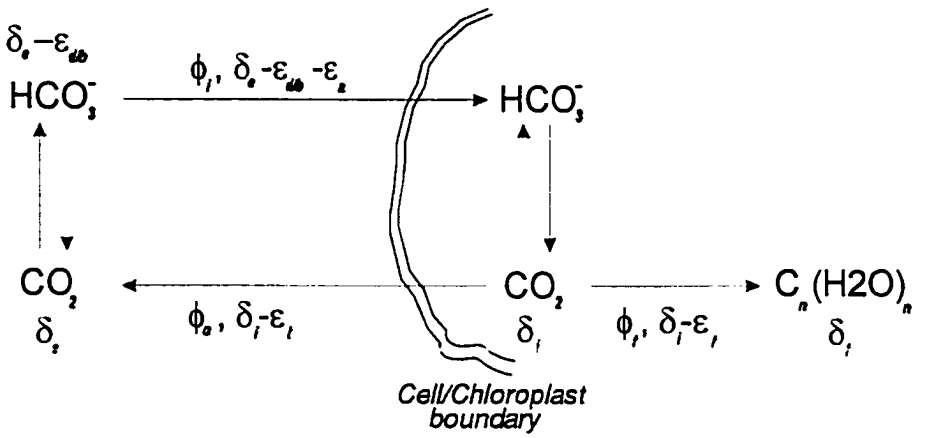

Figure 2.3: Schematic describing carbon flows and isotopic compositions in a cell with active bicarbonate uptake. After Hayes (1993).

inside the cell respectively and δ_f is the carbon isotope composition of the produced biomass. $\varepsilon_{d/b}$ is the equilibrium isotope effect between dissolved CO_2 and HCO_3^-, ε_a is the isotope effect associated with active transport of bicarbonate, ε_t is the isotope fractionation due to diffusion of CO_2 and ε_f is the carbon isotope fractionation occurring during carbon fixation. This isotope effect caused by active uptake of HCO_3^- is not known but is likely to be small (Hayes 1993). Defining $L \equiv \phi_o/\phi_i$ (L is the fraction of bicarbonate entering the cell that leaks back out), $\phi_f/\phi_i = 1 - L$ and with the substitution $\delta_i = \delta_f + \varepsilon_f$ results in an equation describing the carbon isotope fractionation for photosynthesis:

$$\varepsilon_p = \delta_e - \delta_f = \varepsilon_{d/b} + L(\varepsilon_f - \varepsilon_t) \tag{2.19}$$

As indicated by Eq.2.19, the isotope fractionation in this system is controlled by the leakage of CO_2 from the cell: $\varepsilon_p \rightarrow \varepsilon_{d/b}$ when L $\rightarrow$ 0. The leakage is in turn controlled by nutrient availability via calcification. A decline in nutrient concentrations to limiting levels will increase the degree of leakage and subsequently deplete the produced biomass of ^{13}C. i.e.. $\varepsilon_p \rightarrow \varepsilon_{d/b} + \varepsilon_f - \varepsilon_t$ when $L \rightarrow 1$.

During nutrient-replete conditions, the isotope composition of the biomass may also be significantly influenced by β-carboxylation. The effect on the fractionation will depend on which enzyme is utilized. If the cells are using PEP carboxylase with HCO_3^- as substrate, then a small fractionation factor will result e.g. ε_{PEPC}, is only 2 $^\circ/_{oo}$ (Goericke and Montoya 1994) and an enrichment of ^{13}C can be expected. If PEP carboxykinase is used with CO_2 as substrate, a fractionation factor of 30 to 40 $^\circ/_{oo}$ (Goericke and Montoya 1994) will result, and the effect on the fractionation will be indistinguishable from fractionation by Rubisco alone.

Chapter 3

Methods

3.1 Sample Preparation and Analysis

3.1.1 POC: Sample Collection and Preparation

The particulate organic carbon (POC) samples were collected by pumping sea water through pre-combusted glass fiber filters, either *in situ* at predetermined depths between the sea surface and 1000 m (Line P, NE Pacific) or from 5 m depth in an on-board filter manifold (Pacific transect, Victoria-Guam). During the CJGOFS (Canadian Joint Global Ocean Flux Study) cruises in the NE Pacific, samples were obtained as subsamples from the Multi-Unit Large-Volume-Filtration-System, MULVFS (Bishop *et al.* 1985). Up to 12 pumps were deployed at each station providing depth profiles of POC. The samples consisted of 2 subsamples cut from the 53 μm MULVFS filters after recovery of the pumps. The cuts were made with a cookie cutter with a diameter of 44.5 mm. Immediately after sub-sampling, the punches were put into pre-combusted vials filled with a chloroform/methanol (2:1) mixture. The sample vials were first stored on-board and later in the lab at -20°C until extraction.

Sampling during the Pacific Transect from Victoria B.C., to Guam, on-board R/V Sonne (SO112) utilized the "Sea-Loop", a clean sea-water system which has an intake in the bow of the ship at approximately 5 m depth. Measures are taken to keep the

system clean, e.g. it is routinely turned off and closed as the ship enters a port. The cleanliness makes the system well suited for underway collection of surface water and POC. The system is accessed in the on-board labs via a valve, similar to a kitchen faucet, that can be attached to a filter manifold.

As the only geochemist on this cruise, I had to ensure that sampling of POC could be maintained 24 hours a day. This problem was solved by constructing an automated sampling manifold based on a programmable lawn sprinkler system, see Fig. 3.1 (James Hardie Irrigation, part. no 675401). Sprinkler valves were set to control the flow of water to three banks of four 47 mm filter holders (Poretics Corp.). By programming the system to open and close the valves at appropriate intervals, e.g., open to bank 1 for 2 h then close to bank 1, wait 3 h, then open to bank 2 for 2 h and so on, semi-continuous sampling could be maintained along the entire transect. The filters (pre-combusted Gelman A/E) were put into pre-combusted aluminum pockets and frozen at -20°C after the sampling was complete.

3.1.2 Lipid Extraction and Purification

At the time of analysis, solvent in which filters from the NE Pacific cruises had been immersed since shipboard collection was transferred to a separatory funnel. The filter residue was washed 5 times with 2:1 chloroform/methanol which was then added to the separatory funnel. Each time the filters were washed, the sample vial was placed in an ultra-sonic bath filled with an ice-water mixture for 30 seconds. The

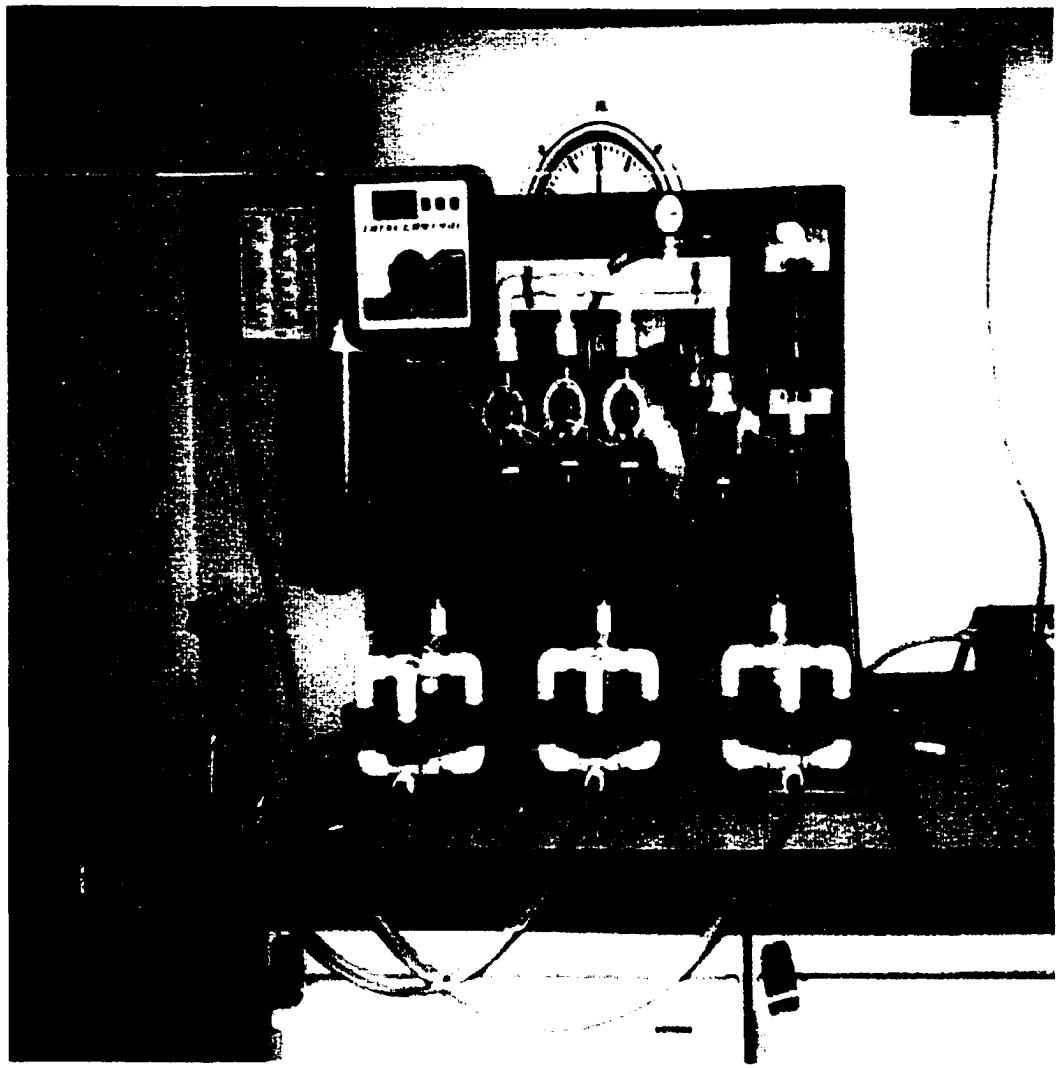

Figure 3.1: Filter manifpold on-board R/V Sonne. The filter setup was controlled by the programmable lawn sprinkler system, which switched between filter banks at pre-programmed times.

preparation of total lipid extracts (TLE) that followed were according to *Wakeham and Pease* (unpublished material, 1992) with the exception that a 5 % $NaHCO_3$ solution was used to wash the organic phase. The neutral fraction from saponification of the TLE was separated into compound groups using a short silica gel column. The column consisted of a Pasteur pipette with 0.3 g of 5 % deactivated silica gel. Each TLE-sample was separated into three fractions: 5 ml hexane, 7 ml 2 % ethylacetate in hexane and finally 5 ml dichloromethane with the alkenones eluting in the middle fraction. The fraction containing alkenones was transferred to a vial with a 150 $\mu\ell$ insert and taken up in *iso*-octane for isotope analysis. The recovery of alkenones using this method varied between 70-90% based on analysis of selected samples with 2-hexadecanone as internal standard.

Use of $NaHCO_3$ solution enabled an estimation of free fatty acids (FFA) in the POM by retaining the fatty acids (FA) in the water phase. The FAs were recovered from the water phase by acidifying with 6N HCl to pH 2 and extracting with dichloromethane.* The resulting FFA sample was methylated according to Wakeham and Pease (unpublished material, 1992) before GCMS analysis.

Samples from the Pacific Transect were treated somewhat differently. First, the

*This method may under-estimate the amount of fatty acids present in the sample due to losses in the water-chloroform interface, where the FA's can be oriented such that the hydrophobic carbon chain is penetrating the organic phase (*de Leeuw J. W.*, personal communication)

frozen filters were thawed and immersed in 2:1 dichloromethane/methanol in pre-combusted vials. After a week at -20°C the samples were extracted in the same way as the NE Pacific samples with the exception that no free fatty acids were recovered. A NaCl-solution was used to separate dichloromethane and methanol and in the subsequent washing of the organic phase. TLEs were saponified and the neutral fractions were taken up in *iso*-octane and used for isotope analysis.

3.1.3 Determination of pCO_2

Concentrations of dissolved CO_2 for the NE Pacific cruises were calculated from measured alkalinity and total CO_2 along with measured concentrations of phosphate and silica. Total alkalinity was measured using a closed-cell potentiometric titration method and total inorganic carbon was determined by coulometric titration. The calculations were made using the DOS-program CO2SYS written by Ernie Lewis at Brookhaven National Laboratory, Upton NY. Constants used by the program were by Weiss, (1974) and Roy *et al.*, (1993). However, while comparing the calculated pCO_2 values with values concurrently obtained with an equilibrator a significant discrepancy was found. Surface PCO_2 calculated from the measured alkalinity and total CO_2 was about 100 μatm lower than the equilibrator values. The latter showed values close to saturation. Literature values (Wong and Chan 1991), provided a control for the same area. They agree with the equilibrator values, i.e. values are close to saturation, ΔP(air - water): -34.9 to 26 .8 μatm (Wong and Chan 1991),

indicating that the calculated values are unreliable. The reason for this discrepancy is not known. The calculation routine from Brookhaven is not thought to be incorrect, which leaves analytical error as a possible cause. However, no such error could be clearly identified, although the total CO_2 values are suspiciously low.

In an attempt to circumvent this problem, alkalinity and total CO_2 was estimated using the temperature-dependent estimates described by Kroopnick, (1985). When calculating the PCO_2 based on these estimates the values are comparable to the equilibrator values, e.g. Δ(equilibrator-measured): 72.9 to 97.7 μatm, Δ(equilibrator-estimated): -8.4 to 11 μatm. These errors corresponds to a discrepancy in C_e relative equilibrator C_e of 2 to 4 μM (average: 3.3 μM) for the measured values and -1 to 0.5 μM (average: -0.2 μM) for the estimated values. Based on this evaluation C_e has therefore been calculated using estimates of alkalinity and total CO_2 according to Kroopnick, (1985) and the Brookhaven program with constants from Weiss, (1974) and Roy *et al.*, (1993).

During the Pacific Transect (SO112), surface pCO_2 was measured continuously using an equilibrator designed by Dr. Gregor Rehder,(GEOMAR- Research Center for Marine Geosciences Christian Albrecht University, Kiel, Germany). The equilibrator consisted of a 2 ℓ glass vessel through which sea water from the sea-loop was led at a rate of 3 ℓ min^{-1} resulting in a residence time for the water in the equilibrator of 40 s. Air was recirculated through the equilibrator with a counter current flow at a rate of

1.6 ℓ min^{-1}. Samples for CO_2 and CH_4 were taken from the recirculating air stream via a multiport valve and measured in a GC equipped with a FID detector. Since CO_2 is not detected by a FID detector the CO_2 in the sample was first converted to CH_4 by passing through a methanizer just upstream of the detector. To enable flux measurements, concentrations of both CH_4 and CO_2 in the air were also measured. The air sample was pumped into the lab from the forward mast at a height over the sea surface of ca 10 m. The residence time in the air line was 1 min. Air, water and two standard gases were measured sequentially. The analyses were calibrated against a gas standard containing 4 ppm CH_4 and 200 ppm CO_2. As a control a second standard gas, 10 ppm CH_4 and 503 ppm CO_2 was measured regularly. The sampling frequency was set to continuously measure air every 40 min and water every 20 min. This provided 36 air and 72 water measurements daily. The measured concentration of CO_2 was corrected for temperature difference between the equilibrator and sea water as measured at the sea loop intake in the bow of the ship.

3.1.4 δ^{13}C-Dissolved Inorganic Carbon

During the NE Pacific cruises, DIC samples were collected in 250-ml glass flasks spiked with HgCl and kept at 4 °C until extraction. The samples were extracted at the Institute of Ocean Sciences (IOS), Sidney B.C. and analyzed at the Biogeochemistry Facility, University of Victoria using the dual inlet on a Finnigan MAT 252 mass spectrometer. IOS standard-1 ($\delta^{13}C$= -1.4 °/$_{oo}$ *vs* PDB) was used as reference gas.

The precision of these measurements was ± 0.05 °/₀₀.

For the Pacific Transect, DIC samples were collected in Vacutainers. Unfortunately all attempts to analyze the samples failed. When setting out to standardize the method, it was discovered that the Vacutainers had rubber stoppers which produced/leaked small amounts of CO_2 with a $\delta^{13}C$ varying between -29 to -35 °/₀₀. This contamination, although in small amounts, was enough to make analysis impossible due to the large isotopic offset between DIC and the CO_2 emanating from the Vacutainers.

$\delta^{13}C_{DIC}$ has instead been set to a constant value of +1.5 °/₀₀, a fairly safe estimate since values of $\delta^{13}C_{DIC}$ do not vary systematically with temperature and the range in surface waters is only 0.8 °/₀₀ (Kroopnick 1985).

3.1.5 Nutrients

In the NE Pacific, hydrocast samples were analyzed on-board for nitrate/nitrite and phosphate with a Technicon Auto Analyzer following modified procedures by Barwell-Clarke and Whitney, (1996).

For the Pacific Transect on-board R/V Sonne nutrient samples were taken from the sea loop, filtered(0.2 μm pore diameter) into acid-washed glass vials and immediately frozen in a -20° freezer. Nutrient analysis from the Pacific Transect were later performed at the Institute of Ocean Sciences, Sidney B.C., using the same instrument and following the same procedures as for the samples from the NE Pacific.

3.1.6 Isotope Measurements of Alkenones

Stable carbon isotope composition of alkenones was measured on a Finnigan MAT 252 Continuous Flow Isotope Ratio Mass Spectrometer (CF-IRMS). The GC used for these samples was equipped with a cold-on-column injector (Carlo Erba adapted to a Varian 3400 GC) and a non-polar column (MDN-1: 30 m, 0.25 mm ID, 0.25 μm film thickness, SUPELCO). Co-injected standards, consisting of C_{36}, C_{38} and C_{40} n-alkanes were used as internal isotopic references (Jasper *et al.* 1994). The C_{36} and C_{40} n-alkane standards were purchased from Chiron A/S, while the C_{38} standard was prepared in the lab by off line combustion with copper oxide and measured with the dual inlet. The precision and accuracy of the analysis were determined by repeated measurements (n=12) of the C_{36} and C_{40} standards at the same conditions as during sample analysis. The precision is reported as two standard deviations ($\pm\sigma$) and the accuracy to be the deviation of the sample average from the expected value, i.e. $\delta^{13}C_{average,n=12} - \delta^{13}C_{Chiron}$. The carbon isotope composition of C_{36} was determined with a precision of $\pm 0.4^{\circ}/_{oo}$ and an accuracy of -0.07 $^{\circ}/_{oo}$, while the C_{40} n-alkane was measured with a precision of $\pm 0.7^{\circ}/_{oo}$ and the accuracy was $0.02^{\circ}/_{oo}$. This relatively low precision is likely to be caused by the high temperature at which the alkenones elute. At this temperature, 320°C, the background is higher due to column bleed; in addition the gas velocity in the column is reduced causing the C_{40} peak to "front", i.e. the peak has a asymmetric left shoulder. These chromatographic problems, together

with the difficulty of volatilizing compounds as large as C_{36} to C_{40}, lead to lower precision. The precision of the alkenone measurements may therefore be assumed to be between 0.4 and 0.7 $^{\circ}/_{\circ\circ}$ since they elute after C_{36} and before C_{40}. A conservative value of 0.55 $^{\circ}/_{\circ\circ}$ for the precision of $\delta^{13}C_{37:2}$ is adopted here.

The isotopic composition of total phytoplankton biomass δ_p, was estimated using an isotopic offset between total biomass and $C_{37:2}$-alkenone of 4 $^{\circ}/_{\circ\circ}$ (Jasper *et al.* 1994; Popp *et al.* 1998), i.e. $\delta_p = \delta_{37:2} + 4$.

3.1.7 Improved Water Trap For The CF-IRMS

Water, if not maintained at a low and constant level, can produce systematic errors during CF-IRMS analysis of stable carbon isotopes. By transferring hydrogen to CO_2 in the ion source via:

$$^{12}C^{16}O_2^+ + H_2O \rightarrow H^{12}C^{16}O_2^+ + OH \cdot \tag{3.1}$$

or related reactions, water causes changes in the 45/44 and the 46/44 ion currents (Merritt *et al.* 1995; Brand 1996). The consequences of these changes are an over-estimation of ^{13}C and a similar over-compensation in the ^{17}O correction. A quantification of water induced errors in the determination of carbon isotopes has been made by Leckrone and Hayes, (1998). They derived a general relationship between the observed error in δ and the ion-current ratio of water to CO_2.

$$error\ in\ \delta = 0.04 + 26 \cdot \frac{i18}{i44} \tag{3.2}$$

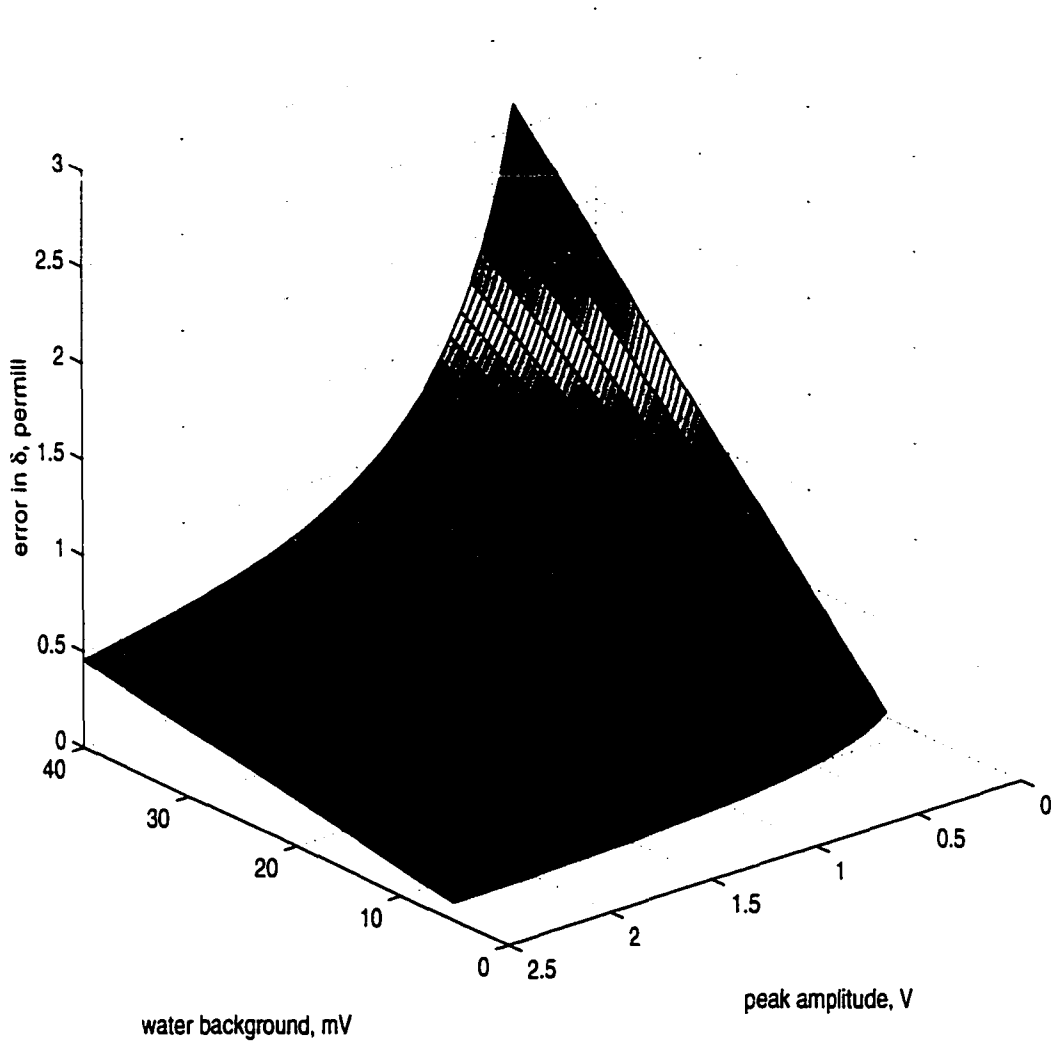

Figure 3.2: Water induced errors at different water background levels and peak amplitudes. Errors are calculated using Eq. 3.2. Peak amplitude is referred to as the mass 44 signal in cup 3. Water levels are referred to as mass 18 signal in cup 3.(Whiticar and Eek 1999)

Following this relationship, it is obvious that the water induced error increases as the background water level gets higher, but it also shows that the error is sensitive to the CO_2 signal. A weak CO_2 signal, i.e. too little material introduced into the source resulting in a small peak, will give rise to an error of larger magnitude than a more substantial peak would for the same water background (Fig. 3.2). Since the water-induced errors affects both reference and sample peaks, the effects on the observed ion current ratios are such that the systematic errors in the resulting δ value can be either positive or negative. If, for example, the reference peak and the sample peak are identical and the water background does not change, then the errors are identical and cancel out. However, if the sample peak is smaller than the reference peak, i.e. the mass 44 ion currents are different, even though the water background remains the same, then the resulting systematic error in the determination of the sample value will be positive, manifested as a heavier bias. Conversely, a sample peak which is larger than the reference peak will produce a negative error with a bias towards a lighter value. Figure 3.3 illustrates the calculated errors as a function of peak size and water background using reference peaks of 1 and 2 volts respectively.

3.1.8 Control of Water-Induced Errors

It is possible to reduce the systematic error by shortening the residence time for the charged ions in the ion source. This can be achieved by increasing the penetration of the accelerating field in the source. A shorter residence time will lead to a lower

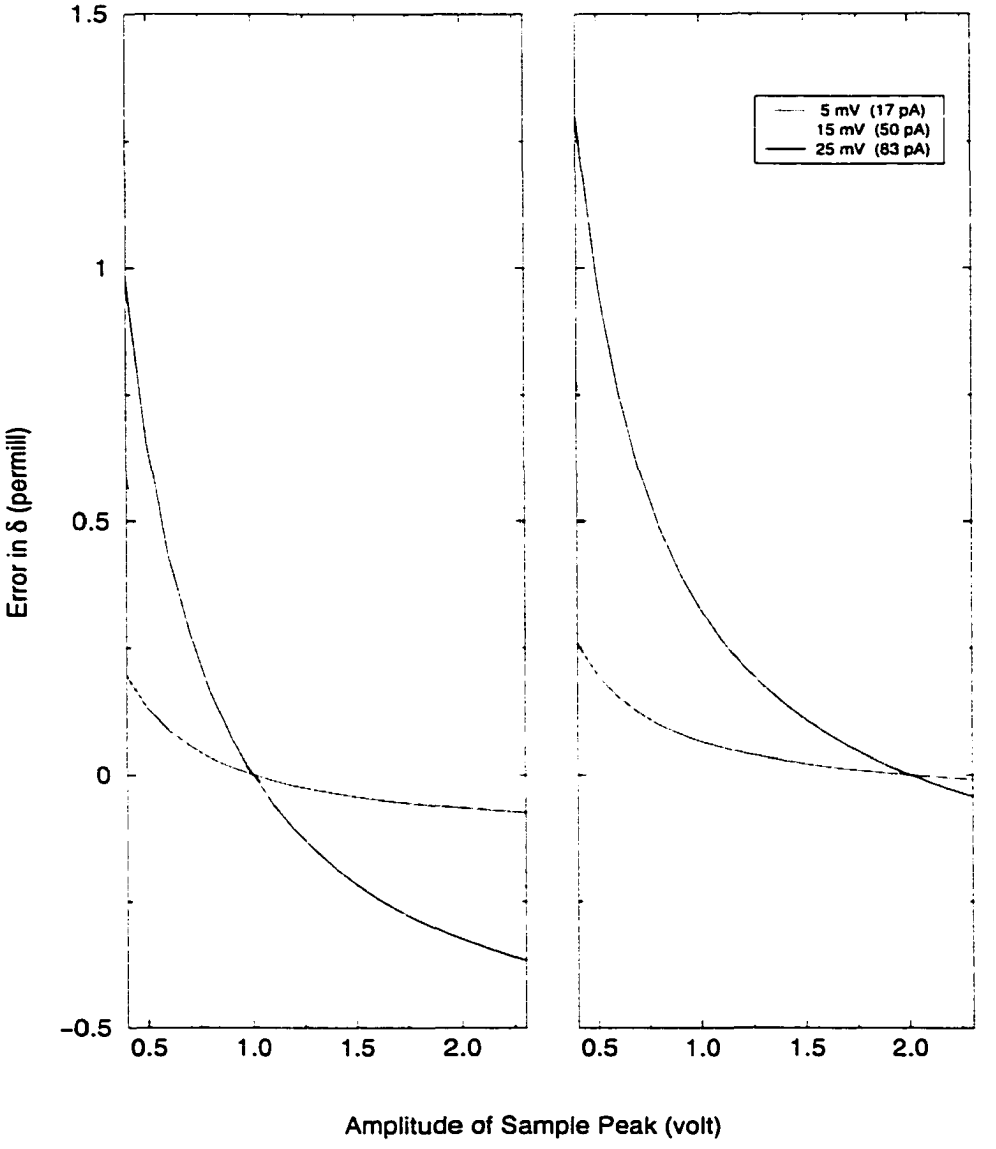

Figure 3.3: Water induced error at different background levels. Errors are calculated using a 1 Volt reference peak in the left panel and a 2 volt reference peak in the right panel. Water levels are referred to as mV signal in cup 3 or as the corresponding signal current.

number of collisions between water molecules and CO_2^+ ions, hence there will be less HCO_2^+ formed and subsequently a smaller error. In Eq. 3.2 the effect of shorter residence time is shown as a lowering the slope factor. Unfortunately, such a change in the accelerating field will decrease the sensitivity of the instrument making this approach less optimal.

While ion extraction affects the residence time for charged species in the source, it will not change the residence time for neutral molecules. The flow rate of neutral gas molecules through the ion source or source conductance can on the Finnigan 252 be changed using the Variable Ion-Source Conductance, (VISC). The VISC regulates the pressure and hence the flow rate in the source by physically closing an opening in the source housing. Leckrone and Hayes, (1998) observed that the water induced errors were only affected during the first 30 % of the VISC span after which no improvement was observed. During the analysis of the alkenones reported in this thesis the VISC was operated at 100 % open. Therefore, the best way to avoid the influence of water background without compromising the sensitivity of the instrument is to remove the water before it reaches the mass spectrometer. Water from leaks in the GC and water formed during combustion of sample molecules is removed in a water trap situated between the combustion reactor and the mass spectrometer. Ideally, this water trap should be able to keep the water entering the source at such a low level that no significant error would be induced. However, the standard water trap is

not efficient enough to completely remove the background. The type of trap used is a so called "Nafion-trap". In this trap the carrier gas is led through a thin (0.33 mm ID) tubular Nafion membrane. This membrane is a copolymer of tetrafluoroethylene (Teflon) and perfluoro3,6-dioxa-4-dimethyl-7-octene-sulfonic acid. The Nafion is mounted coaxially inside a 30 cm long, 1/4" ID stainless steel tube with reducing-tee unions. The steel tube is flushed with a counter current flow of dry helium. Water diffuses from the carrier gas through the Nafion membrane into the helium stream, leaving the carrier gas progressively drier as it passes through the length of the trap. In the system used in the Biogeochemistry Facility this trap was able to maintain the water signal at a ion current of 120 pA or 36 mV of mass 18 in cup 3 (for the corresponding errors see Fig. 3.2).

Modified water-trap

In an attempt to minimize the water induced errors in our mass spectrometer a water trap was constructed using the same Nafion tubing, but with 1/16" glass-lined stainless tubing instead of the 1/4" sheath . The small diameter combined with the glass-lining have the added advantage of keeping surface area where water can adsorb to a minimum. The trap length was increased to 60 cm, partly to increase the residence time of the carrier gas in the trap and partly to enable cooling of the downstream end of the trap. Cooling the trap will lower the vapor pressure of water in equilibrium with sorption sites within the Nafion membrane. The temperature

dependency can be expressed as (Leckrone and Hayes 1997):

$$\log P_{WN} = -\frac{3580}{T} + 10.01 \tag{3.3}$$

Residual water will remain in the gas-stream if insufficient time is allowed for water to diffuse through the membrane. An appropriate length of the trap can be calculated from (Leckrone and Hayes 1997):

$$L \geq F_c \cdot \frac{10^{3.8}}{120\,\pi\,D} \tag{3.4}$$

where L is the length of membrane in cm, F_c is the gas flow rate in ml/min and D is the diffusion coefficient of water in the carrier gas at the operating temperature, $cm^2\ s^{-1}$. For example, using the diffusion coefficient of water in helium at 25°C, 0.908 $cm^2\ s^{-1}$. (Vargaftik *et al.* 1996), Eq. 3.4 calculates a 18.5 cm trap. This trap can dry carrier gas saturated with water to $10.2 \cdot 10^{-3}$ torr. To reach a lower vapor pressure the trap must be cooled. If the trap is cooled to 0°C a 23 cm trap is needed with an equilibrium vapor pressure of $0.8 \cdot 10^{-3}$ torr, D = 0.728 $cm^2\ s^{-1}$ (Leckrone and Hayes 1997). In Fig. 3.4 the theoretical error associated with the "old" trap is compared with the errors corresponding to the water levels in the new trap cooled to -10°C with a ethyleneglycol/dry ice mixture .

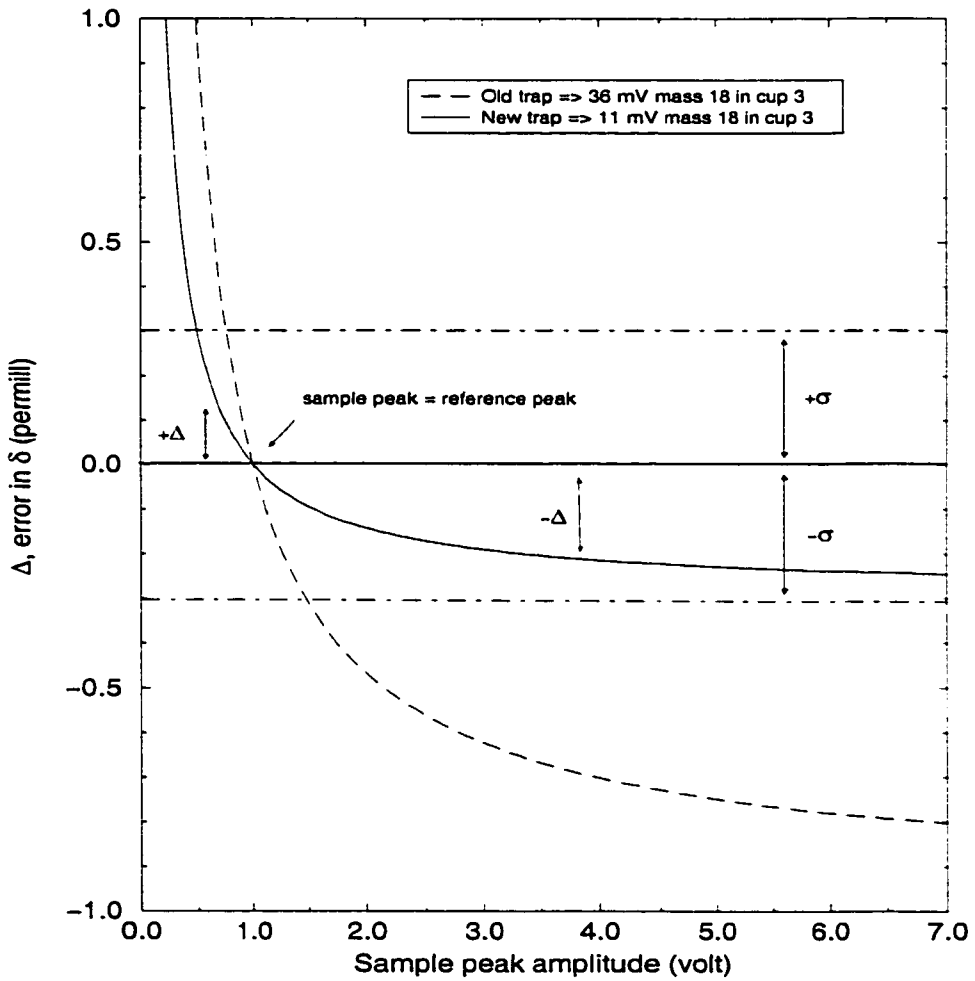

Figure 3.4: Comparison of water induced errors between "old" and "new" water trap. The expected precision ($\sigma = \pm\ 0.3\ ^{\circ}/_{oo}$) is shown for scale. Errors are calculated using a 1 Volt reference peak.

Chapter 4

Influence of Spectral Quality and Irradiance on Carbon Isotope Composition and Growth Rate in a Non-Calcifying Strain of Emiliania huxleyi

4.1 Abstract

Phytoplankton physiology is affected by light intensity and spectral quality of the incoming light. The changes in physiology are expressed as changes in the relative sizes of the different organic constituent pools. Additionally, the carbon isotope fractionation has been shown to be light dependent with a decreasing discrimination with decreasing light intensity. Presented here is an experiment aimed at understanding the effects light and spectral quality may have on growth rate and carbon isotope fractionation in a non-calcifying strain of *Emiliania huxleyi*.

4.2 Introduction

Irradiance has been shown to affect carbon isotope fractionation in cultures of calcifying *E. huxleyi* by a decreasing isotope fractionation with decreasing irradiance (Thompson and Calvert 1995). A consequence of this would be that the carbon isotope fractionation in the ocean is depth dependent, with decreasing fractionation

the deeper the algae grows. However, the conditions in these two cases cannot be compared directly, since in the water column the light environment is also affected by the light attenuation characteristics of the water. This attenuation is wavelength dependent, thus the spectral quality will change with depth. Longer wavelengths are more affected by this attenuation and the spectral quality of light that penetrates into the water column will therefore shift towards blue with depth.

Irradiance and spectral quality have been shown to change the molecular composition of phytoplankton. Rivkin (*1989*) demonstrated significant effects on chlorophyll, carbon and protein content by both irradiance and spectral quality in cultures of *Dunaliella tertiolecta* and *Thallassiosira rotula.* Irradiance also affected the relative amounts of polysaccharides and lipids in these cultures while the spectral quality had no effect on these molecular groups. However, spectral quality, specifically blue light, stimulates nitrate reductase and thereby promotes nitrate uptake. This may lead to increased demand for carbon skeleton, via β-carboxylation, and subsequently to an increased production of amino acids.

The different constituent groups that make up the biomass in phytoplankton have distinctly different isotope signatures. Lipids for example, are depleted in ^{13}C by 3 to 4 $^{\circ}/_{\circ\circ}$ relative to the total biomass while amino acids generally are more enriched in ^{13}C by 1 to 4$^{\circ}/_{\circ\circ}$ (Abelson and Hoering 1961). These light-associated effects may act to change the carbon isotope composition of phytoplankton biomass by altering

the relative sizes of the pools of different compound classes within the cells.

The results of an experiment aimed at the effects of irradiance and spectral quality on the isotopic composition of an non-calcifying strain of *Emiliania huxleyi* are discussed below.

4.3 Materials and Methods

4.3.1 Culture conditions

Cultures of a non-calcifying clone of *Emiliania huxleyi* (clone 732a NEPCC-University of British Columbia, collected and isolated from Station P in the NE Pacific) were grown in 4 replicates of 400 ml batch cultures. Culture media were made from sea water collected at Station P, sterilized by micro-waving for 10 minutes and nutrient enhanced according to Harrison *et. al.*, 1980. At the start of each treatment, the cultures were inoculated with cells corresponding to 6000 cells/ml. The inoculates were taken in exponential growth phase from cultures that had been adapted to the conditions of the specific treatment. The cells were kept suspended by gentle air bubbling. The air was passed through a 0.2 μm filter prior to entering the cultures. Cell enumeration was made by measuring light absorption at 750 nm in a spectrophotometer. A haemocytometer was used to calibrate the absorption *vs* cell density relationship. During the experiment, the culture flasks were placed in a incubator cabinet capable of controlling temperature within $\pm$ 0.3 °C. Light was

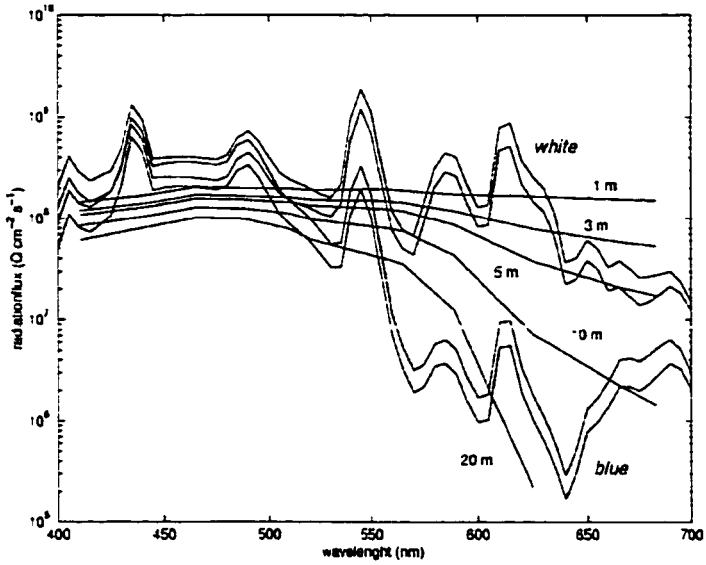

Figure 4.1: Light spectra for the two color treatments compared to field data from Bermuda (BATS). The laboratory conditions are described by to pair of curves, each pair representing the two light intensities at white and blue light respectively.

supplied from a bank of 6 fluorescent light bulbs (Coralife Trichromatic) selected to produce a light spectrum similar to that of sunlight. Light levels were controlled by placing neutral density filters in front of the light bank (Roscolux no. 298, 209) and spectral quality was changed from white to blue light by adding a blue filter (Roscolux no. 69). Light levels were calculated from radiometer measurements at the culture flask positions in the incubator cabinet (LI-1800UW Underwater Spectroradiometer, LI-COR Inc.).

A comparison of the light fields produced in this way to field measurements from the *Bermuda Time Series Experiment* (http://www.icess.ucsb.edu/bbop/bbop/

aarchive.html), shows that the white light (using only neutral density filters) corresponded to a light field at approximately 3-5 m depth while the blue light compared to a light field of approximately 20 m depth (fig. 4.1).

When changing between light colors, the photosynthetically usable radiation (PUR) incident on the culture flasks was adjusted by placing the flasks at different distances from the light source. Photosynthetically usable radiation is the fraction of radiant energy absorbed by the cells (Morel 1978; Gostan *et al.* 1986; Morel *et al.* 1987) and is defined as:

$$PUR = \int_{400nm}^{700nm} PAR(\lambda)A(\lambda)d\lambda \qquad (4.1)$$

where $PAR(\lambda)$ is the incident light field, $A(\lambda)$ is a weighted probability that a photon of a given wavelength will be absorbed by an algal cell. A was estimated by normalizing an absorption spectrum [a(λ)] with respect to its absorption maximum (a_{max}), i.e. ($A(\lambda) = \frac{a(\lambda)}{a_{max}}$ (Gostan *et al.* 1986; Morel *et al.* 1987). The absorption spectrum was obtained from measurements of intact cells filtered onto a glass fiber filter (Truper and Yentsch 1967) (fig. 4.2).

4.3.2 Sample preparation

The cultures were allowed to reach a cell density of $1 \cdot 10^6$ cells/ml at which time the cells were filtered onto pre-combusted glass fiber filters (Gelman A/E) in 100 ml batches. The filters were then kept in -20 °C until analysis. The isotopic composition

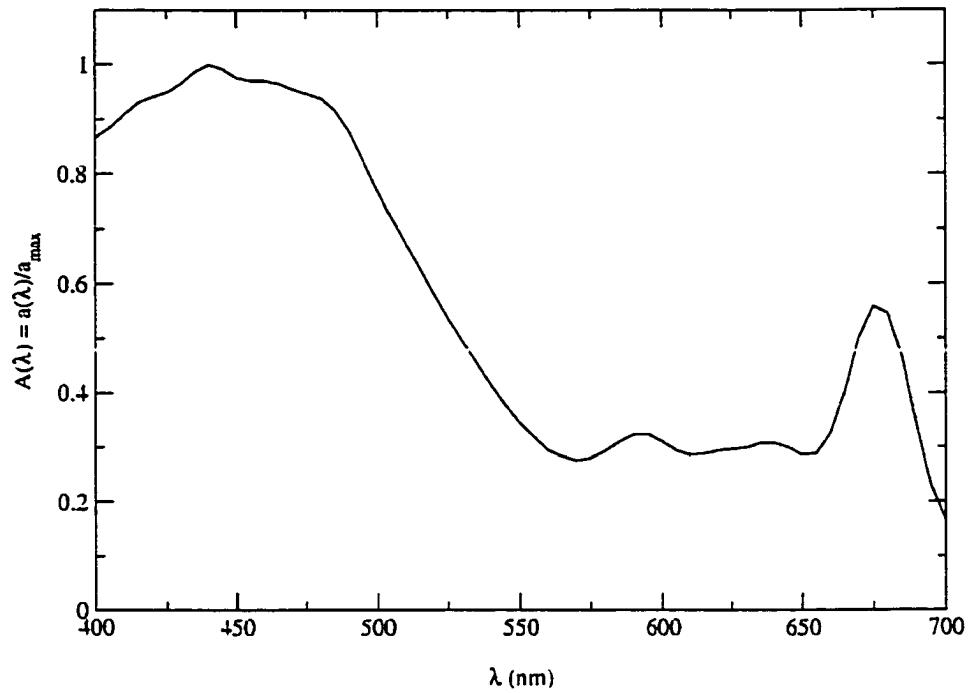

Figure 4.2: Absorption spectra of Emiliania huxleyi *obtained by measurements of intact cells filtered onto a glass fiber filter. The absorption at each wavelength was calculated as the difference between a empty filter and a filter with cells as measured in a spectrophotometer.*

of the produced biomass was measured by placing a subsample cut from one of the filters into a silver capsule and adding two to three drops of 1 N HCl to remove any traces of inorganic carbon. The capsules containing the samples were then placed in a desiccator for 3-7 days after which the isotope composition was measured using an Carlo Erba elemental analyzer online with the Finnigan MAT 252 isotope ratio mass spectrometer. Acetanilide was used as carbon isotope standard ($\delta^{13}C$ *vs* $\delta^{13}C_{PDB}$ = -30.54 °/$_{oo}$). The precision of the measurements was 0.1 °/$_{oo}$.

4.3.3 Dissolved Inorganic Carbon

At the beginning and at the end of each experiment two aliquotes of the media were collected from each replicate culture. For analysis of the carbon isotope composition of Dissolved Inorganic Carbon (DIC) 4 ml of the media were injected into a 7 ml evacuated Vacutainer via a 0.2 μm syringe filter. The Vacutainer was then kept at 4°C until analysis. To determine the concentration of total inorganic carbon (TCO_2), a second aliquote was filtered through a 0.2 μm syringe filter into a 3 ml vial. The vial was then sealed with a rubber stopper while ensuring that no air was left in the vial. This vial was also stored at 4°C until analysis. At this time the pH of the media was determined using a pH-meter. During each treatment, one of the replicate cultures was sampled every day for both DIC and Total CO_2.

4.3.4 Experimental Design

In order to study the effect of depth in the water column irradiance, spectral quality and temperature or a combined effect of the three, a 2^3-factorial design was used. In this design the two levels of spectral quality were white and blue light, temperature levels were 16°C and 8°C. The irradiance was set to a PUR level of 5.8 and 3.2 μE m^{-2} s^{-1}. The light levels were chosen, using the Photosynthesis-Irradiance (P-I) curve in Figure 4.3, so that the high value would provide a saturating amount of light while for the low level light would be limiting. The P-I curve for this clone of *E. huxleyi* was measured using the same setup as for the experiment with white light

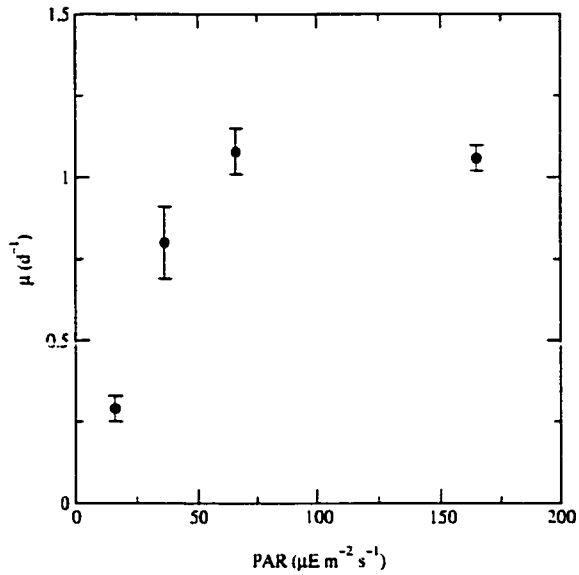

Figure 4.3: P-I curve for non-calcifying clone of Emiliania huxleyi *at 16 °C, white light.*

at 16 °C.

4.4 Results and Discussion

4.4.1 Growth rate

The resulting growth rate for the different treatments are shown in figure 4.4. Growth rates at the higher light level (PUR = 5.8 μE m^{-2} s^{-1}) were 1.1 (d^{-1}) at 16°C and 0.6 (d^{-1}) at 8°C. However, growth rate was independent of spectral quality, i.e. the same for both white and blue light. At the lower light level, PUR = 3.2 μE m^{-2} s^{-1}, blue light resulted in a lower growth rate than that in white light at both temperature levels. A statistical evaluation of the factorial design reveals that effects of all three main factors had a significant effect on growth rate (Table 4.1).

The calculated mean effects show however, that the magnitude of the effect of color is very small; -0.04 compared to the effects of irradiance and temperature of 0.12 and 0.23 respectively (Fig. 4.5).

4.4.2 Isotopic composition of organic carbon

Results from the P-I curve

Analysis of the isotope composition of bulk cellular organic carbon was made for three different light intensities. Using white light at 16 °C, decreasing light levels resulted in more ^{13}C depleted organic material. Considering that non-calcifying clones of *E. huxleyi* are only able to use dissolved CO_2 via passive diffusion as carbon source (Nimer *et al.* 1994a), an increased discrimination against ^{13}C is expected with a lower

Factor	df	Adj MS	F	p
Color	1	0.03990	29.13	0.000
Irradiance	1	0.46803	341.68	0.000
Temperature	1	1.70663	1245.90	0.000
Color*Irradiance	1	0.05528	40.36	0.000
Color*Temperature	1	0.00300	2.19	0.152
Irradiance*Temperature	1	0.08925	65.16	0.000
Color*Irradiance*Temperature	1	0.00945	6.90	0.015
error	24	0.00137		
total	31			

Table 4.1: ANOVA table for growth rate

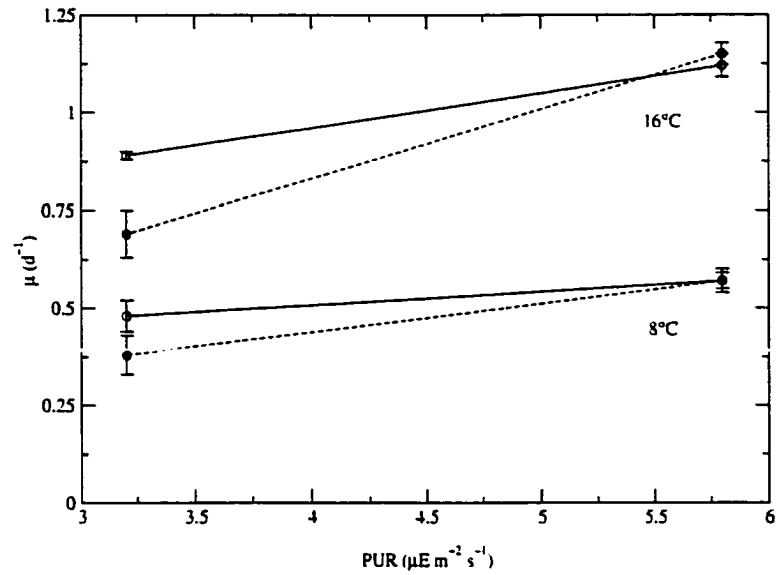

Figure 4.4: Growth rates for the different treatments in the 2^3-design. Solid circles, dashed line: blue light, open circles, solid line: white light. Top pair : 16 °C, bottom pair: 8 °C

carbon demand (Hayes 1993). However, the results of Thompson and Calvert, (1995) have an opposite sign of the slope compared to the data presented here (fig. 4.6). This may indicate that there is a difference in carbon utilization between light limited calcifying and non-calcifying cells. The non-calcifying cells are unable to use bicarbonate and are exclusively diffusive CO_2 users while the calcifying clones are able to take up bicarbonate which may be used for both calcification and photosynthesis. As has been discussed previously calcification, or more specifically an imbalance between calcification and photosynthesis, can affect the availability of CO_2 in calcifying cells and change the extent to which CO_2 is leaking out of the cells. As described later in Chapter 5, light limitation may theoretically, cause an imbalance in the Calcification/Photosynthesis ratio such that the sign of the calcifying slope shown in Fig. 4.6

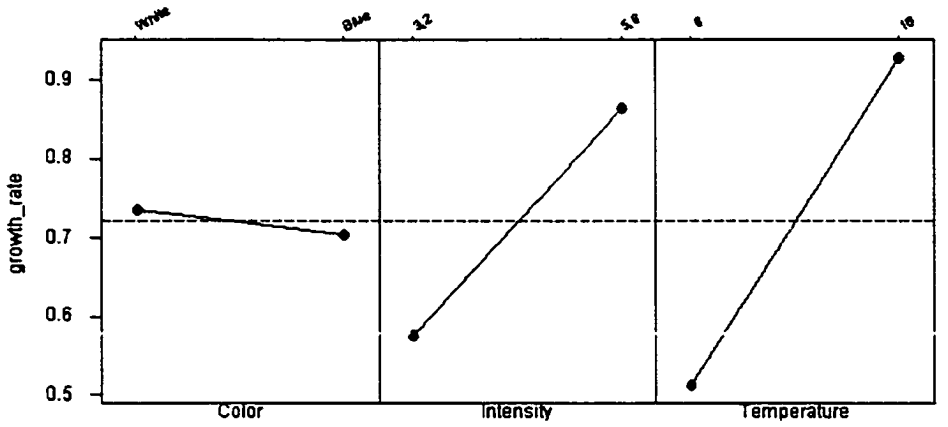

Figure 4.5: Effect of color, intensity and temperature on growth rate. The dashed line represents the overall average of the growth rate.

can be explained. These results support the view of the calcifying *Emiliania huxleyi* as a species that rely on a carbon supply different from passive uptake of dissolved CO_2.

Blue Light Experiment

Due to contamination from degassing of the rubber stoppers (see Chapter 3) all DIC and TCO_2 samples were lost. Unfortunately, without the carbon isotope composition of the dissolved CO_2 no isotope fractionation could be calculated, hence the possible influence of blue light could not be properly evaluated. However, below is an evaluation of the effect of irradiance, spectral quality and temperature on the carbon isotope composition of *Emiliania huxleyi*. The validity of these results are somewhat doubtful since it is possible that the isotope composition of the substrate (CO_2) may change during the course of the experiment. This change of isotope composition is

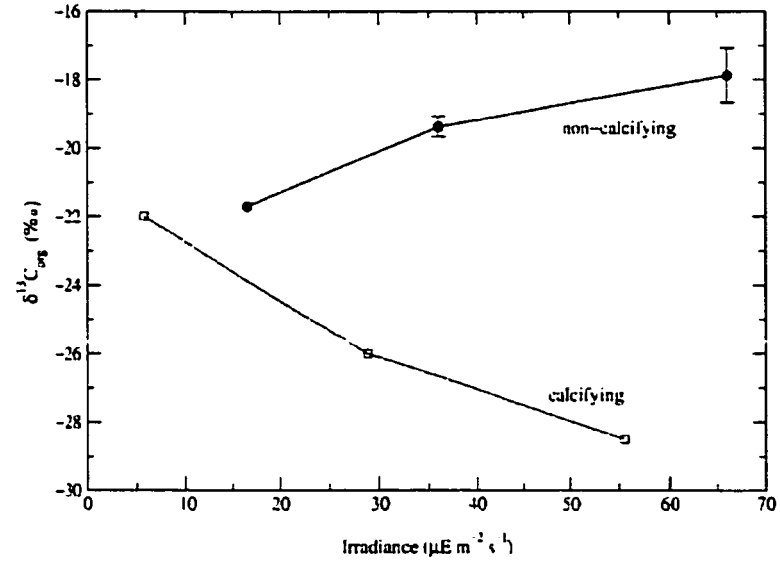

Figure 4.6: Comparison of isotope discrimination in light limited calcifying and non-calcifying clone. Filled circles: non-calcifying clone, this study. Open squares: calcifying clone, (Thompson and Calvert 1995)

caused by selective consumption of $^{12}CO_2$ by the algae, thus the remaining CO_2 in the media will become enriched in ^{13}C over time. The following evaluation is done under the assumption that the isotope composition and the concentration of dissolved CO_2 is the same for all cultures. Although, this is uncertain the media was the same for all cultures, they were all sterilized the same way and the amount of biomass produced during each experiment was approximately the same. The resulting isotope compositions of the cultures are shown in Figure 4.7. The large error-bars for the high intensity results may be a result of varying isotope composition of the dissolved CO_2. Considering the uncertainty of the combination of 8°C and high light intensity, the spectral quality appears not to have any effect.

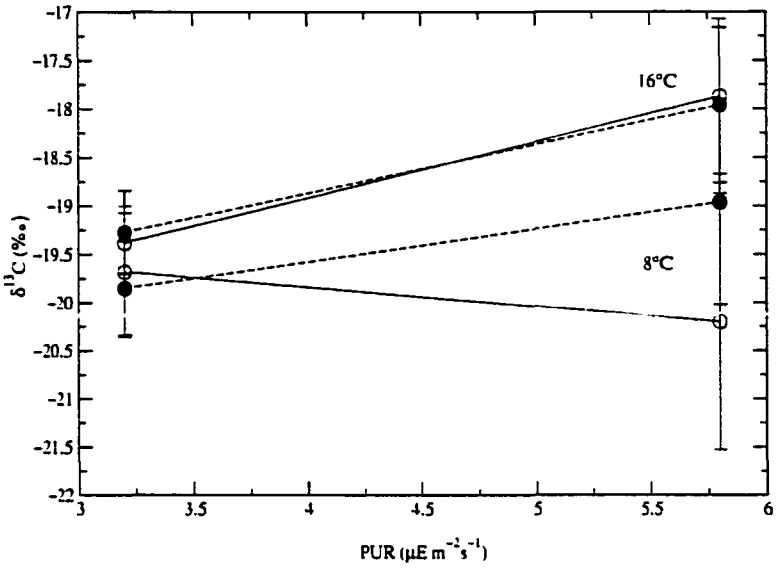

Figure 4.7: Isotope composition for the different treatments in the 2^3-design. Error-bars shown are $\pm\sigma$ for three replicate cultures. Filled circles: Blue light, Open circles: White light

Factor	df	Adj MS	F	p
Irradiance	1	3.8240	6.67	0.020
Color	1	0.4483	0.78	0.390
Temperature	1	6.6150	11.54	0.004
Color*Irradiance	1	0.5340	0.93	0.349
Irradiance*Temperature	1	2.2448	3.92	0.065
Color*Temperature	1	0.4161	0.73	0.4.7
Color*Irradiance*Temperature	1	0.9680	1.69	0.212
error	16	0.5731		
total	23			

Table 4.2: ANOVA table for $\delta^{13}C$

A test for significance of the three factors on the isotope composition of the whole cells shows that only irradiance and temperature produced significant differences between treatments (Table 4.2). The spectral quality showed no effect. This agrees with the growth rate results, where, although spectral quality had a significant effect on growth rate the magnitude of the effect was very small. Therefore, the effects on isotope composition seen in this experiment may be attributed to a primary effect on growth rate. Thus, parameters that affect the growth rate significantly will also affect the carbon isotope composition. Based on this assumption, it can be implied that spectral quality does not influence carbon isotope fractionation. Hence, any possible shift in carbon flow within the cell due to a blue light induced stimulation of nitrate reductase appears not to affect the isotope composition of the cell.

4.5 Conclusion

These results indicate that spectral quality appears to have a very modest effect on the growth rate in non-calcifying *Emiliania huxleyi*. In this experiment growth rate was mainly controlled by temperature and light intensity. The carbon isotope results imply, although the interpretation is hampered by the lack of $\delta^{13}C_{DIC}$, that the spectral quality does not affect the isotope composition either.

The contrasting slopes between the non-calcifying clone in this experiment and the calcifying clone of Thompson and Calvert, (1995) suggest that *E. huxleyi* should not

be considered as an alga relying solely on diffusive uptake of CO_2 but rather a complex carbon supply controlled by calcification and the factors affecting the calcification to photosynthesis ratio.

Chapter 5

Line P, North East Pacific, CJGOFS: Influence of Environmental parameters on Carbon Isotope Composition of Alkenones

5.1 Abstract

Isotope fractionation by Prymnesiophyte algae was determined in samples of marine particulate organic material collected by MULVFS pumps during three CJGOFS cruises on board R/V *Tully* along Line P in the North East Pacific. Carbon isotope fractionation associated with photosynthetic carbon uptake within the euphotic zone is calculated from $^{13}C/^{12}C$ ratios of dissolved carbon dioxide and the $C_{37:2}$ alkenone, a biomarker originating from Prymnesiophyte algae. The use of the MULVFS pumps enabled the determination of depth profiles of alkenone isotope composition from simultaneously collected POM samples within the top 900 m of the water column. Profiles from seven stations, separated both spatially and temporarily are reported.

The profiles demonstrate a larger variability in $\delta^{13}C_{37:2}$-alkenone from samples taken within the euphotic zone than samples taken at depth. The isotope composition of alkenones are generally depleted in ^{13}C at the surface relative the bottom of the euphotic zone, while in two deep profiles the isotope composition returned to more ^{13}C depleted values below 200 m. These results indicate that the variability in isotope

fractionation by Prymnesiophyte algae seen in field samples is affected by their vertical position within the euphotic zone. The availability of light is therefore suggested to play an important role in the control of isotope fractionation. A mechanism for this control is suggested, where light affects the ratio of calcification to photosynthesis which in turn regulates the intra-cellular CO_2 concentration via the cytosolic pH. The carbon isotope fractionation is then a function of the direction and magnitude of CO_2 diffusion in or out of the cell. In addition to investigating changes in isotope composition with depth, a possible relationship between nutrient availability and carbon isotope fractionation was also studied. The results show a linear relationship between carbon isotope fractionation and concentration of phosphate normalized to dissolved CO_2. Based on this relationship, fractionation increases as the ratio of dissolved phosphate to CO_2 decreases. This is in agreement with data presented previously by Bidigare *et al.*, (1997). However, the results presented in this chapter show that the relationship between carbon isotope fractionation and PO_4/CO_2 breaks down when the dissolved nitrate is depleted. Under these circumstances the carbon isotope fractionation is much lower than predicted by the concentration of phosphate and CO_2, and a biomass which is more enriched in ^{13}C is produced.

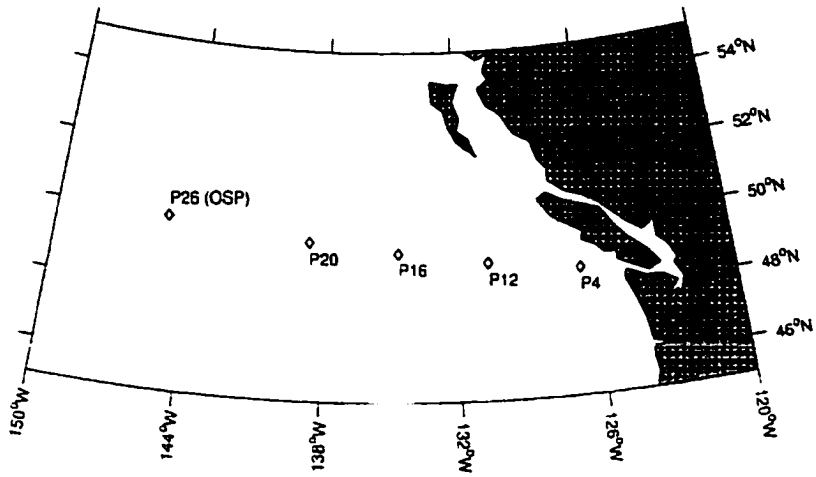

Figure 5.1: Map of Line P off Vancouver Island, North East Pacific

5.2 Introduction

During 1996 and 1997 CJGOFS (Canadian component of the Joint Global Ocean Flux Study) conducted a series of cruises along line P in the North-East Pacific. These cruises gave an opportunity to study carbon isotope fractionation by Prymnesiophyte algae in the field. The goal was to gain understanding of the control exerted by the environment on the carbon isotope fractionation. Environmental factors that were considered were availability of CO_2 and nutrients (phosphate, nitrate), vertical position in the water column and irradiance.

Line P is a 1500 km long oceanographic section between Ocean Station Papa, (50°N, 145°W) and the southern tip of Vancouver Island (Fig. 5.1). Near the coast, Line P stretches over approximately 100 km of continental shelf and a similar distance over the continental slope. The average depth along the line is about 3000 m. Station

PAPA is situated at the offshore end of the line, approximately where the Sub-Arctic Current splits to form the pole-ward-flowing Alaska Current and the equator-ward-flowing California Current. Line P intercepts the Alaska Current and the flow across the line is that of, or at least a part of, the Alaska Current. Basic open-ocean oceanographic characteristics of the water prevail from station P26 to about 500 km from the coast, and coastal features are apparent only over the 200 km of continental slope and shelf (Tabata 1991). A dominant feature along the whole line is a strong year round salinity stratification of the upper 100 m (Bishop *et al.* 1999).

These cruises provided a sample set representing three different seasons - spring, summer and winter at five different locations (Fig. 5.1); three in-shore stations, P4, P12 and P16, which are characterized by spring and late summer phytoplankton blooms dominated by diatoms and two offshore stations, P20 and P26, featuring low biomass dominated by small phytoplankton. The spatial and temporal distribution of the sample stations resulted in a variety of observed environmental conditions. Dissolved carbon dioxide varied between 17.5 and 12.6 μmol/kg, phosphate from 0.33 to 2.2 μmol/kg and nitrate showed values between 0 and 9 μmol/kg. Nutrient concentrations tended to be higher in February and May than in August, consistent with both a lower primary production rate and convective mixing resulting from surface cooling facilitated by wind driven stirring during the winter months. Mixed layer depth also changed with season from 50-100 m during winter to about 20 m for all

stations in late summer.

5.3 Results

At Station P12 in May 1996. nutrients were well mixed down to approximately 60 m. Although not showing up in the nutrient profiles, a thermal stratification was super-imposed at shallower depths, (Fig.5.2). The thermal surface layer was only 10 m deep and likely to have been formed shortly before the station was occupied since the concentrations of nutrients at the surface were unaffected. The nutrient state at this station was moderate, within the top 60 m nitrate was 3.9 μmol kg^{-1} and phosphate 0.7 μmol kg^{-1}. The estimated concentration of dissolved CO_2 was 15.2 μmol kg^{-1} along with silica values of 7 μmol kg^{-1}. Isotopic composition of alkenones, was almost constant within the top 135 m at $\delta^{13}C_{pdb}$ = -24 $^{\circ}/_{\circ\circ}$ with the exception of the surface sample at 10 m which was almost 1$^{\circ}/_{\circ\circ}$ depleted in ^{13}C ($\delta^{13}C_{pdb}$ = -24.7 $^{\circ}/_{\circ\circ}$) than the deeper samples (Fig. 5.2).

Further west at Station P16 in May 1996, the mixed layer was slightly deeper at approximately 80 m with no sign of any recent thermal stratification, (Fig. 5.3). Nutrient concentrations were higher, concentrations of nitrate and phosphate were 7 and 0.9 μmol kg^{-1} respectively. Silica had a value of 9 μmol kg^{-1} within the mixed layer and CO_2 was high at 15.9 μmol kg^{-1}. The carbon isotope values of

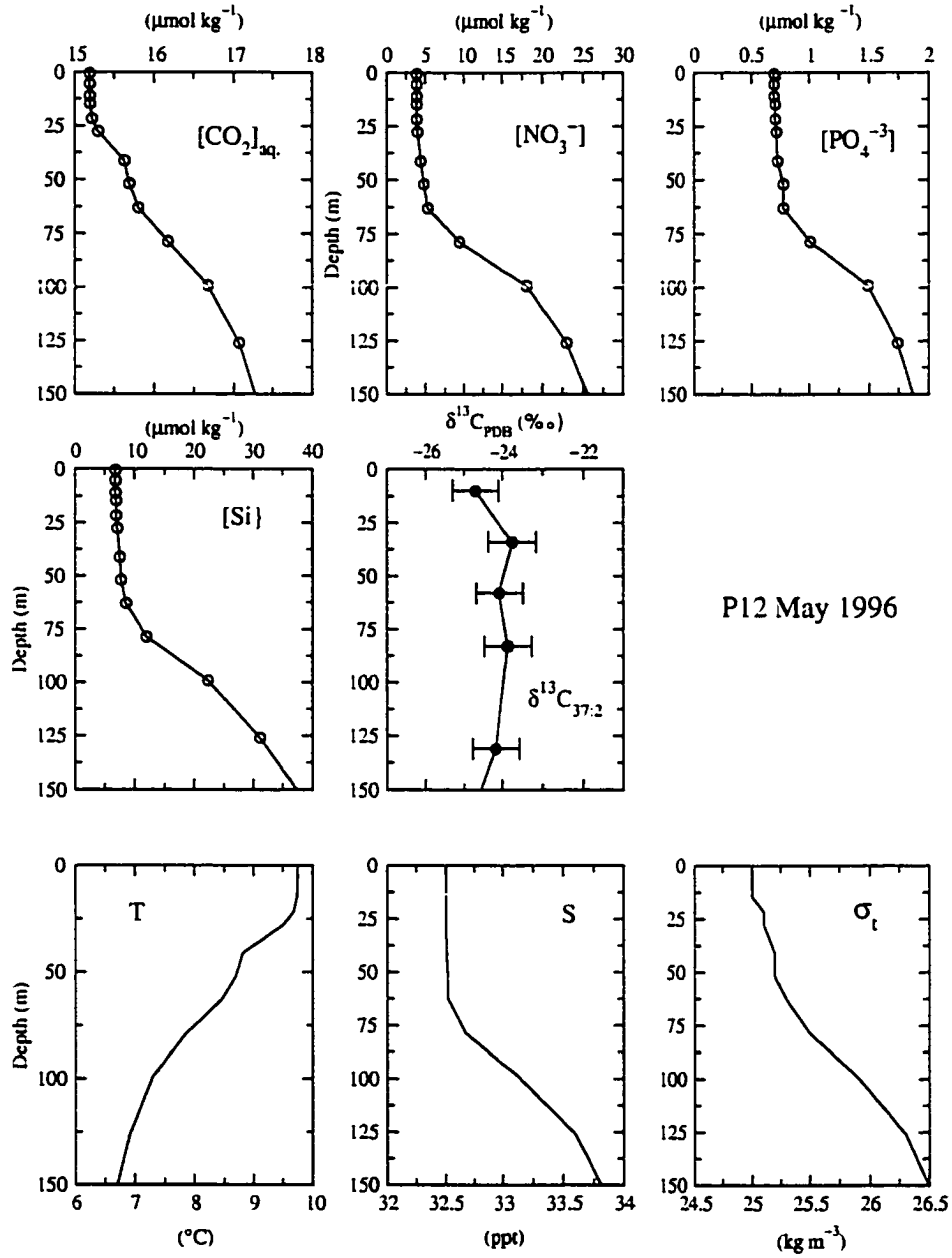

Figure 5.2: Station P12 in May 1996. Environmental parameters and carbon isotope composition of $C_{37:2}$-alkenone as a function of depth. Error bars show the precision of the isotope measurements (± 0.6‰).

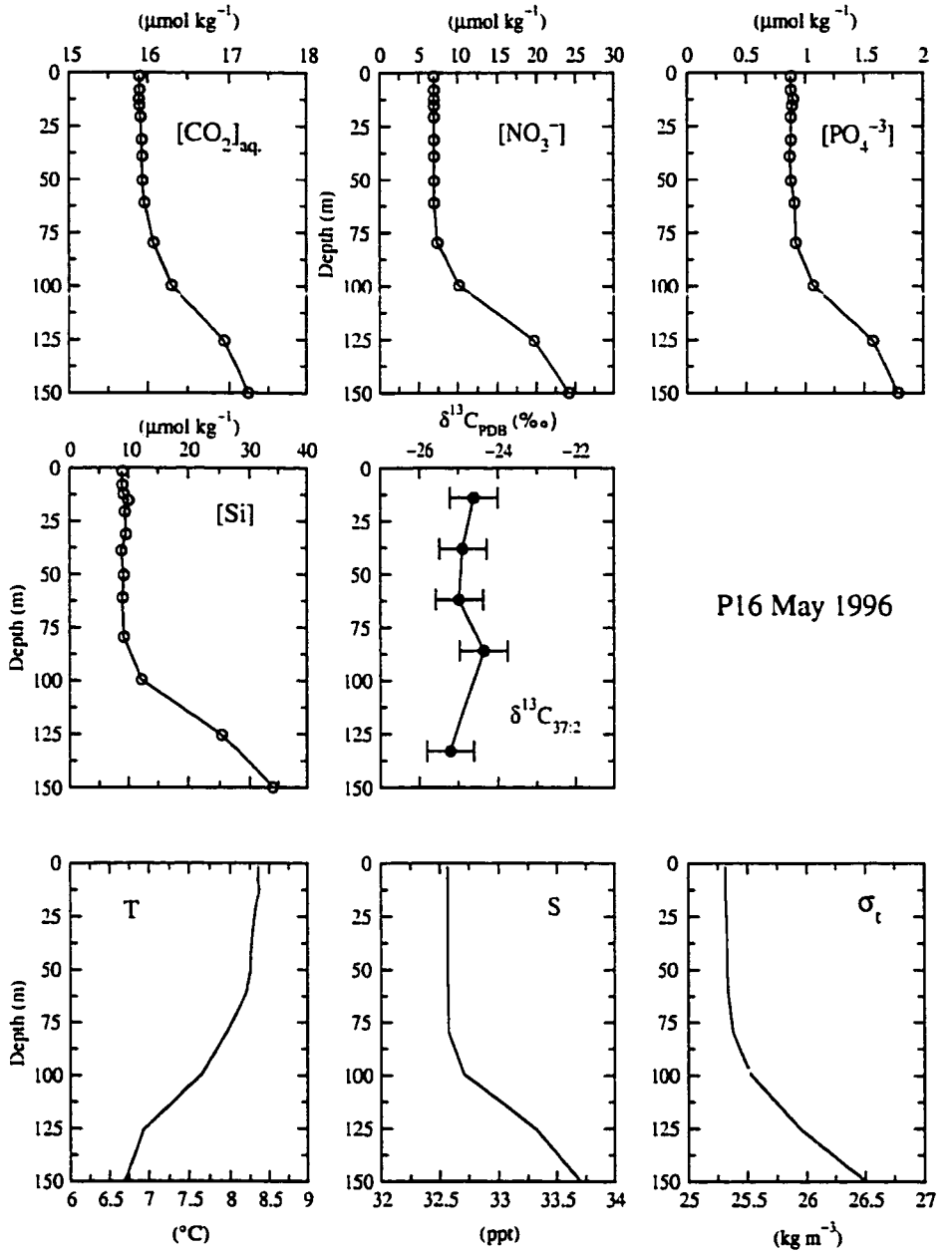

Figure 5.3: Station P16 in May 1996. Environmental parameters and carbon isotope composition of $C_{37:2}$-alkenone as a function of depth. Error bars show the precision of the isotope measurements (± 0.6°/$_{oo}$).

$C_{37:2}$-alkenone varied very little even here, but with a trend towards lighter values with depth: $\delta^{13}C_{pdb}$= -24.6 °/₀₀ at the surface and $\delta^{13}C_{pdb}$= -25.2 °/₀₀ at 133 m. The sample at 86 m deviates from the trend by showing the most ^{13}C enriched value within the profile of $\delta^{13}C_{pdb}$= -24.4 °/₀₀.

Station P20 in May 1996 had a mixed layer of 50 m with a hint of thermal stratification within the top 30 m. Nutrient and CO_2 levels were the highest of all of the May stations (Fig.5.4). Nitrate and phosphate in the mixed layer were 9.0 and 1.0 μmol kg^{-1} respectively and dissolved CO_2 was 16.4 μmol kg^{-1}. Silica was consistent with nitrate and phosphate at 11 μmol kg^{-1} throughout the mixed layer. $\delta^{13}C_{37:2}$-alkenone showed little variation with depth (-25 to -24.3 °/₀₀), except at 85 m depth where the value again was enriched in ^{13}C ($\delta^{13}C$=-23.4 °/₀₀).

While depth profiles of nutrient concentrations and temperature at Station P4 in August show quite dramatic changes with depth, the isotopic composition of the alkenones was strikingly constant (Fig. 5.5). Values varied only 0.7 °/₀₀ with the more ^{13}C depleted values found at depth. The mixed layer was shallow at 15 m with nitrate values reaching 0 between 5 and 10 meters depth and phosphate values at a constant 0.33 μmol kg^{-1}. The silica profile showed a minima coinciding with the nitrate minimum between 5 and 10 m suggesting that the presence of diatoms was responsible for the drawdown of nitrate.

Station P12 in August had a well developed stratification with the thermocline,

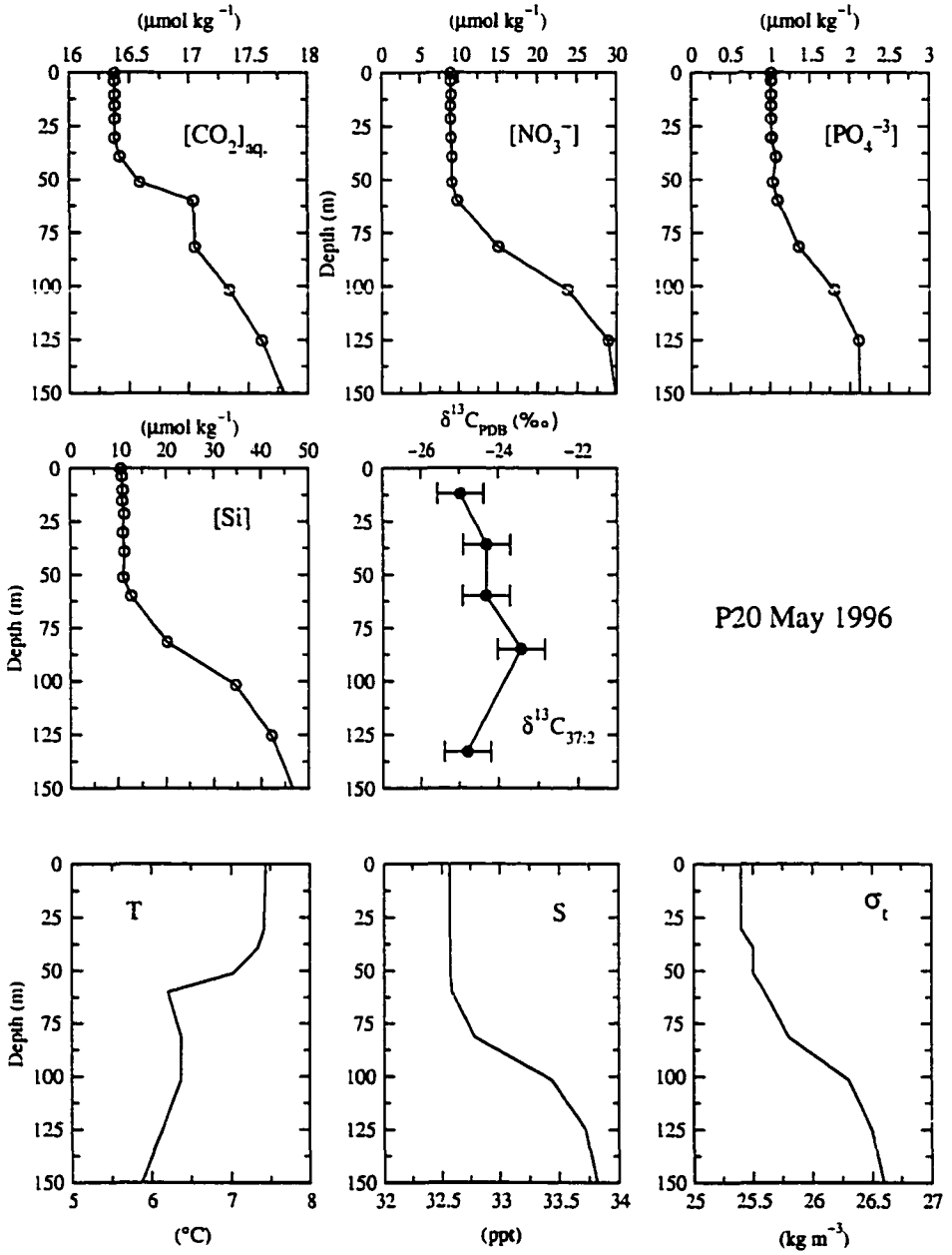

Figure 5.4: Station P20 in May 1996. Environmental parameters and carbon isotope composition of $C_{37:2}$-alkenone as a function of depth. Error bars show the precision of the isotope measurements (± 0.6°/$_{oo}$).

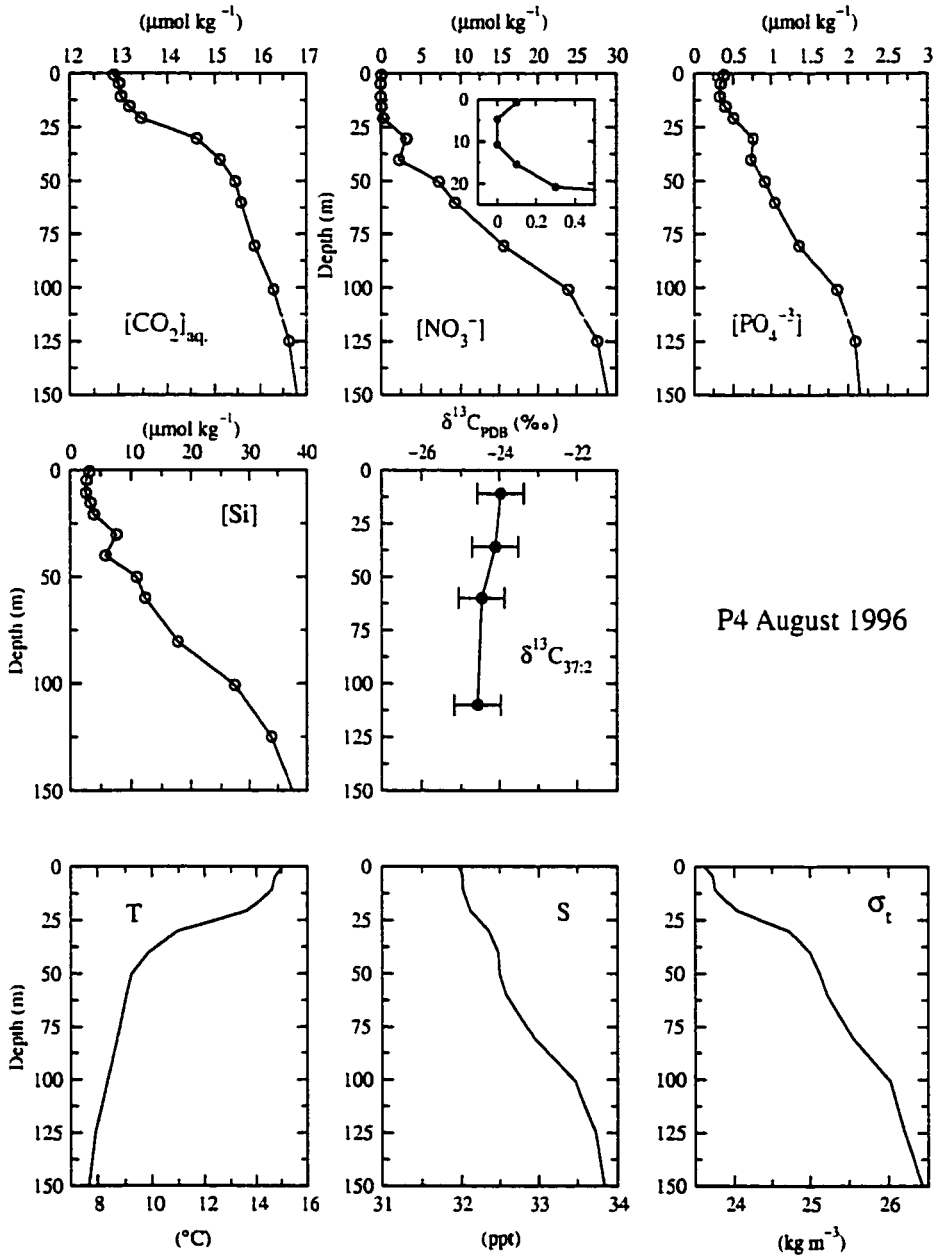

Figure 5.5: Station P4 in August 1996. Environmental parameters and carbon isotope composition of $C_{37:2}$-alkenone as a function of depth. Error bars show the precision of the isotope measurements (± 0.6‰). The insert in the nitrate graph shows the surface minima between 5-10 m depth.

halocline and the pycnocline all coinciding at about 20 m depth (fig. 5.6). Nitrate was completely depleted within the surface layer along with a depletion of silica, which reached a minimum of 1 μmol kg^{-1} just below the mixed layer. Phosphate levels were also low, 0.33 μmol kg^{-1} within the top 20 m. Dissolved CO_2 showed values of 12.6 μmol kg^{-1}. At this station the carbon isotope value of the $C_{37:2}$-alkenone in the 11 m sample, was more than 2 °/$_{oo}$ depleted in ^{13}C ($\delta^{13}C$=-26.3 °/$_{oo}$) relative to samples taken between 36 and 134 m. These samples had an almost constant value of $\delta^{13}C_{37:2}$ between -24.4 and -23.9 °/$_{oo}$.

At Ocean Station Papa (P26) in August 1996, the carbon isotope values of $C_{37:2}$-alkenones were quite different relative to the other stations. Within the top 80 m the values were more enriched in ^{13}C than those seen at the other stations; values for $\delta^{13}C_{37:2}$ varied between -22.3 and -21.7 °/$_{oo}$. At 134 m the value became more depleted in ^{13}C with $\delta^{13}C$ = -23.8 °/$_{oo}$, a value similar to previous stations. The oceanography at this station was similar to station P12, with a shallow mixed layer of about 20 m. Both the thermocline and pycnocline indicated a mature stratification, although the salinity profile still showed the permanent halocline at approximately 80 meters depth. Nutrients were present in relatively high concentrations in spite of the shallow mixed layer, with nitrate values of 7.5 and a phosphate concentration of 0.9 μmol kg^{-1}. Estimates of dissolved CO_2 values were slightly higher than station P12 at 13.7 μmol kg^{-1} while silica was much higher at 13.6 μmol kg^{-1}.

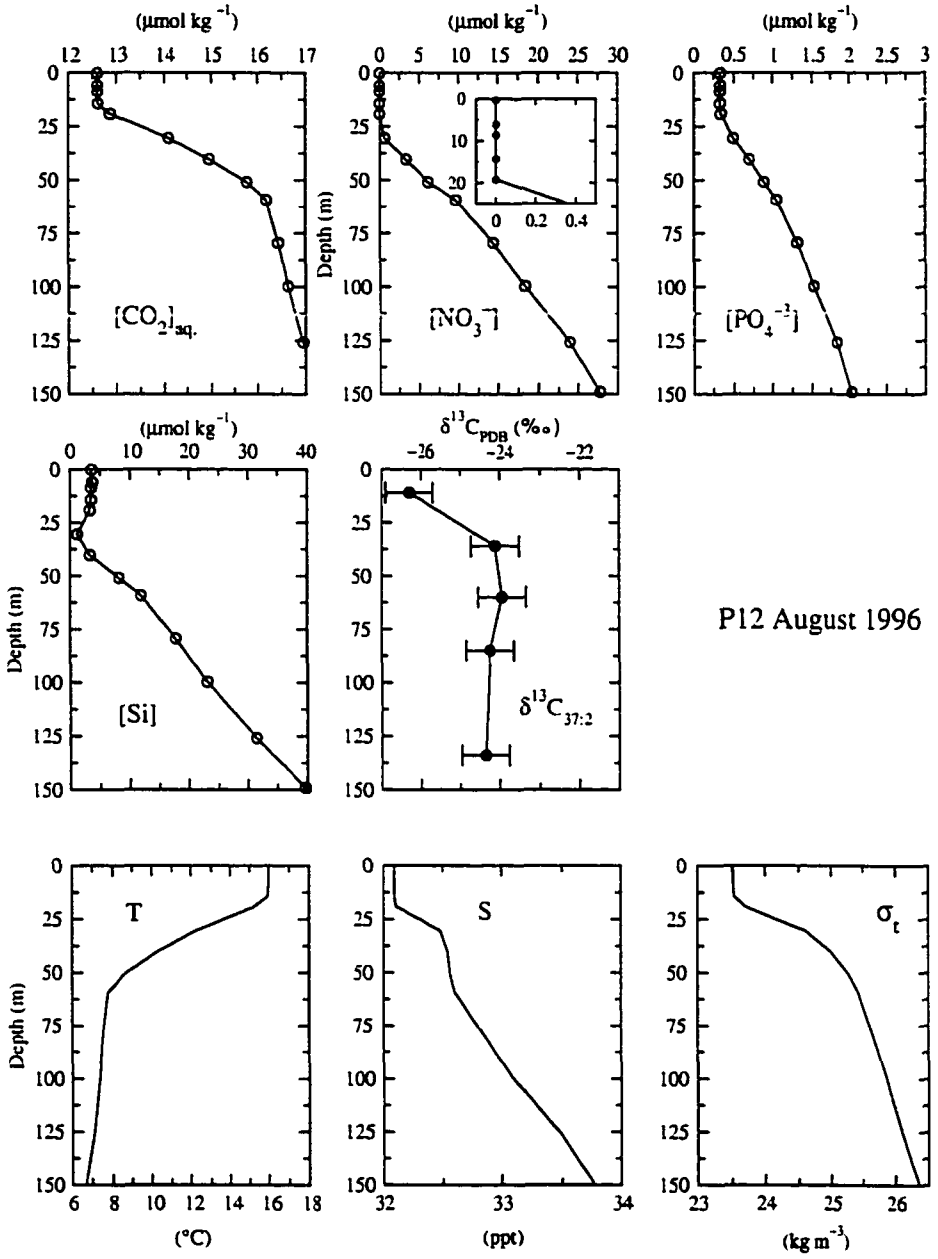

Figure 5.6: Station P12 in August 1996. Environmental parameters and carbon isotope composition of $C_{37:2}$-alkenone as a function of depth. Error bars show the precision of the isotope measurements (± 0.6‰). The insert in the nitrate graph shows the top 25 m at with different scale.

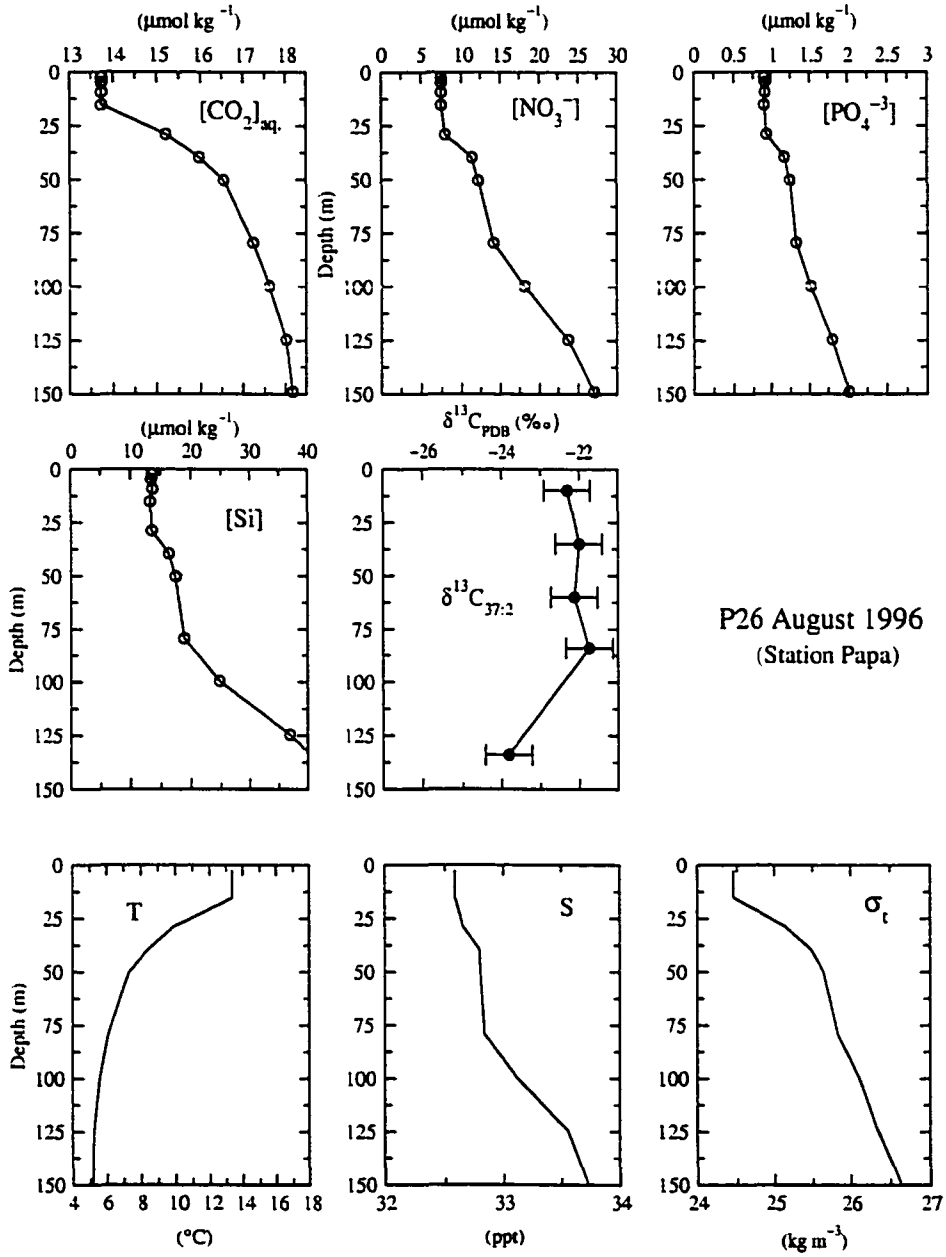

Figure 5.7: Station P26 (Station Papa) in August 1996. Environmental parameters and carbon isotope composition of $C_{37:2}$-alkenone as a function of depth. Error bars show the precision of the isotope measurements (± 0.6‰).

The last station reported here is Station P12 occupied in February 1997. As this was a winter station a deep stratification was observed, with the pycnocline at about 100 m (fig. 5.8). Nutrient values were relatively high with nitrate at 5.9 μmol kg^{-1} and phosphate and silica at 0.8 and 8.5 μmol kg^{-1} respectively. Estimated CO_2 was 15.8 μmol kg^{-1}. Alkenone isotope values at this station resembled the values in August with the surface sample being δ^{13}C = -26.5 $^{\circ}/_{oo}$ and the deeper samples about a permil enriched in ^{13}C. The deeper values differ relative to the August values by one permil, -25 $^{\circ}/_{oo}$ instead of -24 $^{\circ}/_{oo}$. However, the deepest sample at 134 m was again similar to all the previous stations at δ^{13}C = -23.8 $^{\circ}/_{oo}$.

Isotope composition of dissolved inorganic carbon from the surface is shown in Table 5.1. At three stations profiles of $\delta^{13}C_{DIC}$ samples were collected, the resulting isotope profiles are shown in Figure 5.9. Surface samples from three additional stations (P4 in May 1996, P16 in August 1996 and P4 in February 1997) were also measured. The isotope composition of the $C_{37:2}$-alkenones for these stations are shown in Table 5.1 along with carbon data for all surface samples. In Table 5.2 a similar compilation is made for samples from the bottom of the euphotic zone.

5.3.1 Light Conditions

The depth of the euphotic zone was measured for each station with either a LiCOr 2-pi sensor (calibrated using external standards) or a factory calibrated Biospherical instruments INF-300 integrating natural fluorometer and a 4-pi PAR sensor. Light

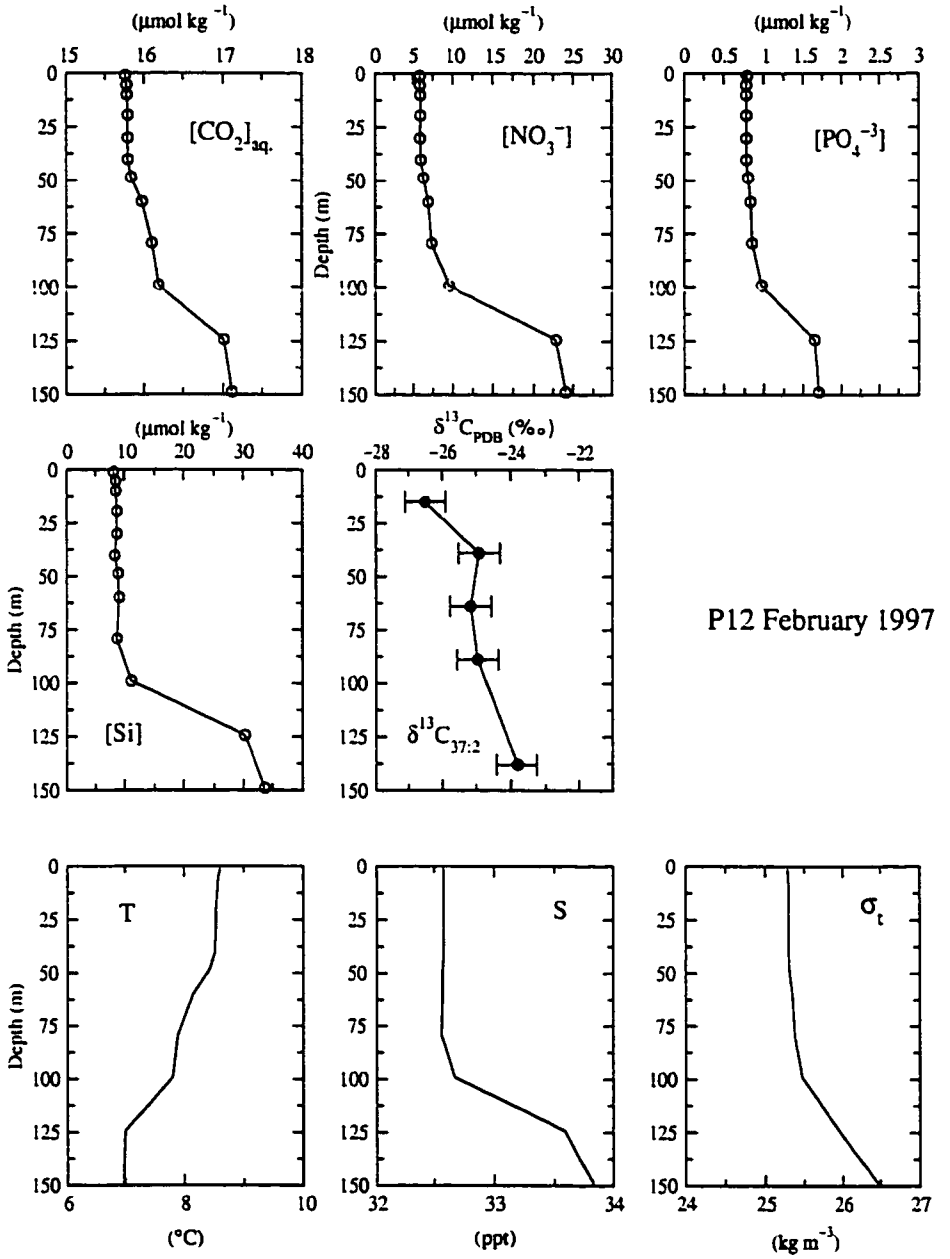

Figure 5.8: Station P12 in February 1997. Environmental parameters and carbon isotope composition of $C_{37:2}$-alkenone as a function of depth. Error bars show the precision of the isotope measurements (± 0.6 °/₀₀).

Station	Depth	Temp.	Salinity	PO_4^{3-}	NO_2^-, NO_3^-	SiO_4	Alk.	ΣCO_2	C_e	$\delta^{13}C_{DIC}$	$\delta^{13}C_e$	$\delta^{13}C_{37:2}$	ϵ_p
	(m)	(°C)	(ppt)	μmol/kg	μmol/kg	μmol/kg	μeq./kg	μmol/kg	μmol/kg	°/₀₀	°/₀₀	°/₀₀	
P4 May 1996	15	10.3	31.27	0.48	1.9	8.6	2343	2126	14.7	1.4	-8.0	-23.8	12.1
P4 August 1996	11	14.6	32.02	0.34	0	2.6	2330	2081	13.1	1.3	-7.6	-24.0	12.7
P4 February 1997	14	8.3	32.44	0.92	7.9	11.1	2348	2146	15.9	0.9	-8.6	-24.7	12.3
P12 May 1996	10	9.8	32.51	0. 70	3.9	6.9	2344	2131	15.2	1.7	-7.7	-24.7	13.3
P12 August 1996	11	16.0	32.10	0.33	0	3.5	2327	2067	12.6	1.5	-7.1	-26.3	15.5
P12 February 1997	15	8.6	31.58	0.78	5.9	8.5	2348	2141	15.5	1.3	8.3	26.5	14.5
P16 May 1996	11	8.4	32.57	0.9	7.0	9.2	2348	2146	15.9	1.3	-8.3	-24.6	12.6
P16 August 1996	10	14.8	32.35	0.37	0	1.5	2330	2079	13.1	1.5	-7.3	-23.6	12.6
P20 May 1996	12	7.7	32.56	1.02	9.0	11.0	2350	2153	16.2	1.6	-8.1	-25.0	13.2
P26 August 1996	10	13.4	32.59	0.92	7.5	13.7	2334	2094	13.7	1.6	-7.4	-22.4	11.2

Table 5.1: Environmental and isotope data for the surface samples. The estimated error in ϵ_p *is* $\pm\sqrt{\sigma^2_{DIC} + \sigma^2_{37:2}}$=0.552≈0.6. *Note that the carbon data except* $\delta^{13}C_{DIC}$ *are estimates based on the temperature relationship between total alkalinity,* ΣCO_2 *and temperature (Kroopnick 1985).*

Station	Depth	Temp.	Salinity	PO_4^{3-}	NO_2^-, NO_3^-	SiO_4	Alk.	ΣCO_2	C_c	$\delta^{13}C_{DIC}$	$\delta^{13}C_c$	$\delta^{13}C_{37:2}$	ε_p
	(m)	(°C)	(ppt)	μmol/kg	μmol/kg	μmol/kg	μeq./kg	μmol/kg	μmol/kg	°/oo	°/oo	°/oo	
P4 August 1996	36	10.3	32.42	0.74	2.7	6.6	2342	2126	14.9	1.2	-8.1	-24.1	12.2
P12 May 1996	58	8.6	32.52	0.78	5.1	8.2	2347	2144	15.8	1.2	-8.4	-24.1	12.0
P12 August 1996	36	11.1	32.52	0.61	2.2	2.4	2340	2118	14.6	1.2	-8.0	-24.1	12.3
P12 February 1997	61	8.2	32.56	0.88	6.5	8.6	2349	2148	15.9	1.2	-8.4	-25.2	13.1
P16 May 1996	38	8.3	32.57	0.9	7.0	8.8	2348	2146	15.9	1.2	-8.4	-24.9	12.8
P20 May 1996	36	7.4	32.57	1.06	9.2	11.1	2351	2157	16.4	1.2	-8.5	-24.3	12.1
P26 August 1996	35	9.0	32.73	1.07	9.9	15.1	2346	2139	15.6	1.2	-8.3	-22.1	9.9

Table 5.2: Environmental and isotope data for the 1% I_0 samples. ε_p refers to fractionation relative CO_2, which isotope composition calculated using a constant $\delta^{13}C_{DIC}$ of 1.2 °/oo. The estimated error in ε_p is $\pm\sqrt{\sigma^2_{DIC} + \sigma^2_{37:2}}$=0.552≈0.6. Note that the carbon data are estimates based on the temperature relationship between total alkalinity, ΣCO_2 and temperature (Kroopnick 1985).

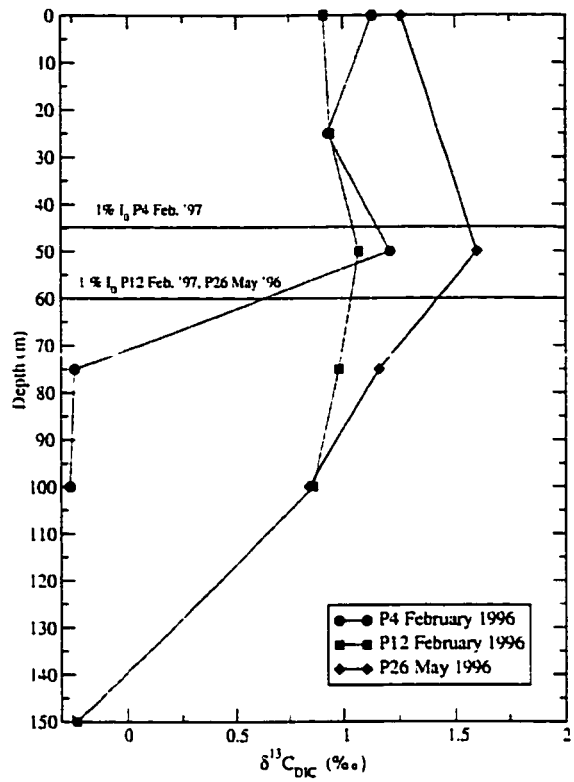

Figure 5.9: Depth profiles of $\delta^{13}C_{DIC}$, used to estimate $\delta^{13}C_{DIC}$ at the bottom of the euphotic zone.

profiles were measured midday the day of sampling (Boyd and Harrison 1999). The depth of both the euphotic zone and the mixed layer are shown in Table 5.3.1. Also shown are the cruise averages of PAR as measured on deck.

5.3.2 SEM micrographs

Attached to the side of each MULVFS pump was a sub-micron filter manifold. One of the filter holders held a 3M-Empore absorption disk for dissolved organic material. To prevent particles from reaching the absorption disk a 1 μm polycarbonate filter

Station	Mixed layer depth (m)	Depth of euphotic zone 1% I_0 (m)	Average PAR $\mu E\ m^{-2}\ s^{-1}$
P12 May '96	10	60	583
P16 May '96	80	40	583
P20 May '96	30	35	583
P4 August '96	15	30	391
P12 August '96	20	40	391
P26 August '96	15	40	391
P12 February '97	40	60	254

Table 5.3: Depth of mixed layer and euphotic zone along Line P

was used. The flow through the "sub-micron" setup was much less than the main MULVFS filters resulting in a moderate accumulation of material on the filters. This made it possible to use the filters directly for Scanning Electron Microscopy, without any preparations except gold sputtering.

The first sample is from 11 m, (Fig. 5.10) and in Panel A the presence of *Gephyrocapsa oceanica*, a alkenone producing species other than *E.huxleyi* is confirmed (Volkman *et al.* 1995). The isotope fractionation in *G. oceanica* have not been tested and may differ from *E. huxleyi* as do their U_{37}^K index* (Volkman *et al.* 1995). In the next panel an intact *E. huxleyi* cell is shown along with many detached coccoliths. A broken coccosphere in the lower right corner seems to consist of two layers

*$U_{37}^K = \frac{[C_{37:2}]}{[C_{37:2}]+[C_{37:3}]}$

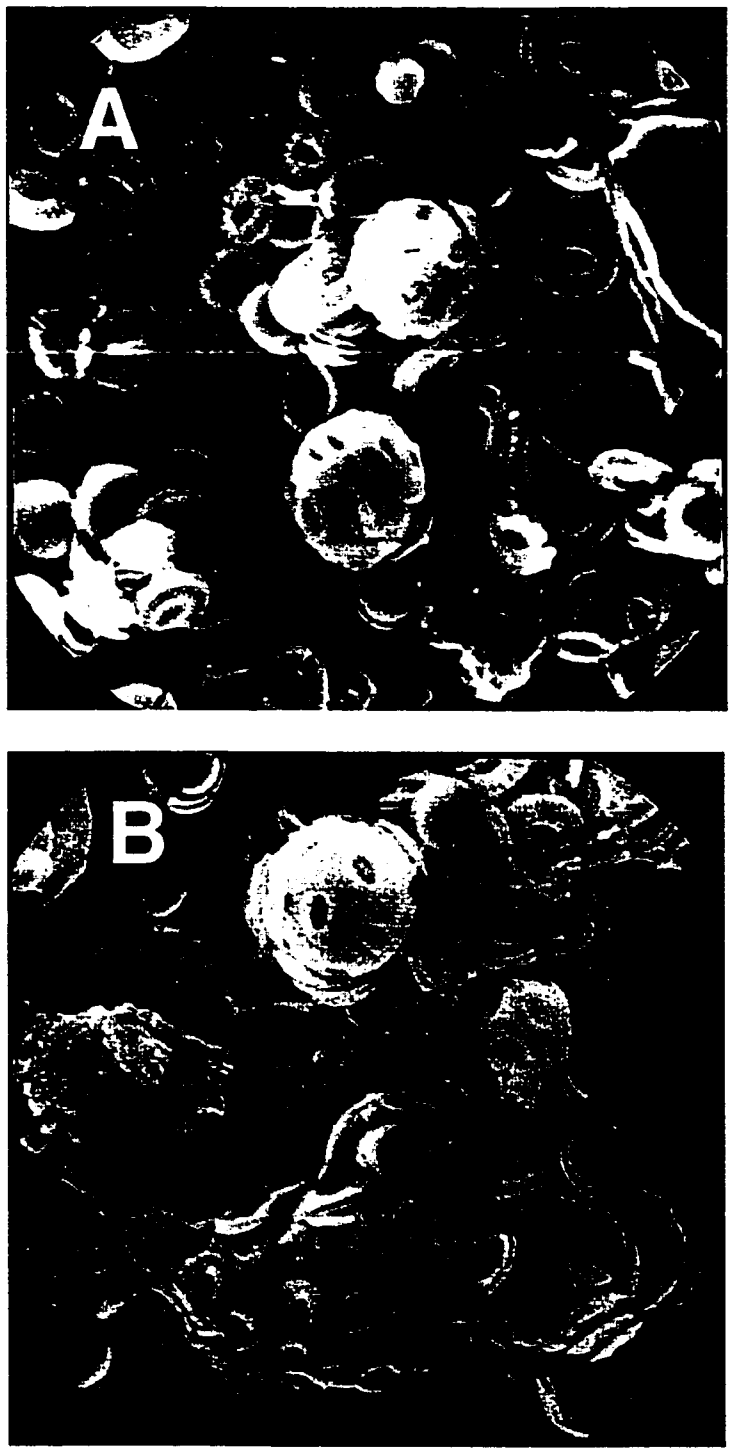

Figure 5.10: SEM Micrographs from 11 m depth at Station P12 in August 1996. Panel A: 3200x, Panel B: 3200x

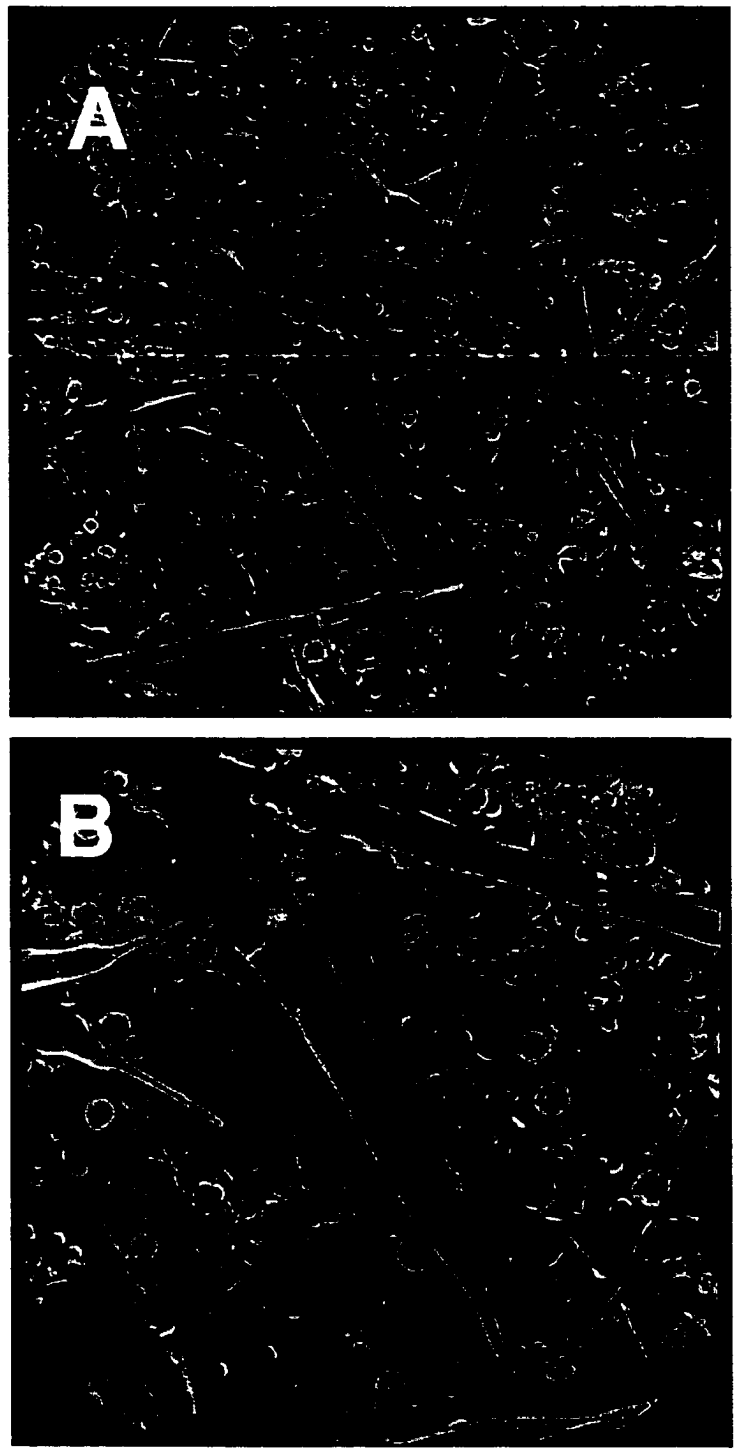

Figure 5.11: SEM Micrographs from 36 m depth at Station P12 in August 1996. Panel A: 400x, Panel B: 860x

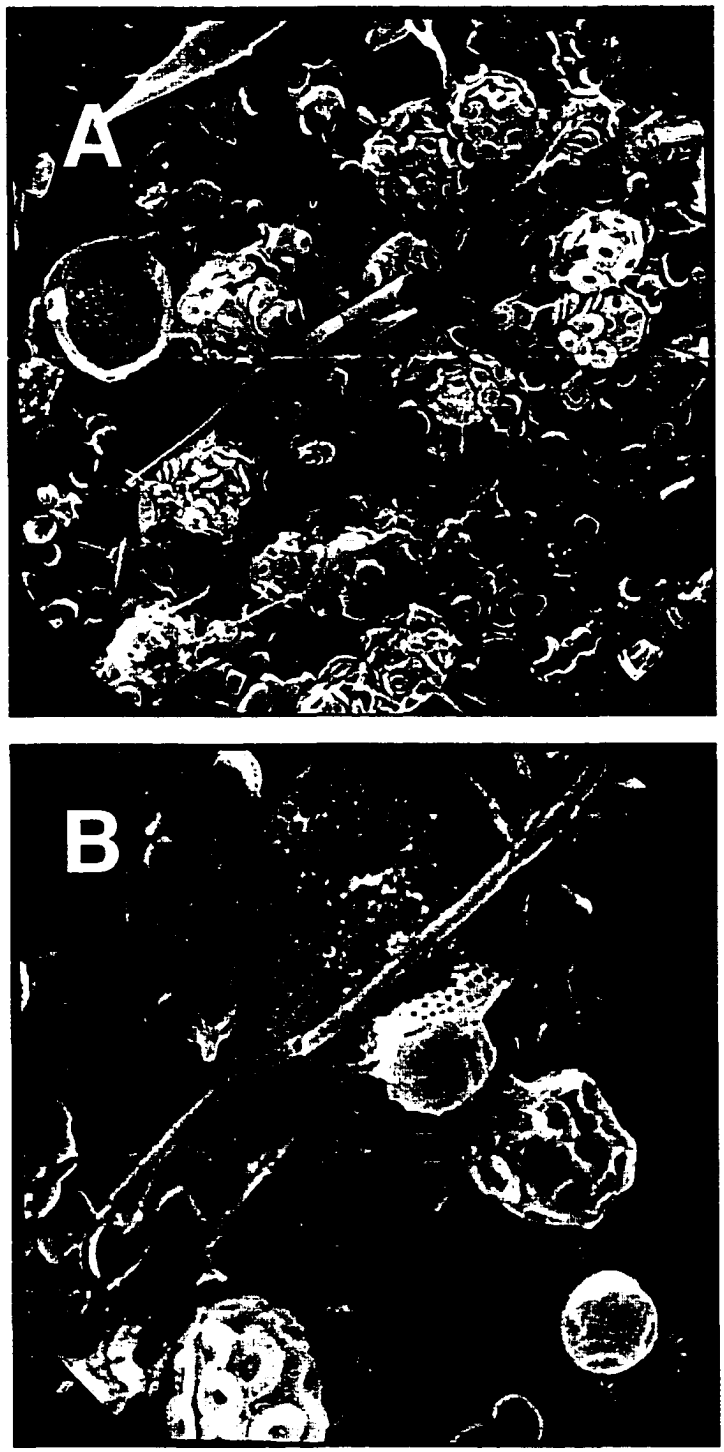

Figure 5.12: SEM Micrographs from 60 m depth at Station P12 in August 1996. Panel A: 1300x, Panel B: 3000x

of coccoliths which along with the detached coccoliths may be an indication of enhanced calcification. At the next depth, 36m (still within the euphotic zone, which reaches down to 40 m), (Fig. 5.11), there is an abundance of coccoliths and in Panel A coccolithophores are forming the background for several pennate diatoms. Panel B shows a few cells of *E. huxleyi* that are not extensively calcified.

Continuing deeper to 60 m, (Fig. 5.12), the cells appears to be heavily calcified and more resemble formless aggregates of coccoliths rather than coccospheres. Interesting to note here is that although *E. huxleyi* cells are heavily calcified, the *G. oceanica* cells appear to be calcified to a lesser degree. If this is typical, then, based on the C/P ratio hypothesis, one might suspect the carbon isotope fractionation to be different in the two species, a subject that merits further study.

At 300 meters depth (Fig. 5.13)the particulate material is mostly made up of debris, such as broken diatom frustrules and detached coccoliths. A few intact cells of *E. huxleyi* var. *Corona* and *G. oceanica* are present at this depth.

At the deepest MULVFS depth at 900 m (Fig. 5.14), the filter collected a mix of detached coccoliths originating from both *E. huxleyi* and *G. oceanica.* Also, a large aggregate that appears to be a fecal pellet filled with coccoliths is present. *Cadée* (1985) found similar aggregates of coccolithophores embedded in mucoid material in the North Sea. Cadée claimed that although the aggregates shape resembled that of copepod fecal pellets the length to width ratio was less than that of copepods of ($\sim$

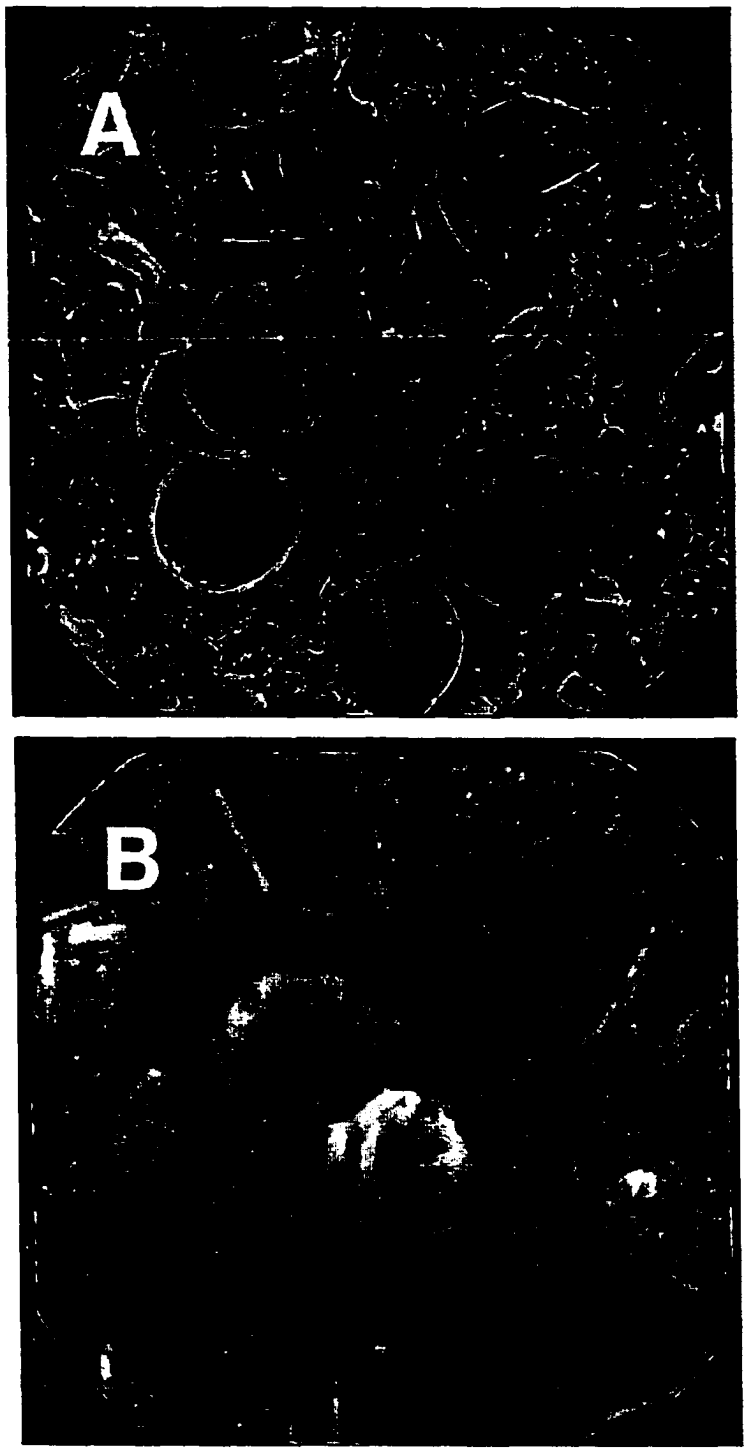

Figure 5.13: SEM Micrographs from 307 m depth at Station P12 in August 1996. Panel A: 3000x, Panel B: 4800x

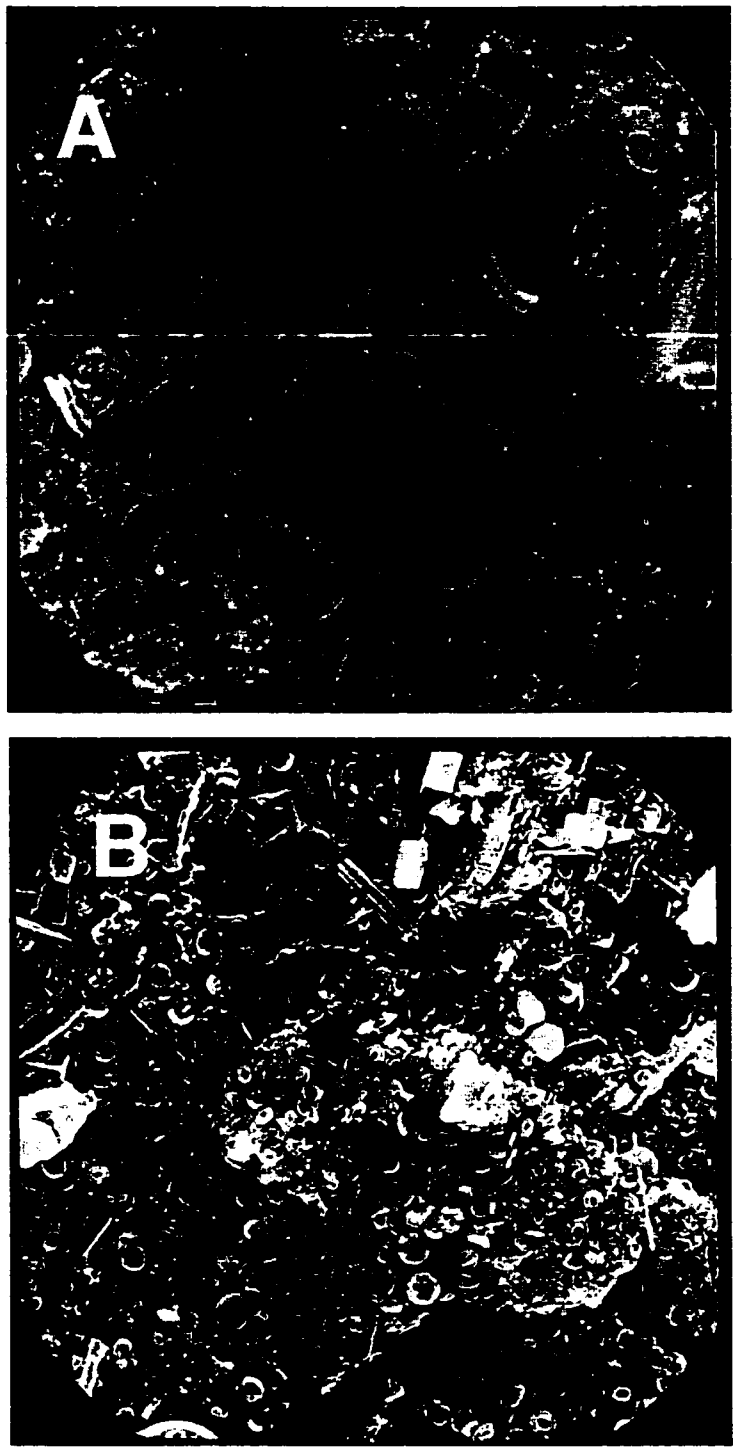

Figure 5.14: SEM Micrographs from 901 m depth at Station P12 in August 1996. Panel A: 4000x, Panel B: 1000x

7). The length to width ratio of the aggregate found here is about 2, thus implying a non-copepod origin.

5.4 Discussion

A comparison of the depth profiles of $\delta^{13}C_{37:2}$-alkenone from the CJGOFS cruises show a surface zone above the permanent pycnocline at 100 m. This zone is characterized by a variable isotope composition ($\delta^{13}C$ = -21.5 to -26.5°/$_{oo}$) reflecting differences in growth conditions between stations. Below the pycnocline at depths deeper than 100 m, the isotope compositions appear to converge towards a common value of $\delta^{13}C_{37:2} \approx -25°/_{oo}$. At these depths, very little, or no light is available for growth and most of the alkenones found here are likely to have been derived from the surface zone. The different processes affecting the carbon isotope composition of the alkenones within and below the euphotic zone are discussed below.

5.4.1 The Euphotic zone

The Euphotic or photic zone is defined as the part of the water column in which the light levels are above the compensation point for photosynthesis. This is defined to be at 1 % of the surface irradiation (I_0). By definition, the euphotic zone is where the majority of the photosynthesis and carbon assimilation takes place. It is therefore likely that the variability in isotope values seen in this zone is a consequence

of differences in the processes responsible for carbon assimilation. Among the factors affecting these processes are irradiance, (which will differ between stations depending on weather and time of year), and nutrient supply (which will also vary, both spatially and temporally as affected by up-welling and biological activity). Both irradiance and nutrient availability will also change vertically in the water column, i.e. the depth to which light penetrates into the water is affected by the intensity of the incident light and the turbidity of the water, while nutrient concentration is mainly affected by the vertical distribution of phytoplankton. To examine the effect of varying environmental factors in the euphotic zone on carbon isotope fractionation, a comparison of isotope values of alkenones found in the surface (mixed layer)and the bottom of the euphotic zone was made.

The variability in isotope composition of the mixed layer samples (10-15m) was accompanied by equally variable environmental parameters. For example, ε_p was 15.5 $^{\circ}/_{\circ\circ}$ at Station P12 in August and 11.2 $^{\circ}/_{\circ\circ}$ at Station P26 in August, nitrate varied between 0 and 9 μmol kg^{-1}, phosphate concentration was 0.3 μmol kg^{-1} at the depleted stations and 1 μmol kg^{-1} at the more replete stations (Table 5.1, Fig. 5.17). Meanwhile at the bottom of the euphotic zone (1% of surface irradiance, I_0) the variation in ε_p was not as large, 13.1 to 9.9 $^{\circ}/_{\circ\circ}$, (Table 5.2, Fig. 5.18). ε_p is here calculated relative to dissolved CO_2 by adopting a constant value for $\delta^{13}C_{DIC}$ of 1.2$^{\circ}/_{\circ\circ}$, based on the average $\delta^{13}C_{DIC}$ at the respective 1%I_0 depths from Station

P26 in May 1996 and P4, P12 in February 1997 (see Fig. 5.9).

Nutrient and dissolved CO_2 levels at the bottom of the euphotic zone were generally higher than in the mixed layer. Light levels were also different for cells growing in the mixed layer and cells at the bottom of the euphotic zone, except for Station P16 in May 1996 which had a mixed layer that reached below the euphotic zone. Measurements of alkenone concentrations at Station P12 in May reveal that production at the $1\%I_0$ depth was comparable to that near the surface, Table 5.4, which suggests that both locations are important to the overall production of alkenones. A comparison of the fractionation in the mixed layer and at the bottom of the euphotic zone is shown in Figure 5.15. The average ε_p of the mixed layer samples was 13.4 °/₀₀ with a range of 5.1 °/₀₀, while at $1\%I_0$ the average fractionation was 12.4 °/₀₀ and the range was lower at 3.1 °/₀₀. The difference in ε_p between surface and $1\%I_0$ varied from 3.2 to 0.2 °/₀₀. For station P16 in May for which both samples where taken within the mixed layer the ε_p was 12.6 °/₀₀ in the 10 m sample and 12.8 °/₀₀ for the deep sample. This similarity is consistent with the mixed layer being well mixed - hence sample depth is of little consequence. For the remaining stations the surface samples showed a larger fractionation than the deeper samples. For four of these stations the difference in ε_p was 1.1 to 1.4 °/₀₀ while for Station P12 in August the difference was 3.2 °/₀₀ and for Station P4 in August it was only 0.5 °/₀₀. Station P4 in August also showed an unusual feature in the nutrient profiles, where at 30 m depth the concentrations

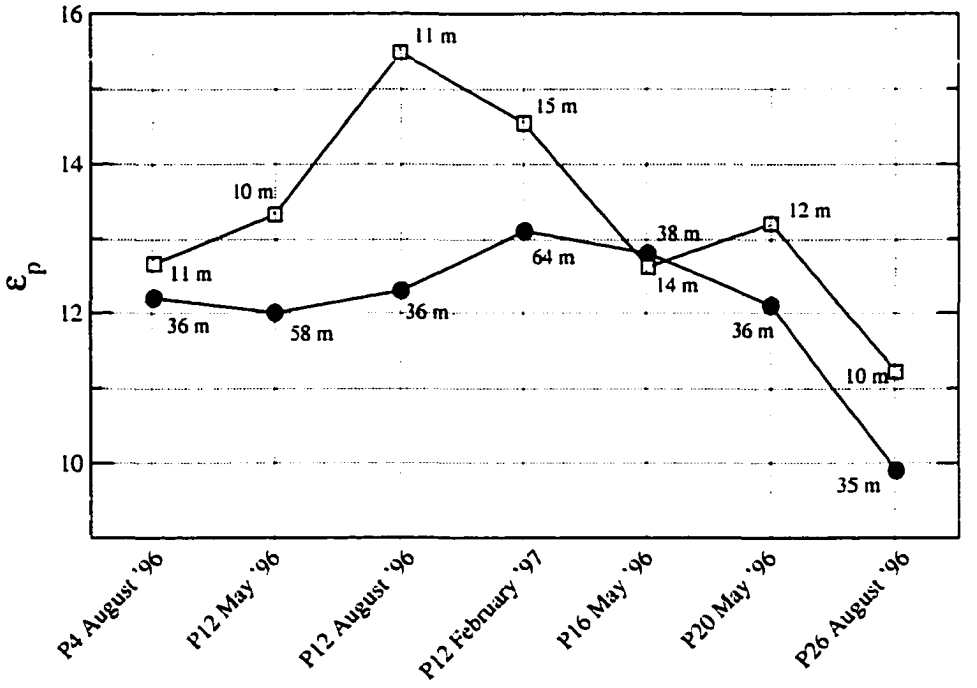

Figure 5.15: Isotope fractionation for mixed layer (open squares) and 1%I_0 (filled circles) samples. ε_p calculated from measured $\delta^{13}C_{DIC}$ and $\delta^{13}C_p$ - the carbon isotope composition of the produced biomass. $\delta^{13}C_p$ is calculated from $\delta^{13}C_{37:2}$-alkenone by adding a constant 4 °/₀₀, the isotopic offset between alkenones and total biomass ((Jasper et al. *1994)). Sample depths are indicated next to the symbols.*

of nitrate, phosphate and silicate all departed from the general increasing trend and suddenly decreased. This decrease lasted about 10 m where after the concentrations started to increase again (see Fig. 5.5). This layer may be a parcel of water which was entrained from a shallower position; thus, the observed nutrient concentrations were lower than in the surrounding water. The $1\%I_0$ sample at station P4 was taken in the middle of this "layer" and may therefore not be representative of a low light environment. It is also possible that growth of *E. huxleyi* was already light limited at the shallow depth due to high turbidity as shown by the shallow euphotic zone at this station.

In contrast Station P12 in August showed an increased fractionation at the surface with a large difference in fractionation between surface and deeper water. The significance of the difference in carbon isotope fractionation between surface and bottom of the euphotic zone was tested for all stations using a paired sample t-test. If Station P16 was excluded the difference in ε_p between surface (mixed layer) and $1\%I_0$ was significant with a 95 % confidence interval (p=0.011, n=6). To test the sensitivity of the estimated carbon isotope composition of the DIC at the bottom of the euphotic zone, the t-test was used for the two measured extreme values of $\delta^{13}C_{DIC}$: 0.98 °/$_{oo}$ and 1.6 °/$_{oo}$. Both tests showed a significant difference at the 95 % confidence level between surface and bottom of the euphotic zone with p = 0.006 and p = 0.034 respectively.

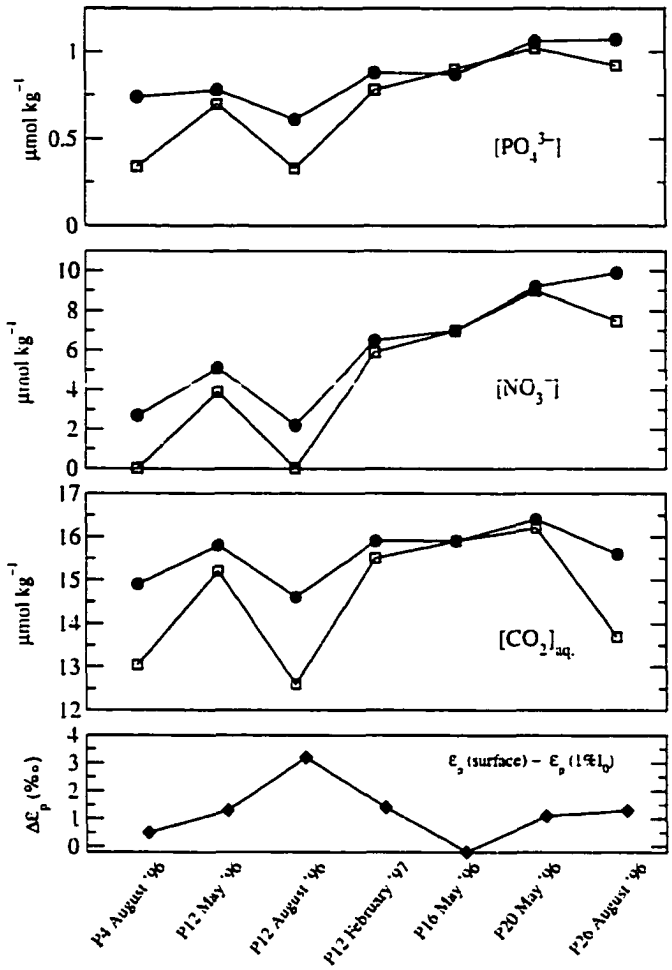

Figure 5.16: Comparison of nutrient concentrations in the mixed layer and at 1 % I_0.Open squares: surface (mixed layer), Filled circles: 1%I_0. The bottom panel show the difference in ϵ_p between surface (mixed layer) and at 1%I_0.

In Figure 5.16 the differences in environmental parameters and isotope fractionation between the surface and 1%I_0 are explored. For the stations reported here neither dissolved CO_2, phosphate nor nitrate concentration alone seems to be responsible for the difference in isotope fractionation between the two depths. Nutrient concentrations were generally higher at the deeper sample locations providing a situation of

light limited but not nutrient limited growth, while nutrient limitation did occur in the surface at station P4 and P12 in August. However, if Station P4 was at the onset of nutrient depletion then it is possible that the conditions recorded when the station was occupied may not have prevailed long enough to have effect on the physiology of *E. huxleyi*. Light limitation cannot be ruled out for the surface samples and the isotope fractionation in the surface could therefore be the result of the combination of light and nutrient influence. The overall lower variation between stations in the deeper samples implies a common controlling factor, for which light is the most likely candidate. Figure 5.17 and 5.18 show the different environmental parameters plotted against ε_p for the surface and 1% I_0 samples respectively. As indicated by figure 5.16 there are no apparent correlations between any of the environmental parameters and carbon isotope fractionation for samples collected within the euphotic zone.

5.4.2 Fractionation at depth

The extent to which material produced at a certain depth may be mixed with sinking material produced at a shallower depth has to be considered when interpreting depth profiles of $\delta^{13}C_{37:2}$-alkenone. Boyd and Harrison, (1999) suggested that the fate of phytoplankton along Line P during the post-bloom periods is sedimentation. Pelagic recycling is the dominant process for the rest of the time at the in-shore stations (P4-P16) and a year round recycling at the offshore stations (P20, P26). This view was refined slightly by Thibault *et al.*, (1999). Based on pigment data from the

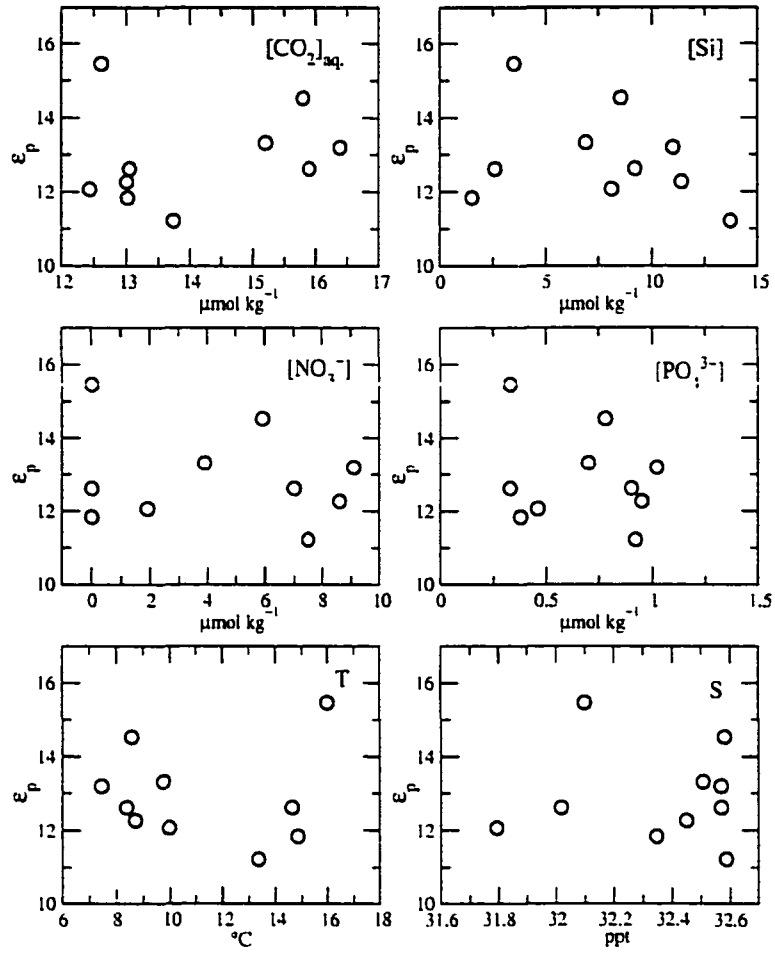

Figure 5.17: ε_p versus *environmental parameters in the mixed layer.* ε_p *calculated as the fractionation between dissolved* CO_2 *and* $\delta^{13}C_{org}$. *based on measured values of* $\delta^{13}C_{DIC}$ *and* $\delta^{13}C_{37:2}$*-alkenone.)*

CJGOFS cruises they suggested that large copepods had a significant influence on the downward flux of POC during the spring. In the winter unidentified herbivores (e.g salps, pteropods) have an impact, together with an equal contribution of sinking algae. Neither algal sinking nor herbivore grazing seem to have significant influence on the magnitude of the downward flux of biogenic material during summer. Extending

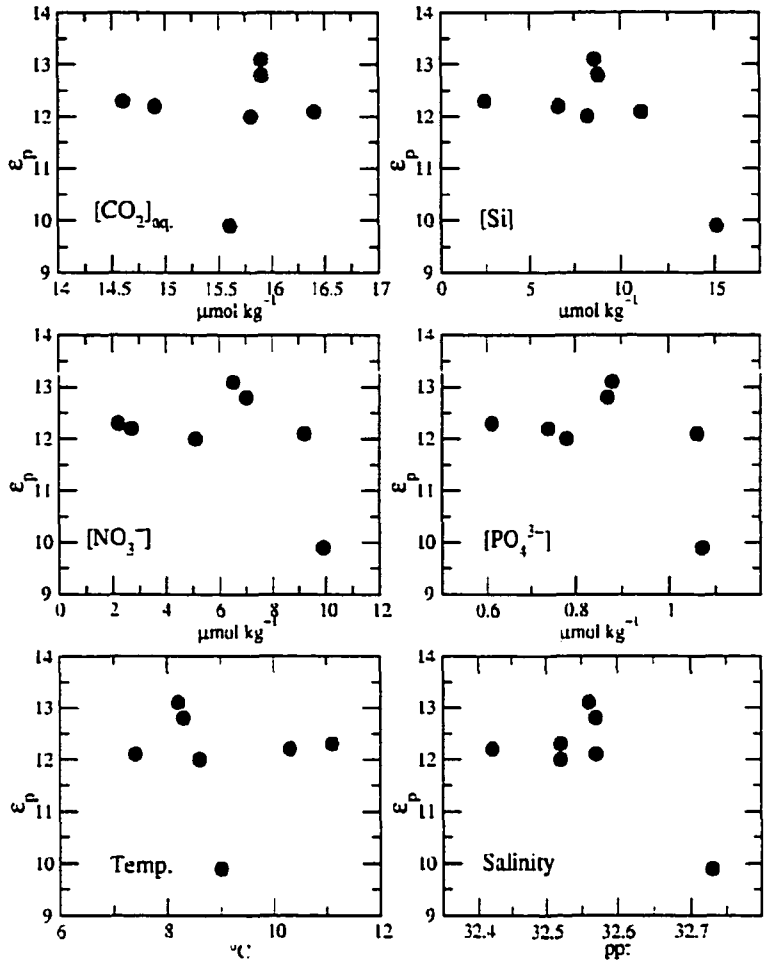

Figure 5.18: ε_p *versus environmental parameter at 1 % I_0.* ε_p *calculated as the fractionation between dissolved CO_2 and $\delta^{13}C_{org}$, based on an estimated value of $\delta^{13}C_{DIC}$ and measured values of $\delta^{13}C_{37:2}$-alkenone.*

the profiles to depths beyond the euphotic zone, the vertical variation in $\delta^{13}C_{37:2}$-alkenone for the spring stations was very low between 35 and 135 m at Station P12 while at Station P16 and P20 there was a positive departure at 85 m coinciding with a maximum in pyrophaeophorbide *a* (Thibault *et al.* 1999), a marker associated with fecal matter originating from copepods. However, there was a similar concentration of

pyropheophorbide *a* at Station P12 without any shift in isotope value. An increase in copepod fecal matter could be perceived as mixing of *in situ* produced material with material produced at shallower depths. The sinking rate for copepod fecal pellets containing *E. huxleyi* coccoliths exceed 100 $m\ d^{-1}$ (Harris 1994) making it difficult to estimate the true depth of origin. With the assumption that the concentration of pyropheophorbide is elevated at the depth of grazing then the increased concentration of pyropheophorbide *a* can also be used to indicate elevated concentrations of phytoplankton cells. Therefore, it may be interpreted as an indicator of the location of production. Hence the isotope signal at 85 m for Station P16 and 20 in May could be caused by alkenones being produced with a carbon isotope fractionation according to the local conditions.

A simple mass balance can be used to test the sensitivity of the isotope signal to vertical mixing . The isotope mass balance is written as:

$$\delta^{13}C_{mix} \cdot m_{mix} = \delta^{13}C_{z_1} \cdot (x \cdot m_{z_0}) + \delta^{13}C_{z_1} \cdot m_{z_1} \tag{5.1}$$

where $\delta^{13}C_{mix}$ is the measured δ-value and $\delta^{13}C_{z_1}$ the isotope composition of material produced at z_1 m. The amount of material (m) at the deeper level is the sum of the material being mixed in and the material being produced at the depth in question.:

$$m_{mix} = (x \cdot m_{z_0}) + m_{z_1} \tag{5.2}$$

x being the fraction of the material at depth z_0 that is mixed in with the material at depth z_1. Since these fluxes are unknown an assumed value of 25 % of the "standing

Depth (m)	Conc. $C_{37:2}$-alkenone ng l^{-1}	measured $\delta^{13}C_{37:2}$ (°/₀₀)	adjusted $\delta^{13}C_{37:2}$ (°/₀₀)	$\Delta\delta^{13}C_{37:2}$ (°/₀₀)
10	4.4	-24.7	-	-
34	3.0	-23.8	-23.2	0.6
58	3.6	-24.1	-24.2	-0.1
83	1.8	-23.9	-23.5	0.4

Table 5.4: Calculation of isotope composition of "in situ" *produced alkenones at Station P12 in May 1996, assuming a downward flux corresponding to 25 % of the alkenones produced in the mixed layer.*

stock" in the surface layer is used here. The adjusted values are shown together with the concentration of $C_{37:2}$-alkenone for the top 83 m at Station P12 in May in table 5.4. This shows that under the assumption that the downward flux of alkenones corresponds to 25 % of the mixed layer "standing stock", the isotope composition at the 1% I_0 depth is virtually unaffected. This calculation implies that the previously calculated fractionation is indeed the *in situ* fractionation. The adjusted isotope composition at 83 m depth is 0.4 °/₀₀ more enriched in ^{13}C than the measured value. This suggests that the enriched material produced at depth acts to attenuate the isotopically-depleted isotope signal in the mixed layer, and thus the downward mixing of alkenones dampens the variation and the signal approaches an integrated value of production over an period of time proportional to the rate of downward mixing. The carbon isotope signal is then a function of the proportions of fast sinking fecal material to sinking single cells of *E. huxleyi*. The seasonal average of isotope composition in the

euphotic zone is strikingly similar to the average composition at depth for Station P12. The average for the euphotic zone (all stations) was $\delta^{13}C_{37:2}$ = -24.9 °/₀₀ (n=8) and the corresponding average for all the deep samples was $\delta^{13}C_{37:2}$ = -24.8 °/₀₀ (n=17). It should be pointed out that the average for the deep samples does not include any samples from February, however since little or no production is expected at these depths the turnover time must be quite long. As a result the signal is not likely to change quickly and the values can be expected to be similar to those of May and August. To test that the changes in carbon isotope fractionation with depth is not a result of changes in species composition the $U^{K_{37}}$-index was calculated for Station P12 in May 1996. The $U^{K_{37}}$-index is a sea surface temperature proxy based on the ratio of di-unsaturated and the sum of di- and tri-unsaturated alkenones. Temperatures were estimated using a calibration curve from Conte *et al.*, (1998) for a non-calcifying strain of *E. huxleyi* isolated at Ocean Station Papa (P26): $U_{37}^{K} = 0.014 + 0.03 \cdot T$. The results are shown in Table 5.5 and the estimated temperatures in Figure 5.19. The values of the U_{37}^{K} index decrease proportionally to the decrease in temperature, however the calculated temperatures, using the calibration curve of Conte *et al.*, (1998) , were offset relative to the measured values by about 3°C. The *E. huxleyi* strain used for the calibration was not calcifying. Therefore, due to physiological differences, the offset may not be representative of the strain of *E. huxleyi* found along Line P. Another possibility for the under estimation of the actual temperature

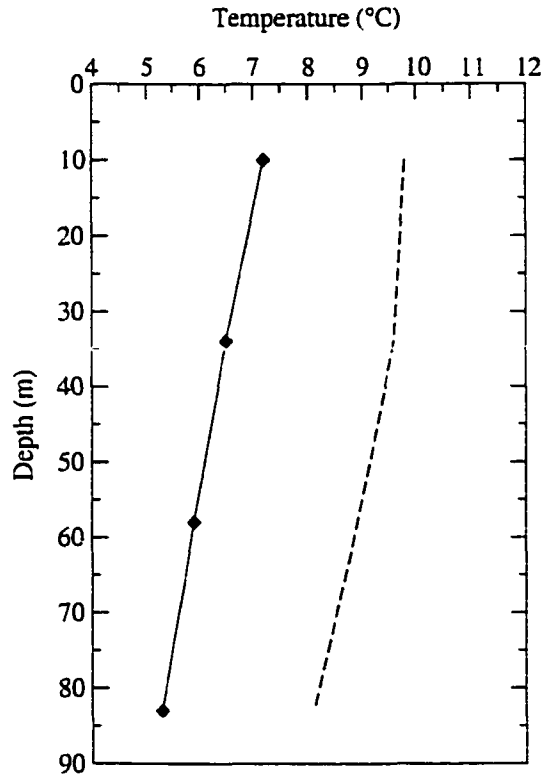

Figure 5.19: Temperature estimates based on the U^K_{37}-index at Station P12 in May (filled diamonds)and measured temperature (dashed line). A calibration curve from Conte et al *(1998) for a non-calcifying strain from OPS is used: $U^K_{37} = 0.014 + 0.03 \cdot T$.*

Depth (m)	U^K_{37}	C_{37}/C_{38}
10	0.23	1.75
34	0.21	NA
58	0.19	1.73
83	0.18	1.78

Table 5.5: U^K_{37} and C_{37}/C_{38} ratios for Station P12 in May. The C_{37}/C_{38} ratio for a calcifying strain isolated at OSP (732a) is 1.25 (n=9).

by the U_{37}^{K}-index would be the presence of a significant population of *Gephyrocapsa oceanica*. The calibration curve for this species is offset to that of *E. huxleyi*. Since the two species are different with respect to the production of C_{37} and C_{38} alkenones (Volkman *et al.* 1995), *E. huxleyi* has generally a ratio of C_{37}/C_{38} larger than 1 while the ratio for *G. oceanica* is less then 1 (Volkman *et al.* 1995). A calcifying strain isolated at OSP (732a) grown in our laboratory had a ratio of C_{37}/C_{38} of 1.25 (n=9). The ratios for the euphotic zone at Station P12 in May were between 1.7 and 1.8 (Table 5.5) indicating a constant species or mix of species. The latter is less likely since the value of the ratio was so high, although it may indicate that the *E. huxleyi* growing at Station P12 is different from the 732a-strain.

For the summer stations the 35 to 135 m samples showed very little variation in $\delta_{37:2}$. Since mixing can be ruled out, in accordance with a very slow vertical transport found by Thibault *et al.*, (1999) these results imply that the measured carbon isotope compositions reflect the fractionation at each depth. The variability in $\delta^{13}C_{37:2}$-alkenone between stations for depths between 35-135 m remained approximately the same as for the bottom of the euphotic zone, (Fig. 5.20).

The results for P26 in August are unique in that the isotope composition within the top 80 m is heavier than any of the other stations. At 135 m depth however, all seven stations have a $\delta^{13}C_{37:2}$ between -25.2 °/$_{oo}$ and -23.9 °/$_{oo}$ The reasons for the apparent tendency of the isotope values to converge at depth is not fully understood. Apart

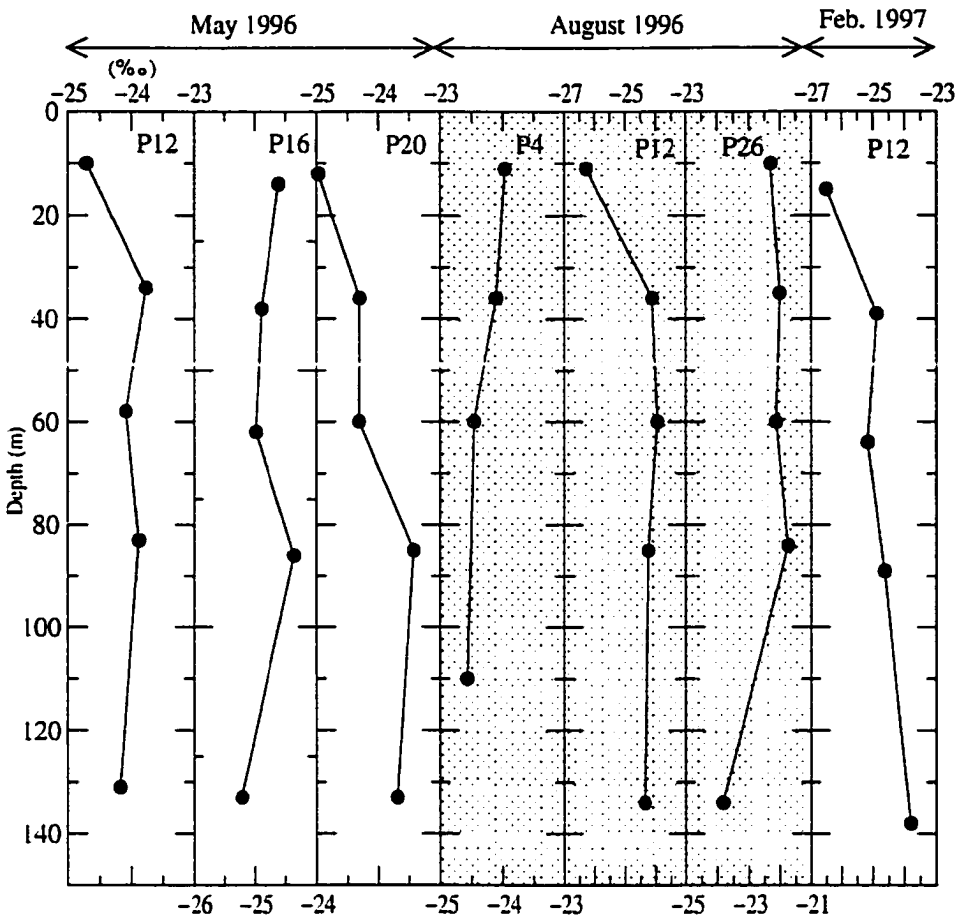

Figure 5.20: .

$\delta^{13}C_{37:2}$-alkenone profiles for all stations.

from the mixing of material from shallower depths as suggested earlier, production of alkenones at these depth may be possible. Algae have been shown to be able to maintain the photosynthetic activity at light levels below the compensation point for extended periods of time (Hellebust and Terborgh 1967). For example, Anderson, (1969) detected active photosynthesis at 90 m depth off the Oregon coast where the light levels were less than 0.1 % I_0. Cells that sink out of the euphotic zone may still

be fixing carbon, albeit at a very low rate. In addition, van Bleijswijk *et al.*, (1994) showed that the ratio of production of calcite carbon to production of organic carbon decreases dramatically at low light levels. Therefore calcification is likely to assume a low rate relative to the rate of photosynthesis. At these depths light limitation will be the dominating factor in controlling both photosynthesis and calcification. Therefore carbon isotope fractionation will be less dependent on local nutrient and C_e conditions, resulting in a more uniform $\delta^{13}C_{37:2}$ at depth.

5.4.3 Nutrient influence

Recent efforts to quantify the isotope fractionation associated with carbon assimilation in phytoplankton have shown that, in addition to dissolved carbon dioxide, the phytoplankton growth rate plays an important role (Laws *et al.* 1995; Laws *et al.* 1997; Bidigare *et al.* 1997). Bidigare *et al.*, (1997) demonstrated with cultures of *E. huxleyi* that the isotope fractionation show a slightly stronger correlation to growth rate (μ) multiplied by the inverse of dissolved carbon dioxide ($1/CO_2$) than to carbon dioxide alone. They also inferred that since phytoplankton growth rate at saturating light conditions is controlled by nutrient availability, nutrient concentration should, by extension also influence isotope fractionation. This is supported by the correlation between ε_p and $[PO_4^{3-}]1/C_e$ (Fig. 5.21). The importance of nitrate for isotope fractionation was demonstrated by Eek *et al.*, (1999). They showed that during nitrate

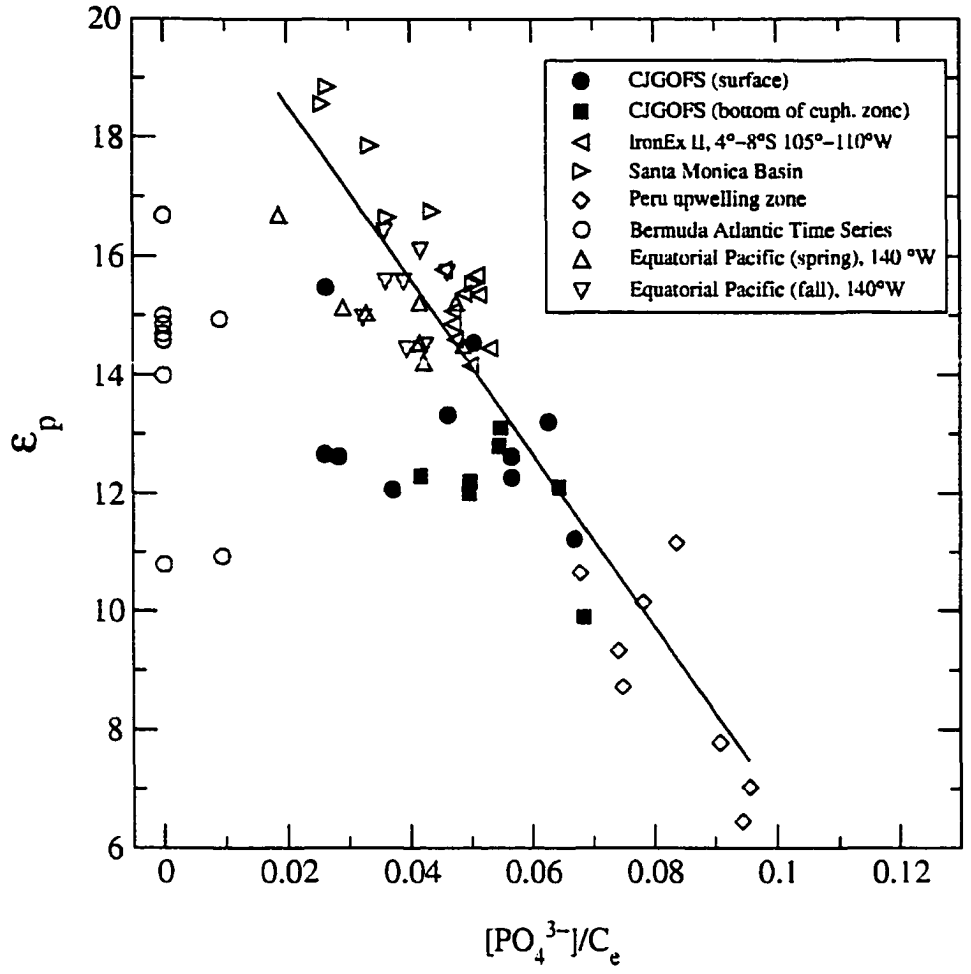

depletion the isotope fractionation is less than expected from the ε_p *vs* $[PO_4^{3-}]/C_e$ relationship (Fig. 5.22). To compare the measurements from NE Pacific with previously published material, data by Bidigare *et al.*, (1997) is used. This data set is compiled from several different environments and is therefore especially useful in generating a overview of carbon isotope fractionation by *E. huxleyi* in the world's oceans. The results from the NE Pacific fills a gap in the larger data set as seen in Figure 5.21. In spite of the likelihood that different environments also represent different strains of *E.*

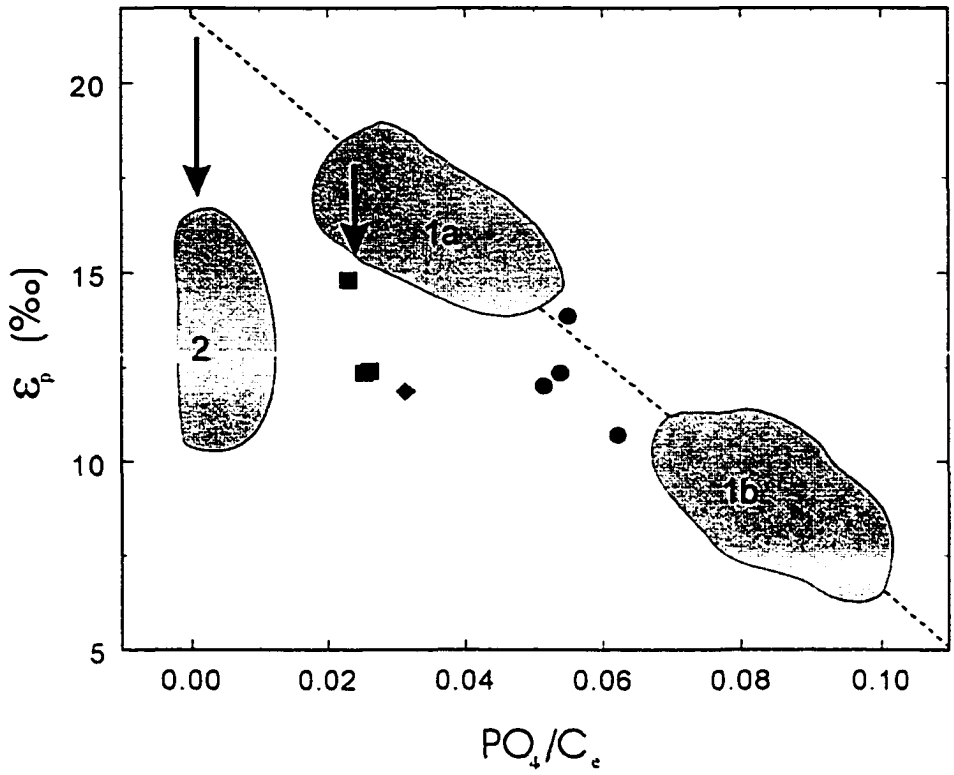

Figure 5.22: Effect of nitrate depletion on the $\varepsilon_p$vs PO_4^{3-}/C_e relationship. Measurements from the NE Pacific are shown with symbols, nitrate replete - filled circles, nitrate depleted - filled squares. The shaded area represent data from Bidigareet al., (1997). Area 1a and 1b represent samples from nitrate replete waters and area 2 represents samples from nitrate depleted water. The dashed line is the linear regression for the nitrate replete samples in area 1a and 1b. Note that the carbon isotope fractionation for the nitrate depleted samples is lower than the regression line.

huxleyi (Brand 1982), there seems to be a relationship between ε_p and the availability of phosphate and dissolved CO_2. There are however some exceptions;for example, ε_p from Bermuda Atlantic Time Series (BATS) are much lower than expected from the bulk of the data. Similarly, some of the stations from NE Pacific also showed lower

fractionation than would be expected from the ε_p *vs* $[PO_4^3-]/C_e$ relationship.

A closer examination shows that the samples from the BATS data set and the anomaly samples from NE Pacific have one thing in common. They have all been collected in nitrate-depleted waters. The minimum concentration of NO_3^- required for growth of *E. huxleyi* is less than 5 μM, with a $K_{0.5}$ for NO_3^- of 0.1 *mu*M (Merrett *et al.* 1993; Eppley *et al.* 1969). It is therefore possible that cells growing in waters with less than 0.1 μM NO_3^- operate in a different physiological mode than cells in nitrogen-replete waters. For example, calcification increases in N-limited cells (Baumann *et al.* 1978; Paasche 1998) as does CO_2-leakage (Nimer and Merrett 1995). In addition experiments performed by Merrett *et al.*, (1993) shows that calcification ultimately has an absolute requirement for NO_3^-, which indicates that nitrate limitation will cause enhanced calcification up to a point, after which calcification will cease. Furthermore, nitrogen starvation causes an accumulation of carbohydrates and neutral lipids in phytoplankton (Uriarte *et al.* 1993; Bell and Pond 1996). Among the neutral lipids are the alkenones, which have been shown to increase in concentration per cell by a factor of 15 after two weeks in zero nitrate media (Epstein *et al.* 1998).

The SEM pictures from Station P12 in August (Fig. 5.10 to 5.14) at which nitrate was exhausted confirms that the cells are heavily calcified as would be expected in a nitrate limited environment. However, an increased calcification causing increased leakage of CO_2 from the cells would produce a relatively high fractionation, which

is the case for Station P12 in August (ϵ_p=15.5 $^\circ/_{oo}$) but not for Stations P4 and P16 in August (ϵ_p=12.7 and 12.6 $^\circ/_{oo}$ respectively). This may be a consequence of timing, i.e. the time between complete exhaustion of NO_3^- and sample collection. For example, if the time of exhaustion and sampling are close together then the isotope signal in the cells may still reflect low but non-zero nitrate conditions. If, on the other hand, the two events are separated in time then the isotope signal would indeed reflect a zero nitrate environment. Therefore cells that are still growing in nitrate depleted waters may show a higher ε_p due to nitrate induced calcification than cells that have had time to become scenecent. Bearing this potential influence of nitrate depletion in mind and excluding the data from the Bermuda Atlantic Time Series, the relationship between ε_p and $[PO_4^{3-}]/C_e$ for the remaining data from Bidigare *et al.*, (1997) can be described as: $\varepsilon_p = 21.8 - 151.7 \cdot [PO_4^{3-}]/C_e$ with $r^2 = 0.93$, P$\leq$ 0.01. *Figure 5.23 shows a plot of the data from NE Pacific with the corresponding linear regression. Nitrate stations; P4, P12 and P16 in August and Station P4 in May are excluded, the linear regressio with a* $r^2 = 0.70$, P$\geq$ 0.05. *The regression for the whole dataset (line 2. in Fig.* 5.23) : *have a much poor* P$\geq$ 0.05, *implying that the fractionation is different in nitrate repleteand nitrate depleteenvironm* from NE Pacific are represented by solid square. As discussed earlier, the fractionation at 1%I_0 was less than in the mixed layer samples even though the phosphate and CO_2 values were slightly higher. This low fractionation at depth may be a response to light limitation.

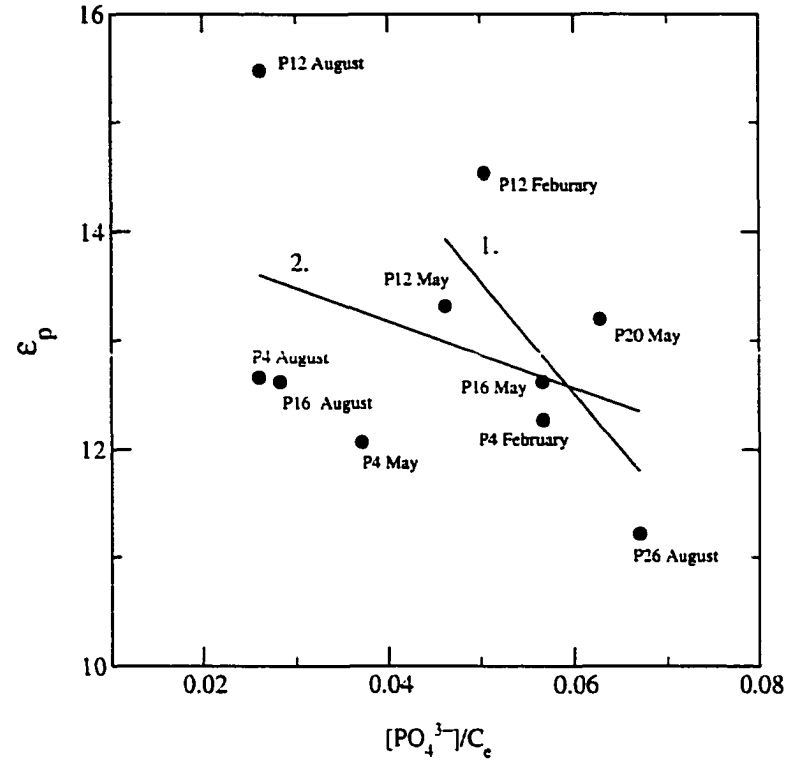

Figure 5.23: Regression of ε_p vs $[PO_4^{3-}]/C_e$. Line 1 is the linear regression for nitrate replete stations, while line 2 is the regression for all stations.

Assuming that *E. huxleyi* is utilizing HCO_3^- and that due to active transport of HCO_3^- the cells are leaking CO_2, the extent of leakage can be calculated by rearranging Eq. 2.19:

$$L = \frac{\varepsilon_p - \varepsilon_{d/b}}{\varepsilon_f} \tag{5.3}$$

If the fractionation by rubisco (ε_f) is assumed to be 29 $^\circ/_{oo}$ and the thermodynamic equilibrium effect between dissolved CO_2 and HCO_3^- is as shown by *Mook et al*

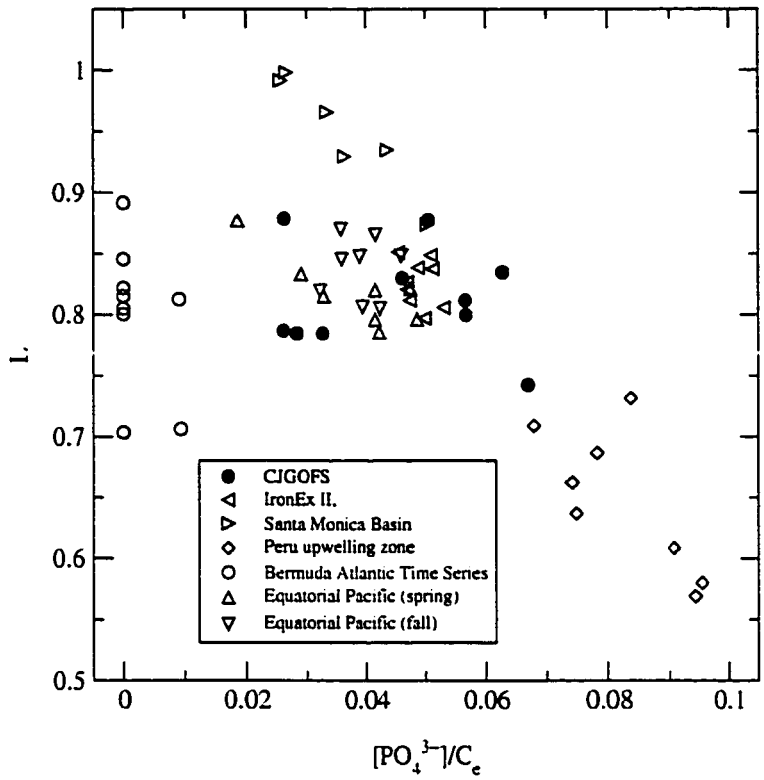

Figure 5.24: Estimates of CO_2 leakage for date from Bidigare et al., *(1997) and the mixed layer samples from Ne Pacific (CJGOFS).*

(1974):

$$\varepsilon_{d/b} = 24.12 - \frac{9866}{T} \tag{5.4}$$

where T is the absolute temperature. Figure 5.24 shows the apparent leakage L *vs.* $[PO_4^{3-}]/C_e$. The calculated leakage is reasonable in that it does not exceed unity, which would have implied that more carbon was leaking out than was transported in.

5.4.4 Estimation of growth rate

Since field measurements of growth rate for specific species are impossible to obtain it has to be estimated. To produce an estimate of growth rate for the NE Pacific samples I have chosen a model by Tyrell and Taylor, (1996). As a part of a model describing phytoplankton succession in the North Atlantic designed, they designed a growth rate model specifically for *E. huxleyi*. The growth rate was estimated using the following equation:

$$\mu_i = \mu_{max} \cdot Q_{10}(T) \cdot \psi(I)\phi(N, A, P) \tag{5.5}$$

where μ_{max} is the maximum growth rate of *E. huxleyi* under optimal conditions(0.6 d^{-1}, NE Pacific strain (Muggli and Harrison 1996), $Q_{10}(T)$ is the temperature dependence of growth rate, $\psi(I)$ is the limitation of growth rate due to low light intensity and $\phi(N, A, P)$ is limitation of growth rate due to low concentrations of nitrate (N), ammonia (A) and phosphate (P). All growth limiting factors vary between 0 (total inhibition of growth) and 1 (no limitation). The equation assumes that the total limitation of growth is equal to the product rather than the minimum of the limitations, with the exception of the nutrients for which the minimum is applied. The limitation due to temperature is calculated as:

$$Q_{10}(T) = 10.0^{[(T-16.0)\cdot\frac{0.301}{10.0}]} \tag{5.6}$$

This equation does not compensate for a decrease in growth rate at higher temperatures, which in this case will not cause a problem since the temperature did not

exceed the optimum temperature of 16 °C for the NE Pacific strain of *E. huxleyi* (Muggli and Harrison 1996). Limitation due to low light intensity is calculated as:

$$\psi(I) = \frac{I}{I + I_H} \tag{5.7}$$

where I_H is the half saturation constant for light, here taken to be 17 μE m^{-2} s^{-1} as measured by Thompson and Calvert, (1995) for a *E. huxleyi* strain isolated at Ocean Station Papa (P26)(Thompson and Calvert 1995). Tyrell and Taylor, (1996) used I_H = 100 μE m^{-2} s^{-1} in their model. The light intensity (I) at each station was calculated by setting I_0 to the average PAR value for the particular cruise and assuming the average irradiance within a depth interval to be (Kirk 1994):

$$I = I_0 \cdot \frac{1}{z_2 - z_1} \int_{z_1}^{z_2} e^{-k \cdot z} dz \tag{5.8}$$

Where z_1 and z_2 are the top and bottom of the depth interval in question (e.g. mixed layer) and k is an attenuation coefficient calculated from (Kirk 1994):

$$D = \log_{10} \frac{I_0}{I_{1\% I_0}} = 2 \tag{5.9}$$

$$k = 2.303 \cdot \frac{D}{r} \tag{5.10}$$

using r as the depth of the euphotic zone. Admittedly, this is an approximation of the attenuation coefficient. In reality k will change with depth in the euphotic zone since it is wavelength dependent, but it will serve as a coarse measure of the combined

attenuation caused by absorption and scatter by particles. Finally, nutrient limitation is estimated as:

$$\phi(N, A, P) = Min[\frac{(N/N_H) + (A/A_H)}{1 + (N/N_H) + (A/A_H)}, [0.7 + (0.3 \cdot \frac{P}{P + P_H})]] \quad (5.11)$$

Half saturation constants for the nutrients are taken from Tyrell and Taylor, (1996) to be N_H= , A_H= and P_H= respectively. The equation for phosphate limitation differs from a Michaelis-Menten function to accommodate growth even when there is no inorganic phosphate in the water. This is because *E.huxleyi* is thought to be able to grow by using organic phosphates. However, in this case it is not a concern since the phosphate concentration was above zero at all stations. Concentrations of ammonia were not measured during these cruises, but data for Line P at other times as shown by Varela and Harrison, (1999), have measured values between 0.1 and 1.0 μg -at l^{-1} NH_4^+ with most concentrations between 0.1 and 0.5 μg-at l^{-1}. As an approximation of ammonia in the model the maximum value of 0.5 μg-at l^{-1} is adopted here, allowing for a maximal nitrogen availability. Finally, the instantaneous growth rate is converted into specific growth rate according to:

$$\mu = \mu_i \cdot \frac{L}{L + D} \quad (5.12)$$

where L and D are the light and dark periods respectively.

In Figure 5.25 the estimated growth rates are plotted against ε_p. Even though there is no apparent correlation between the two parameters some details stand out.

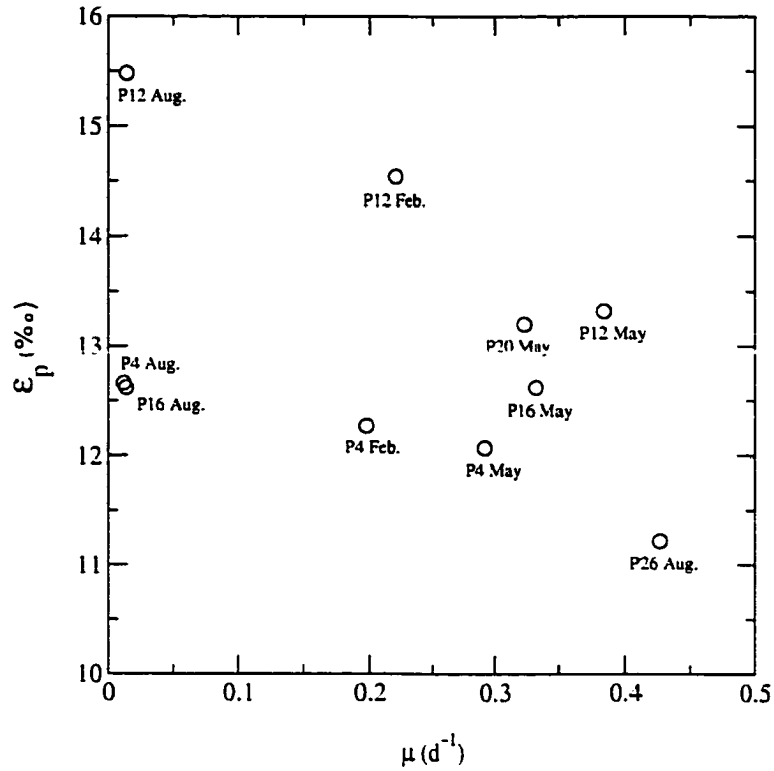

Figure 5.25: Estimated growth rate vs ε_p for surface samples from the NE Pacific. Growth rate estimated using a model by Tyrell and Taylor, (1996).

For example, the low fractionation at Station P26 in August corresponds to the highest growth rate of all stations in agreement with previously published results (Bidigare *et al.* 1997; Laws *et al.* 1995). Also Station P12 in February showed a high fractionation (ε_p=14.5 °/₀₀) and the growth rate here is low. However, Station P4 in February has a similar growth rate estimate but the fractionation is low making the growth rate estimates less conclusive, although the different limiting factors may provide some insight. Figure 5.26 shows the four factors used in the estimate. Four of the stations have a significant limitation due to lack of nitrate; Station P4, P12 and

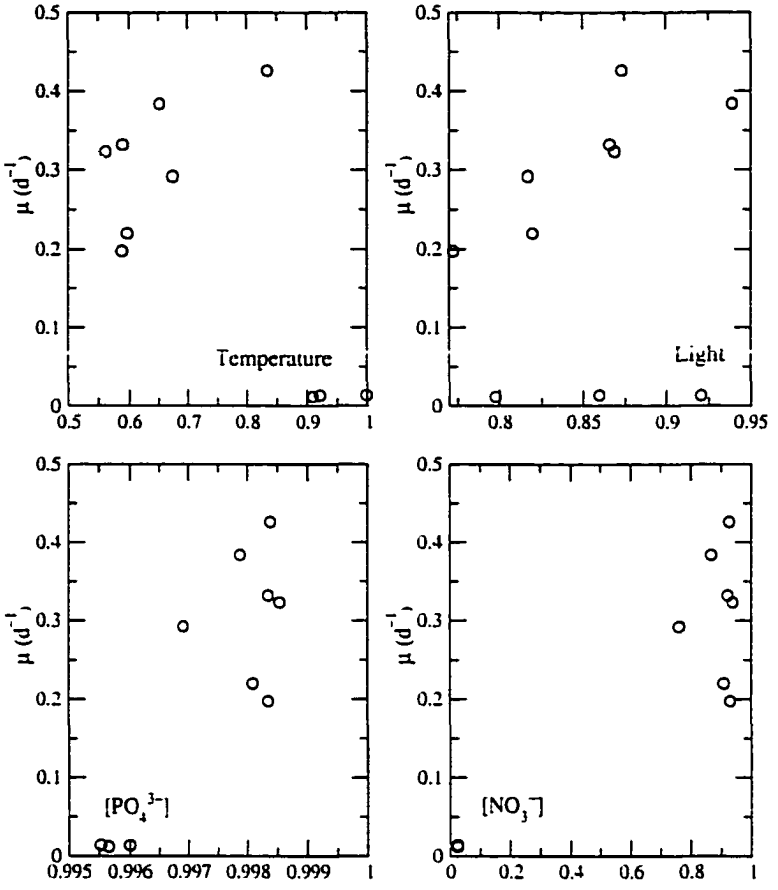

Figure 5.26: Growth limitation by environmental parameters as estimated by the growth model by Tyrell and Taylor, (1996), Eq. 5.6,5.7 and 5.11. Each factor can vary between 0 and 1, with 0 indicating total inhibition of growth and 1 no limitation.

P16 in August were all completely depleted of nitrate and Station P4 in May which in addition to a low nitrate concentration also was collected just below a mixed layer with zero nitrate (Eek *et al.* 1999). The growth rate at the other stations appears to be controlled by light and temperature.

5.4.5 Effect of calcification: theoretical considerations

Due to its ability to actively take up HCO_3^- (Dong *et al.* 1993; Nimer and Merrett 1993) and to the low internal pH (Nimer *et al.* 1994a; Dixon *et al.* 1989), *Emiliania huxleyi* cells are leaking CO_2 (Nimer and Merrett 1995). This has consequences for the isotope fractionation as described in Chapter One, and the resulting isotope composition will be dependent of the extent of leakage (Eq. 2.19). Since calcification is thought to be supplying carbon to photosynthesis by transport of HCO_3^- (Sikes *et al.* 1980; Nimer and Merrett 1992; Nimer *et al.* 1992; Nimer *et al.* 1994a; Anning *et al.* 1996), the ratio of calcification to photosynthesis may serve as a indicator of leakage. This assumption is supported by the fact that nutrient limited cells, which have an enhanced calcification (Paasche 1998; Van Bleijswijk *et al.* 1994; Paasche and Brubak 1994; Anning *et al.* 1996), leak substantially more than nutrient replete cells (Nimer and Merrett 1995). Calcification is light dependent and has a saturating point lower than that of photosynthesis (Paasche 1964; Nimer and Merrett 1993; Van Bleijswijk *et al.* 1994). Results reported by van Bleijswijk *et al.*, (1994) also indicate that the initial slope of calcification is steeper than that of photosynthesis. Figure 5.27 shows simulated Photosynthesis-Irradiance and Calcification-Irradiance curves in panel A according to the previous discussion and the ratio between the two (C/P) in panel B. The shape of the C/P curve mimics measurements of C/P both from van Bleijswijk *et al.*, (1994) and Balch *et al.*, Fig.5.28, (1996), although

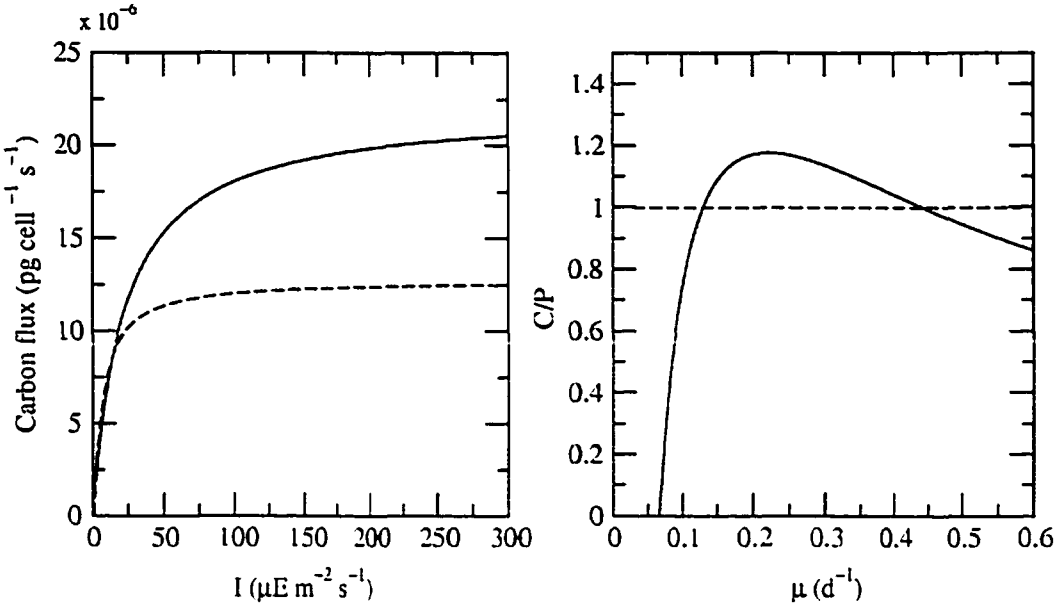

Figure 5.27: Panel A. simulated P-I (solid line)and C-I (dashed line) curves. Panel B. Calcification/Photosynthesis ratio calculated from the curves in panel A. Note the C/P ratio is exceeding 1 for part of the growth rate interval only.

the simulated curve has a higher maximum. The C/P-ratio has here been allowed to exceed 1. Such high values of C/P have been shown in both culture (Van Bleijswijk *et al.* 1994) and in natural populations (Balch *et al.* 1992). Under the assumption that the C/P-ratio is proportional to the extent of leaking, the isotope fractionation can be estimated using Eq 2.19:

$$\varepsilon_p = \delta_e - \delta_f = \varepsilon_{d/b} + L(\varepsilon_f - \varepsilon_t) \tag{5.13}$$

Since C/P and possibly the "leakage" goes through a maximum this idea would accommodate the conflicting observations of increasing fractionation with increased growth rate as seen in the light limited cultures of Thompson and Calvert, (1995) and

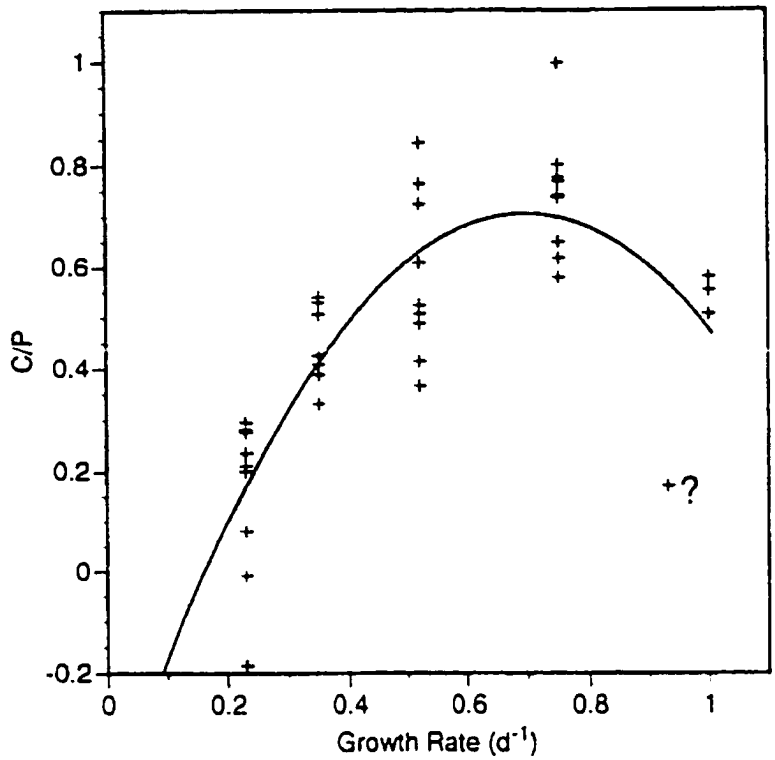

Figure 5.28: Ratio of calcification to photosynthesis as a function of steady state light limited growth rate. Line represents a least-squares polynomial fit to all of the data. From Balch et al., *(1996).*

the increased fractionation with decreasing growth rate in the nitrate limited cultures of Bidigare *et al.*, (1997). The low growth rate in light limited cultures would then correspond to a C/P regime on the left side of the maximum and the higher growth rates in the nitrate limited cultures on the right side. There are, admittedly, other differences between the two data sets; for example, the cultures grown by Bidigare *et al.*, (1997) were nitrate limited which adds the complexity of enhanced calcification due to nutrient limitation.

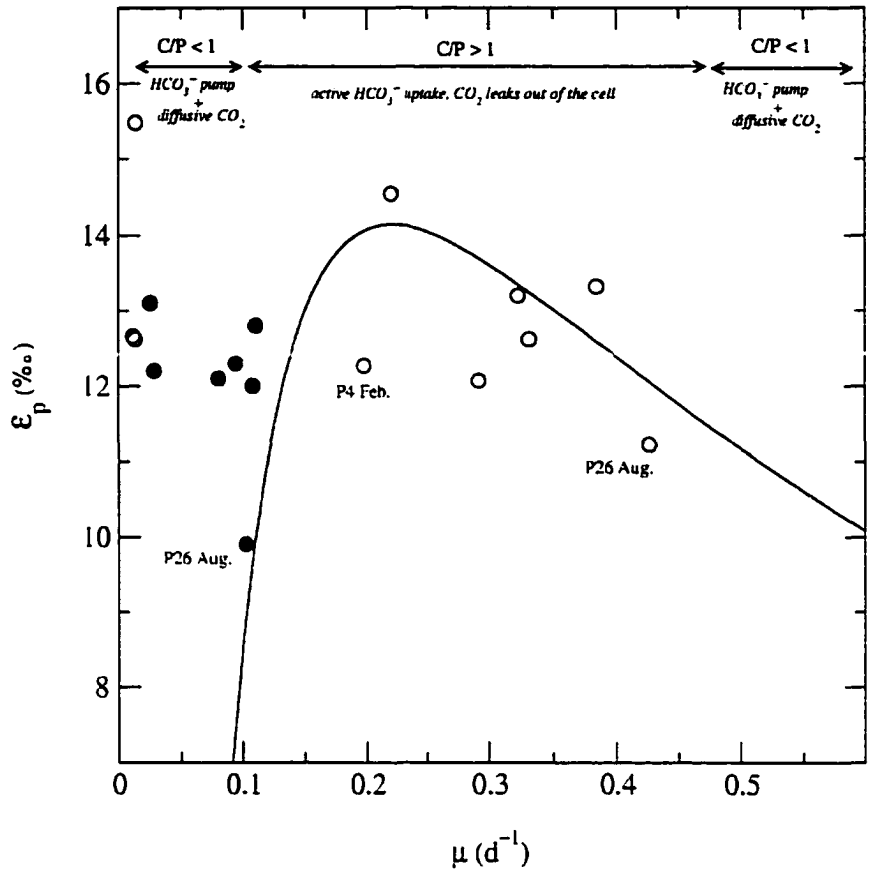

Figure 5.29: Comparison of "leakage" model with CJGOFS data.
In the growth rate interval between approx. 0.1 and 0.45 d^{-1} C/P is above 1 and the cells are subsequently leaking CO_2. At higher growth rates and when the growth rate is less than 0.1 d^{-1} the C/P is less than 1 and cells are no longer leaking and carbon may enter the cell by passive diffusion of CO_2 along with active uptake of HCO_3^-.

In Figure 5.29 the C/P curve is superimposed on the CJGOFS data from the mixed layer and at 1 % I_0. As seen in the figure, Station P26 in August for which the samples had a consistently low fractionation fits in on both sides of the C/P maximum, thus demonstrating two different reasons for similar ε_p. The samples from 1 % I_0 do not follow the curve down to low ε_p, but rather assume a fairly constant

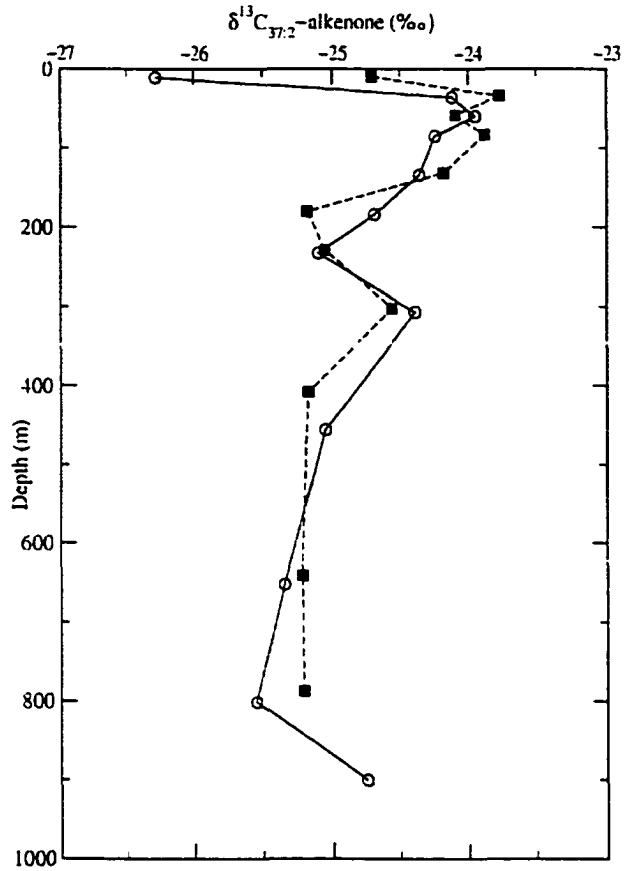

Figure 5.30: Station P12 in May and August 1996.
Isotope composition of $C_{37:2}$-alkenone as a function of depth. Filled squares: May, Open circles: August.

value between 12 and 13 °/₀₀. This may be because the calcification is too slow to contribute to the carbon transport and the cells acquire carbon by passive diffusion only. The extent of fractionation agrees with the two "zero-nitrate" stations P4 and P16 in August, which may reflect carbon assimilation without calcification, since calcification will cease when nitrate is completely depleted.

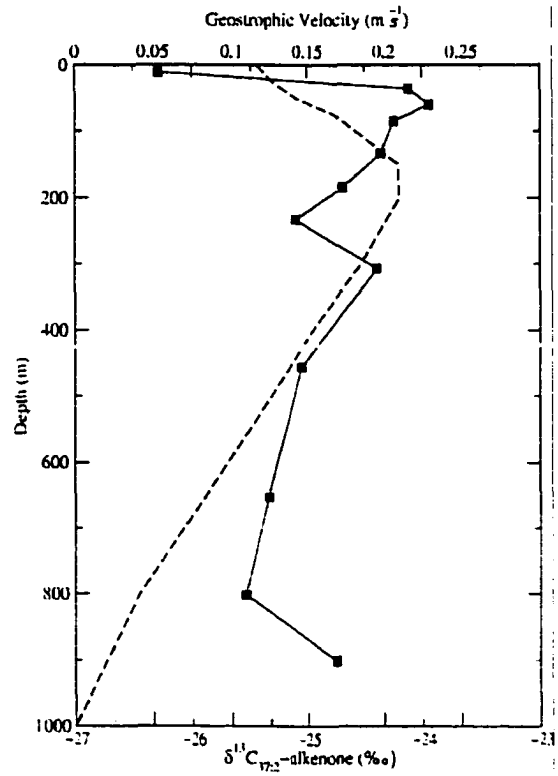

Figure 5.31: Geostrophic velocity between P4 and P12 in August is represented by the dashed line, the solid line and filled squares shows the isotope composition of the alkenones at Station P12.

5.4.6 Deep profiles

Two stations were extended below 135 m; Station P12 in May and August, where samples down to 800 and 900 meters depth were extracted, (Fig 5.30). Both profiles show a negative departure from the general trend between 180 to 300 m. On closer examination this departure was coinciding with a maximum in geostrophic velocity calculated between Station P12 and P4, (Fig. 5.31). At the depth in question there was a southward flow of 15 $km\ d^{-1}$ implying that the isotopically lighter material

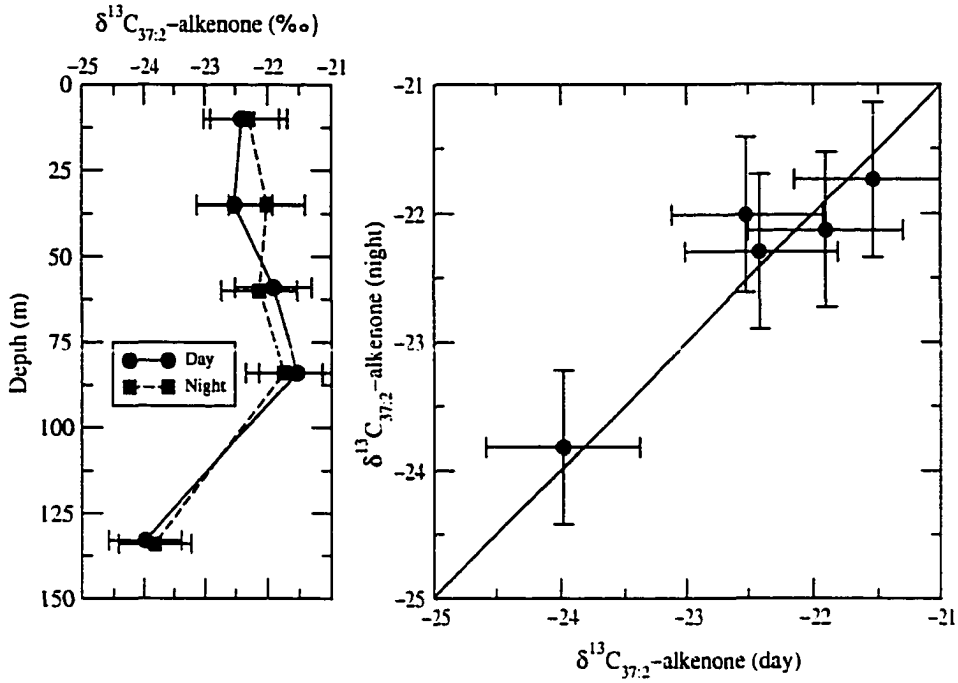

Figure 5.32: Station P26 in August 1996. Isotope composition of $C_{37:2}$-alkenone as a function of depth for two repeated casts 36 hours apart. Filled squares: Night samples, Filled circles: Day samples.

within this layer may be an integrated value of alkenones produced north of Line P.

5.4.7 Sampling reproducibility

During the August cruise of 1996 station P12 was occupied twice within 36 hours. The first cast was done during daylight while the following cast was done at night. Figure 5.32 show depth profiles of isotope composition of $C_{37:2}$-alkenone during the two casts. The profiles are virtually identical; the largest difference between the two casts is at 36 m where the day sample was 0.5 °/$_{oo}$ lighter than the night sample. The fact that there was very little difference between the two casts shows that there

are no diurnal changes in isotope signal within the top 135 m of the water column. A diurnal change in isotope composition may be expected if copepods were to ascend to the surface at night to graze, but since the copepod activity was minimal during the summer a diurnal cycling of the isotope composition of alkenones is unlikely. These stations can therefore be used to demonstrate the reproducibility of the sampling and analytical techniques. In fact, the results from this Station indicate that the estimated precision of the isotope measurenments, as decribed in Chapter One, may be too low.

5.5 Conclusions

The data presented here shows that the control of carbon isotope fractionation in the Prymnesiophyte algae in the North East Pacific is very complex and involves several environmental factors. The differences in fractionation between the mixed layer and at 1% I_0 suggests that light limitation decreases the fractionation contrary to what might be expected based on growth rate. This was previously shown by Thompson and Calvert, (1995) in cultured *Emiliania huxleyi* but this is the first field investigation to support their results. Furthermore, estimates of fractionation at depths below the compensation point appear to be similar for all stations regardless of season. A comparison of the average isotope composition in the euphotic zone with deeper samples at one station (P12) suggests that the isotope composition at depth

reflects a seasonal average of the alkenones produced in or near the euphotic zone. This reduced resolution will have no consequences for the sedimentary record of the isotope signal since sediment samples will have a resolution far less than annual.

The availability of nitrate is shown to play an important role in carbon isotope fractionation by prymnesiophytes, where the absence of nitrate causes the fractionation to depart from the previously demonstrated relationship between ε_p and $[PO_4^{3-}]/C_e$. Samples from nitrate depleted waters show a lower fractionation than that expected based on $[PO_4^{3-}]/C_e$ alone, and will therefore have serious implications for the validity of the ε_p calculation used to predict concentrations of dissolved CO_2.

Finally, a simplified model that assumes that *Emiliania huxleyi* cells leak CO_2 in proportion to the ratio of the rate of calcification to the rate of photosynthesis (C/P) may offer an insight into the complicated interaction between environmental parameters and carbon isotope fractionation in these, for paleo-climate studies, key-algae. The model presents the possibility that the fractionation in *Emiliania huxleyi* may have a maximum at an intermediate growth rate with the consequence that two different growth rates (a high and a low) could show the same carbon isotope fractionation. This dichotomy could have a serious impact on the interpretation of ε_p results.

Chapter 6

Pacific Transect from Victoria, B. C. to Guam: Control of Carbon Isotope Composition in Alkenones by Availability of Phosphate

6.1 Abstract

During the R/V Sonne cruise from Victoria, B.C. to Guam in September 1996, a total of 139 POM samples were collected along with 45 surface water samples for nutrient analysis. Lipids from 35 of the POM samples have been extracted, of which 29 contained sufficient amount of alkenones for isotope analysis. Carbon isotope compositions; $\delta^{13}C_{POM}$ and $\delta^{13}C_{37:2-alkenone}$, are reported here along with concurrent measurements of dissolved CO_2, phosphate and nitrate concentrations.

6.2 Introduction

The main objective for this cruise was to continuously measure the methane and carbon dioxide content in surface water across the Pacific. The cruise also presented an excellent opportunity to collect POM samples that, together with concurrent measurements of pCO_2, could be used to test the CO_2 dependency of carbon isotope fractionation in *E. huxleyi*. The samples reported here span a distance of over 5100 km and represent a North-East to South-West cross section of the North Pacific (Fig. 6.1). Most of the samples that contained sufficient amounts of alkenones for isotope analysis where collected in waters with low nutrient levels. This is consistent with the notion that *E. huxleyi* is well adapted to low nutrient conditions (Brand 1994), and

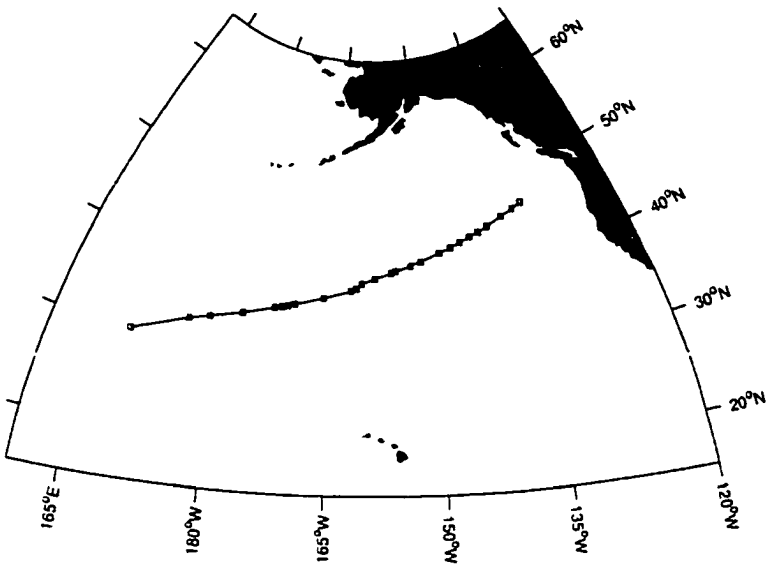

Figure 6.1: Sample locations during the Pacific Transect onboard R/V Sonne

especially to low phosphate levels - which is believed to be a possible trigger factor for *E. huxleyi* blooms (Townsend *et al.* 1994). This data set is especially valuable because it represents the conditions at which *E. huxleyi* is most likely to grow. The data also provide an opportunity to compare $\delta^{13}C_{POM}$ to $\delta^{13}C_{37:2-alkenone}$ from the same samples and thereby give an insight into the carbon isotope fractionation of *E. huxleyi* relative to the carbon isotope fractionation of whole population of phytoplankton.

6.3 Results

6.3.1 Environmental Conditions

This transect followed a South westerly course from Victoria, B.C. to Guam. Temperature and salinity increased continuously along the track. Temperature increased from 17.6 °C to 26.7 °C, while salinity increased by 2 ppt from 32.61 to 34.64 ppt (Fig. 6.2.)

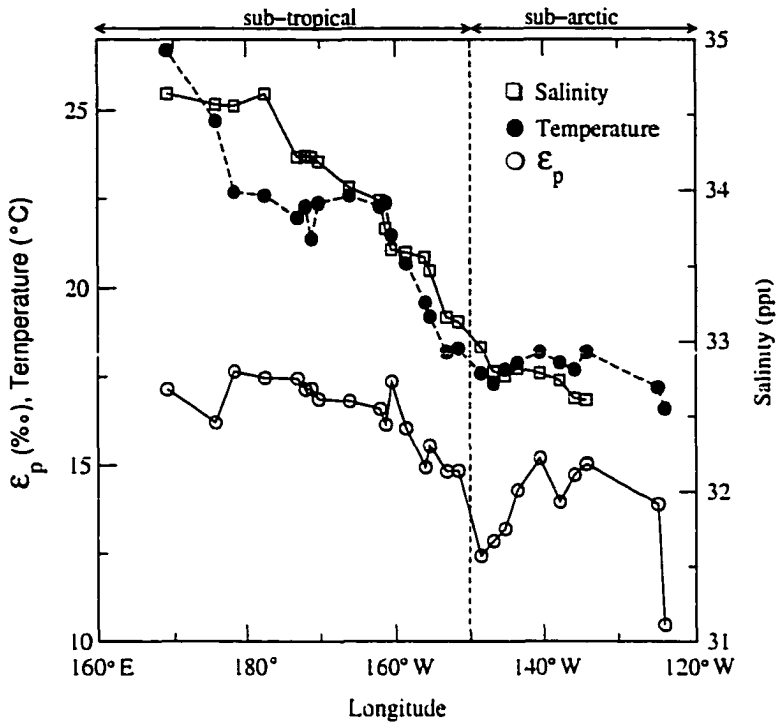

Figure 6.2: Carbon isotope fractionation, temperature and salinity vs *longitude for SO112. ε_p - solid line with open circles. Temperature - dashed line with filled circles, Salinity - solid line with filled diamonds.*

pCO_2 in the surface water was measured every 20 minutes during the entire cruise (see Chapter 3), amounting to approximately 72 measurements daily. From the pCO_2 measurements concentrations of dissolved CO_2 (C_e) was calculated using Henry's law with coefficients according to Weiss, (1974). Concentrations of C_e varied between 13.4 and 10.6 μM. The lowest C_e concentrations are found in the warm South-west (Fig. 6.3). Concentrations of phosphate and nitrate varied in a similar manner to that of C_e, with higher concentrations in the North east (Fig. 6.3). This trend is possibly due to upwelling along the North American continent. Phosphate concentrations range between 0.41 and 0.02 μM, and the nitrate concentration between 1.09 and 0.05 μM. Although the nutrient concentrations are higher in the North-east they are

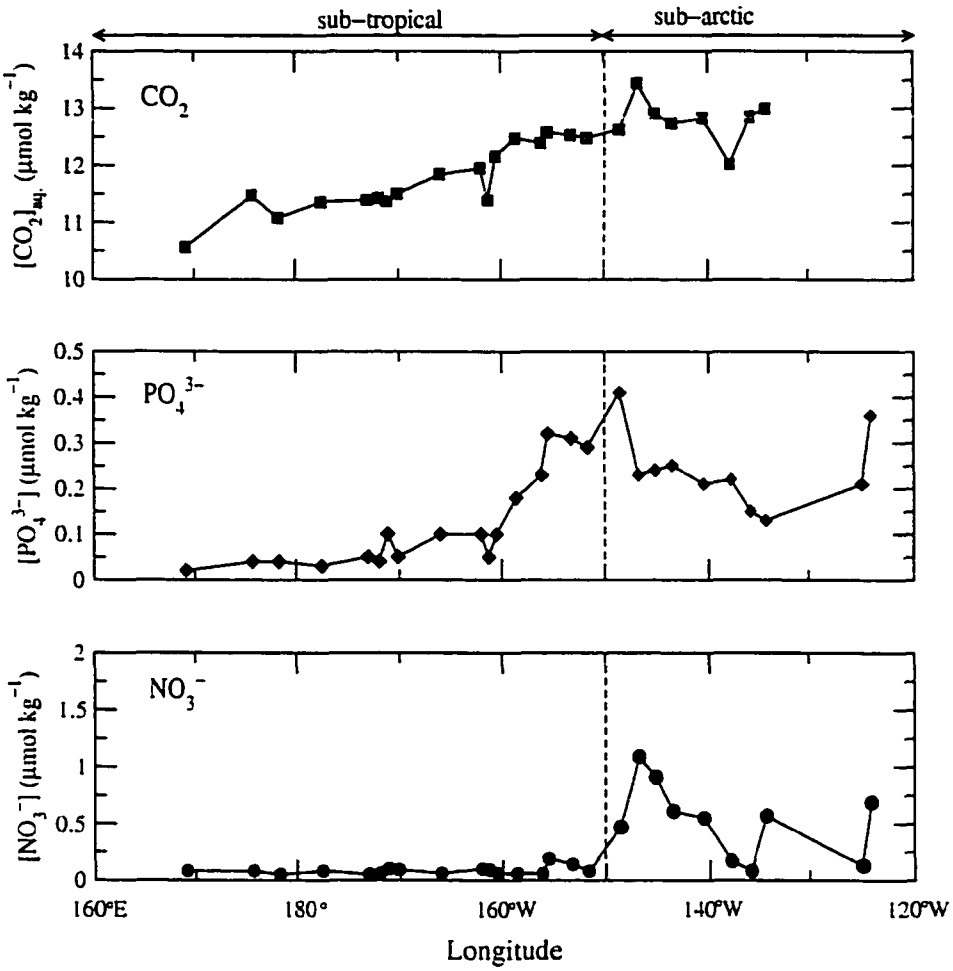

Figure 6.3: Concentration of dissolved CO_2 and macro nutrients at the isotope sample locations along the transect.

still quite low. The waters in the whole data set can be considered to be nutrient deficient, especially west of 150°W. West of this point the concentrations of nitrate are less than the half-saturation constant ($K_{0.5}$) of 0.1 μM for *Emiliania huxleyi*. Overall, the concentration of nitrate is lower than the half-saturation constants determined for nitrate uptake in the sub-arctic (4.21 μM NO_3^-) and tropical Pacific (0.1-0.7 μM NO_3^-) respectively (MacIsaac and Dugdale 1969). Since the transect passes through the transition from sub-arctic to sub-tropical conditions, predictions of nutrient uptake based on the characteristics of the two areas may be inaccurate.

6.3.2 Carbon Isotope composition of POM and $C_{37:2}$-alkenone

The carbon isotope composition of $C_{37:2}$-alkenone follows a trend with ^{13}C-enriched values in the North-east where the nutrient concentrations are higher and ^{13}C-depleted values in the nutrient depleted South-west (Fig. 6.4). The $\delta^{13}C_{37:2}$ values range between -23.2 °/$_{oo}$ and -27.7 °/$_{oo}$, a greater variation than the particulate organic matter which shows much less variation. The range for POM is only about 2.1 °/$_{oo}$ between -21.2 °/$_{oo}$ and -23.3 °/$_{oo}$. POM also differs from the alkenones by showing an opposite trend relative the alkenones in the warmer waters where $\delta^{13}C_{POM}$ becomes more enriched in ^{13}C. This results in an increase in the difference between the isotope composition of alkenones and bulk organic carbon increases the South west.

6.3.3 Isotope composition of Dissolved Inorganic Carbon

To produce an estimate of the isotope composition of dissolved CO_2, estimates of total CO_2 and total alkalinity were calculated. These are based on the temperature relationships presented by Kroopnick, (1985). On the basis of GEOSECS data for surface waters ($\leq$ 100 m), Kroopnick showed that ΣCO_2 and T_{ALK} are linearly

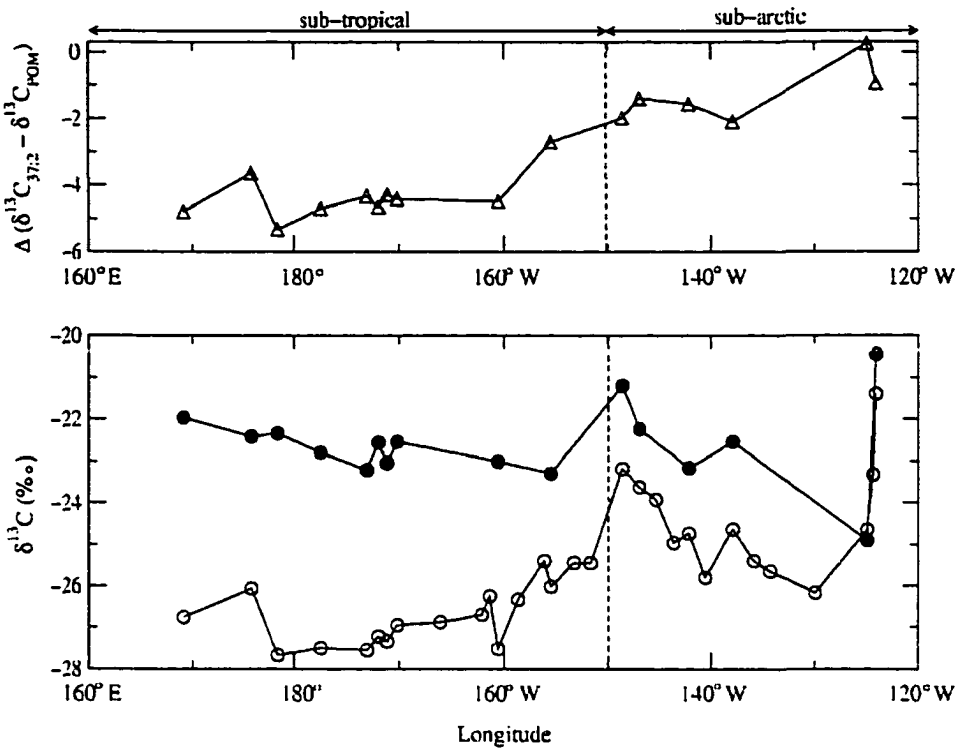

Figure 6.4: Isotopic composition (°/₀₀ relative PDB) of particulate organic matter and $C_{37:2}$-alkenones at 5 meters depth along the transect. Bottom panel shows isotope compositions with $\delta^{13}C_{POM}$ as solid circles and and $\delta^{13}C_{37:2}$ as open circles, top panel shows the difference between the two.

correlated with temperature. These relationships can be summarized as:

$$\Sigma CO_2 = -10.36 \cdot T + 2233 \tag{6.1}$$

$$T_{ALK} = -2.84 \cdot T + 2372 \tag{6.2}$$

By using the estimated values of ΣCO_2 and T_{ALK} the speciation within the carbonate system can be calculated (see Chapter 3, Methods). A comparison of the estimated and the measured C_e values shows an average error in the estimated values of 0.4 μM with a standard deviation of $\pm$ 0.3.

To calculate the isotopic composition of the dissolved CO_2, $\delta^{13}C_{DIC}$ has to be

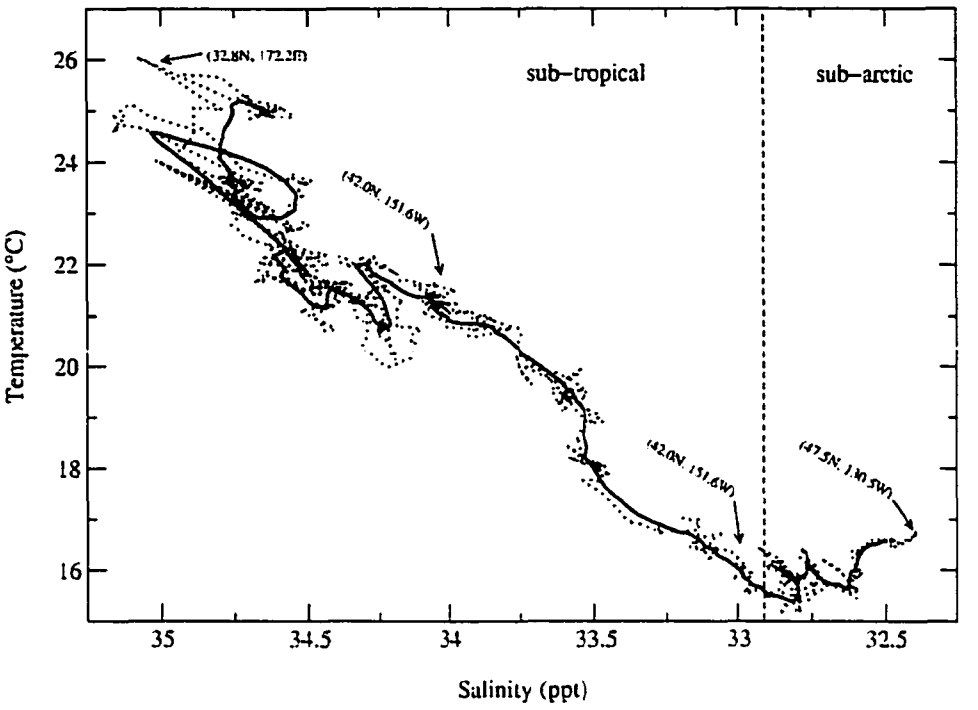

Figure 6.5: Temperature-Salinity relationship along the transect. The sub-arctic waters are characterized by an decreasing salinity as temperature increases, while for the sub-tropical water salinity is increasing with increasing temperature.

known. Since values of $\delta^{13}C_{DIC}$ do not vary systematically with temperature and the range in surface waters is only about 0.8 $^{\circ}/_{\circ\circ}$ (Kroopnick 1985), a value for $\delta^{13}C_{DIC}$ $of + 1.5^{\circ}/_{\circ\circ}$ was used to estimate $\delta^{13}C_{CO_2}$.

6.4 Discussion

6.4.1 Sub-arctic vs Sub-tropical

The transition between sub-arctic and sub-tropical conditions along the transect was clearly shown by the relationship between temperature and salinity (Fig. 6.5). Between 130° W and 150° W temperature decreased with salinity while west of 150°

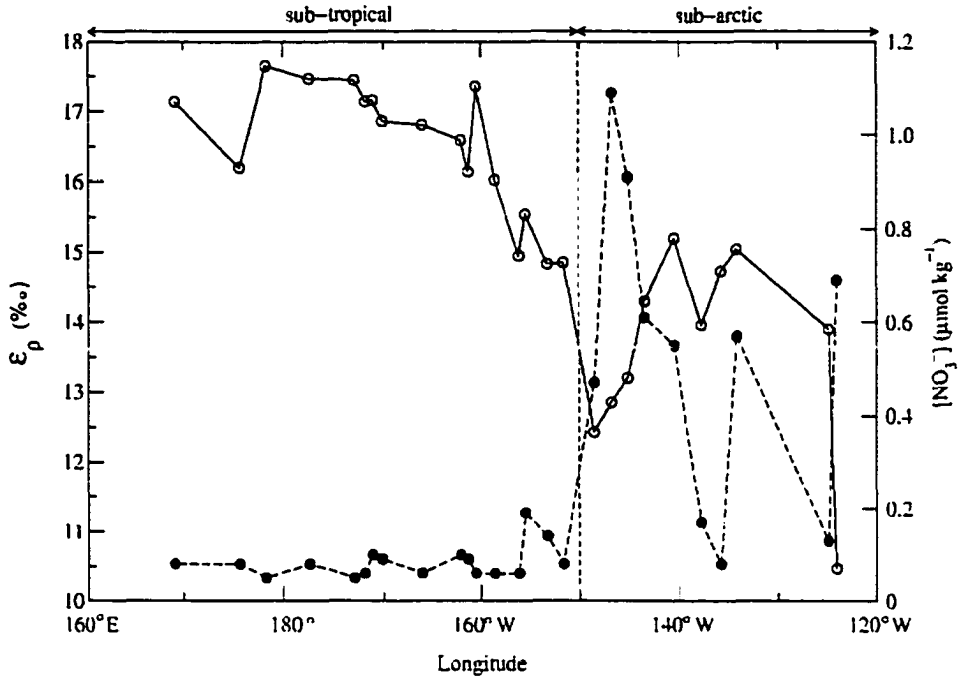

Figure 6.6: Nitrate concentration (filled circles) relative carbon isotope fractionation (open circles) along the cruise track.

W an opposite trend was observed (Fig. 6.5). The location of this transition could also be seen in the estimated isotope fractionation, ε_p (Fig. 6.2) as well as in the nitrate concentration (Fig. 6.6). Phosphate concentration however, did not change as abruptly as ε_p or nitrate (Fig. 6.7), and remained high until 160°W. This may indicate that the low nitrate between 150° W and 160° W was a consequence of late summer depletion rather than the general oligotrophic conditions. This region therefore constitutes a "transition-zone" characterized by higher nutrient concentrations and high sea water temperatures. As shown in Figure 6.8, the beginning of the transect crossed on a shallow angle along the more productive sub-arctic region. Therefore a higher nutrient concentrations would be expected east of 160° W. However, based on the Temperature-Salinity relationship the transition from sub-arctic to sub-tropical conditions is in the following discussion assumed to occur at 150° W. In contrast to

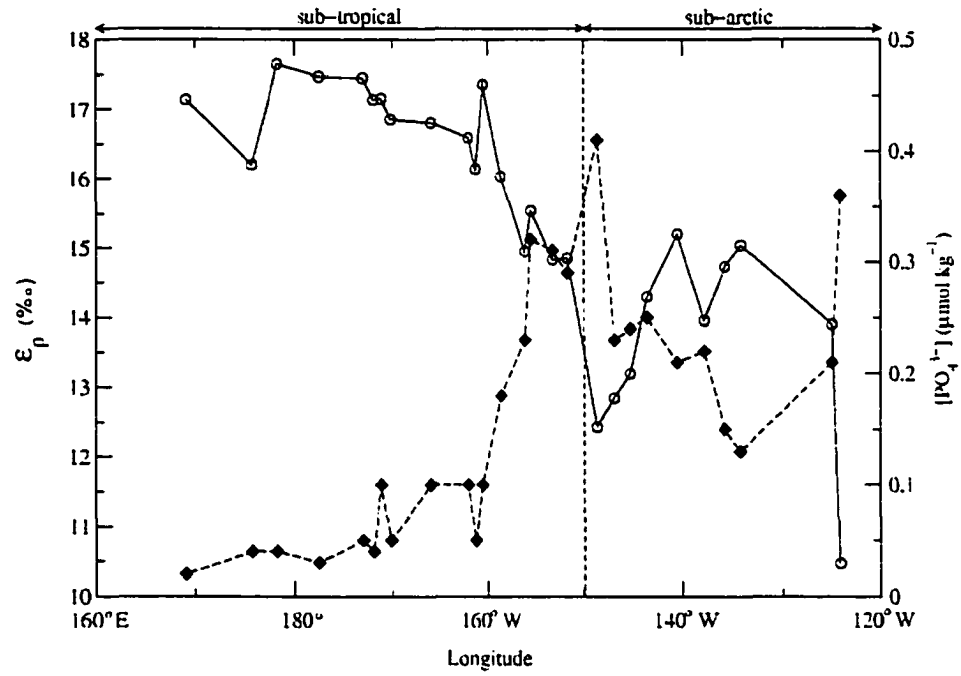

Figure 6.7: Phosphate concentration (filled diamonds) relative carbon isotope fractionation (open circles) along the cruise track.

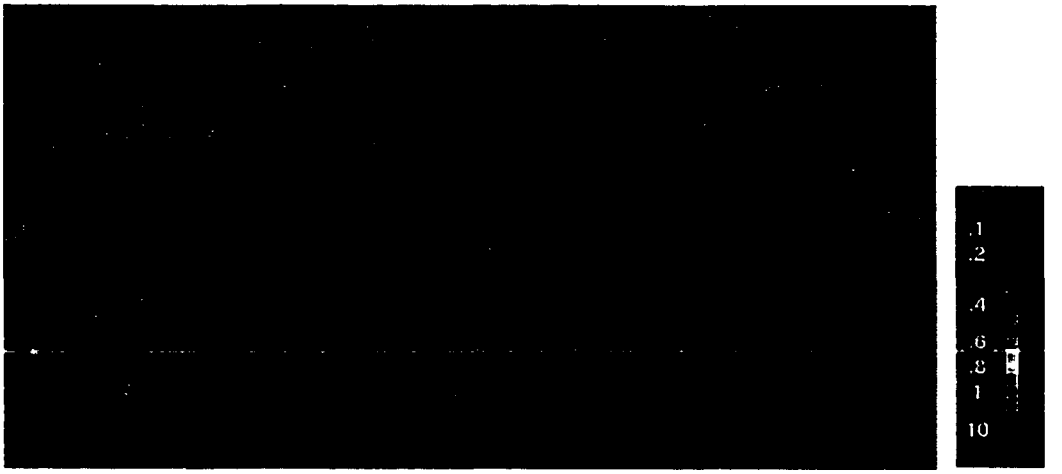

Figure 6.8: Satellite image of ocean color in the Pacific from the SeaWifs project. The data shown is acquired by the satellite Nibmbus-7 from November 1978 to June 1986. An approximation of the cruise track is indicated. The bar to the right shows the color scale of phytoplankton pigment concentration (mg m^{-3}).

the other parameters, dissolved CO_2 did not exhibit any shift coinciding with the assumed transition (Fig. 6.9), but slowly decreased with increasing temperature. It is interesting to note that dissolved CO_2 decreases while fractionation is increases along the cruise track. If the concentration of dissolved CO_2 were controlling carbon isotope fractionation in *Emiliania huxleyi* then the opposite would be expected, i.e. a decrease in isotope fractionation with decreasing CO_2 concentration.

The south-westerly course of the transect meant that surface irradiance increased as the ship approached Guam. Unfortunately, no measurements of irradiance were made during this cruise, so the surface irradiances shown in Figure 6.10 are estimates based on satellite data from the SeaWifs project.* Data consist of monthly averages for September at locations on a 2.5° x 2.5° grid of the earth and are here averaged over a time period from 1983 to 1990. The Seawifs data are not contemporaneous with the cruise, but more importantly the variation between different years was quite high,

*http://www.giss.nasa.gov/data/seawifs/data/index

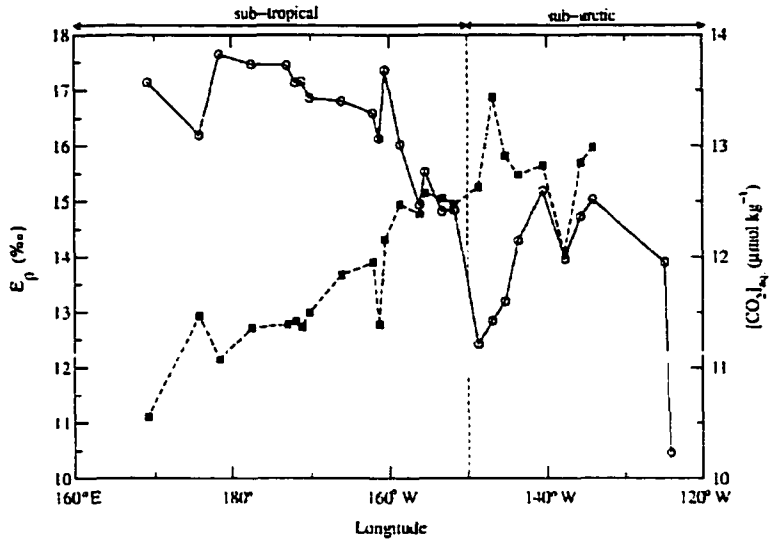

Figure 6.9: Dissolved CO_2 (filled squares) relative carbon isotope fractionation (open circles) along the cruise track.

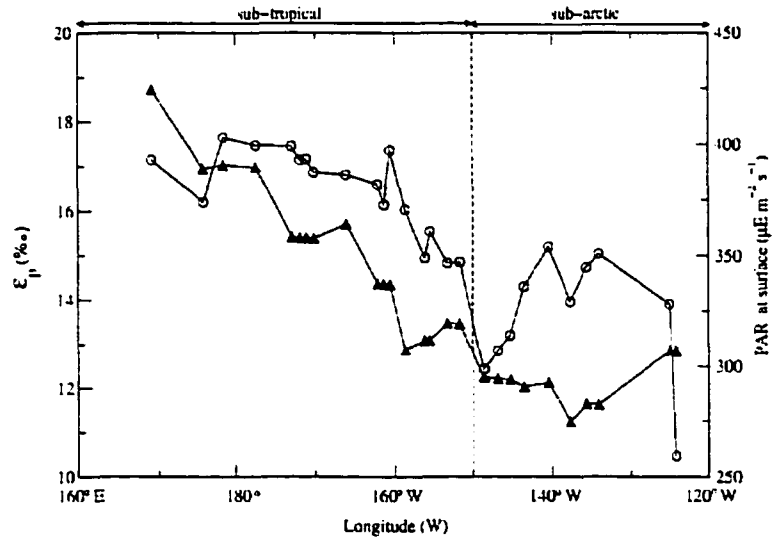

Figure 6.10: Surface Irradiance (filled triangles) relative carbon isotope fractionation (open circles) along the cruise track.

up to 20 % of the estimated value. This makes the absolute values less suitable for evaluation of the data presented here. The trend, however, clearly show an increase

of surface irradiance with decreasing latitude.

Studying an organism in two distinctly different environments leads to some concern. Are the environmental differences large enough and do they prevail long enough to cause natural selection to produce two different strains with different isotope fractionation characteristics within the separate environments? In this case, the two environments differ in respect to both temperature and nutrient availability.

6.4.2 Environmental parameters along the transect

Dissolved Carbon dioxide

Figure 6.11 shows ε_p plotted against the water-column parameters. In panel A, concentration of dissolved CO_2 shows no correlation with ε_p for the samples collected in sub-arctic waters. In the sub-tropical region there is a trend towards increasing ε_p with decreasing CO_2 concentration. The lack of correlation with the sub-arctic samples is consistent with the previously described results from the NE Pacific (CJGOFS). However, the trend in the sub-tropical region is the opposite to what would be expected if the cells were relying on passive diffusion of CO_2 as supply of carbon for photosynthesis. If on the other hand the cells were leaking CO_2 then a decreased external CO_2 concentration would amplify the gradient between the inside and outside the cell. Hence a decreased C_e could increase the leakage and consequently increase the fractionation (see Chapter 2). To test this hypothesis ε_P is plotted versus both $[PO_4^3-]$ and $[PO_4^3-]/C_e$ in Figure 6.12. A linear regression for both cases have a r^2 which is virtually the same (r^2= 0.82 and 0.81 respectively). With the data from the Pacific Transect, CO_2 appears not to have any influence on the ε_p *vs.* $[PO_4^3-]/C_e$ relationship. Therefore, it is more likely that the apparent trend between ε_p and CO_2 is caused by other factors that covary with CO_2.

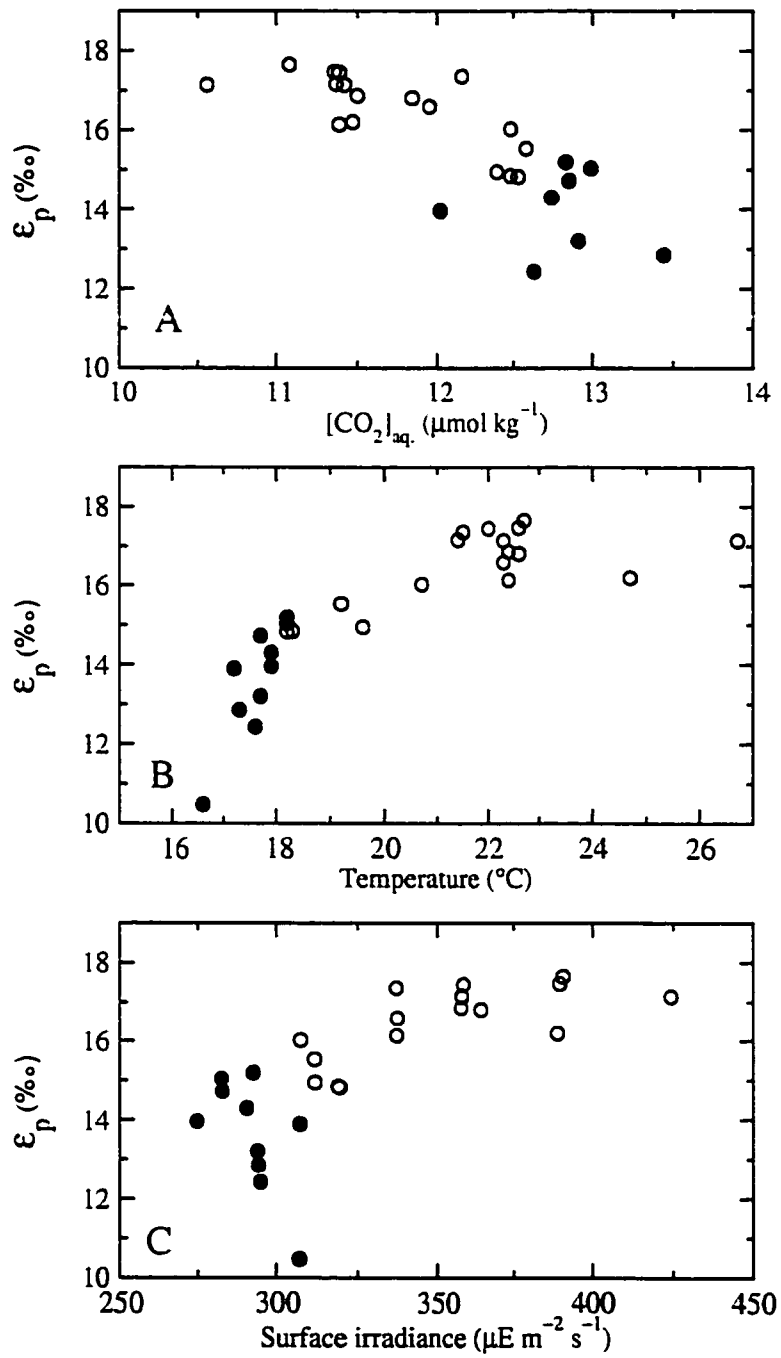

Figure 6.11: Dissolved CO_2, temperature and surface irradiance vs. ε_p. *Sub-arctic samples: filled circles, sub-tropical samples: open circles.*

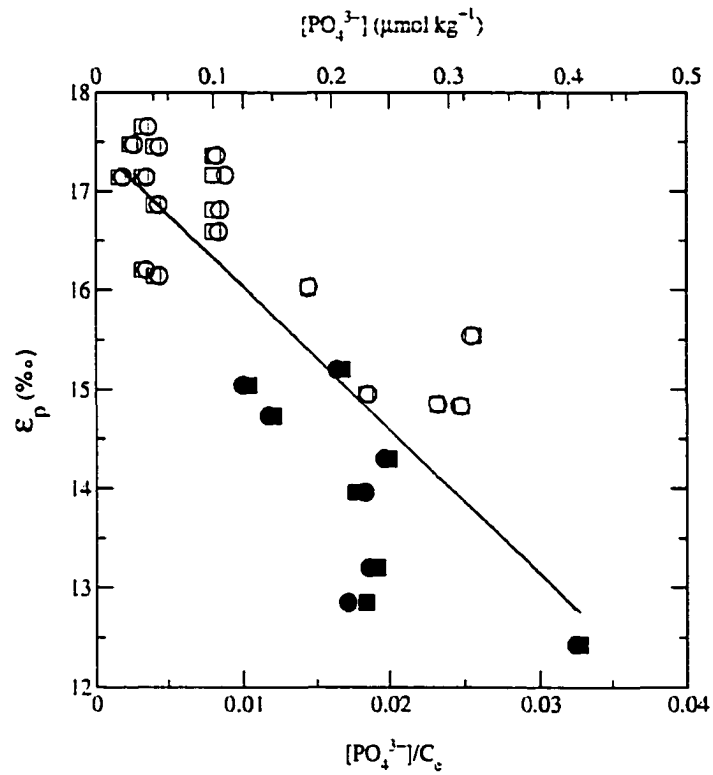

Figure 6.12: Comparison of ε_p vs $[PO_4^{3-}]/C_e and [PO_4^{3-}]$. Squares: $[PO_4^{3-}]$, circles: $[PO_4^{3-}]/C_e$, Filled symbols: Sub-arctic samples, open symbols: sub-tropical samples.

Temperature

Temperature shown in panel B (Fig. 6.11) displays a similar behavior with ε_p, i.e. an increasing trend with increasing temperature with a different slope for the sub-arctic samples relative the sub-tropic samples. There are several ways temperature can influence carbon isotope fractionation. It has an effect on the $\delta^{13}C_{Ce}$ at equilibrium with $\delta^{13}C_{DIC}$ with about 0.1 $^{\circ}/_{\circ\circ}$ per degree Celsius. This would in this case cause a shift of about 1 $^{\circ}/_{\circ\circ}$ over the temperature range and does not explain the 6-7$^{\circ}/_{\circ\circ}$ change in carbon isotope fractionation seen in the data. Temperature also increases the diffusitivity of CO_2 which could affect the transport of CO_2 out of the cell and thereby increase the leakage and subsequently the isotope fractionation (see Chapter 2). Growth rate of *Emiliania huxleyi* is a function of temperature, e.g. the optimal temperature for an isolate from the NE Pacific is 16°C (Muggli and Harrison 1996). Temperatures above optimal will, if the cells are relying on diffusive uptake of CO_2, lead to an increased isotope fractionation. In Figure 6.11, Panel C, the estimated surface irradiance shows a similar pattern.

Nutrients

In contrast, the nutrients, as shown in Figure 6.13, have a different relationship to ε_p. Both nitrate and phosphate are inversely correlated with ε_p. Although the relationship between ε_p and nitrate in the sub-arctic was quite weak, it is virtually non-existent in the sub-tropical region. The shift in slope for nitrate between sub-arctic and sub-tropical samples was similar to that of CO_2. For phosphate the slope appeared to change only slightly between sub-arctic and sub-tropical samples (Fig. 6.13, top panel). The more consistent trend implies that phosphate may be exerting the major control on the carbon isotope fractionation along the transect. This agrees with the notion that a high phosphate concentration (i.e. high growth rate and a balanced calcification-photosynthesis) should result in a low fractionation. Also

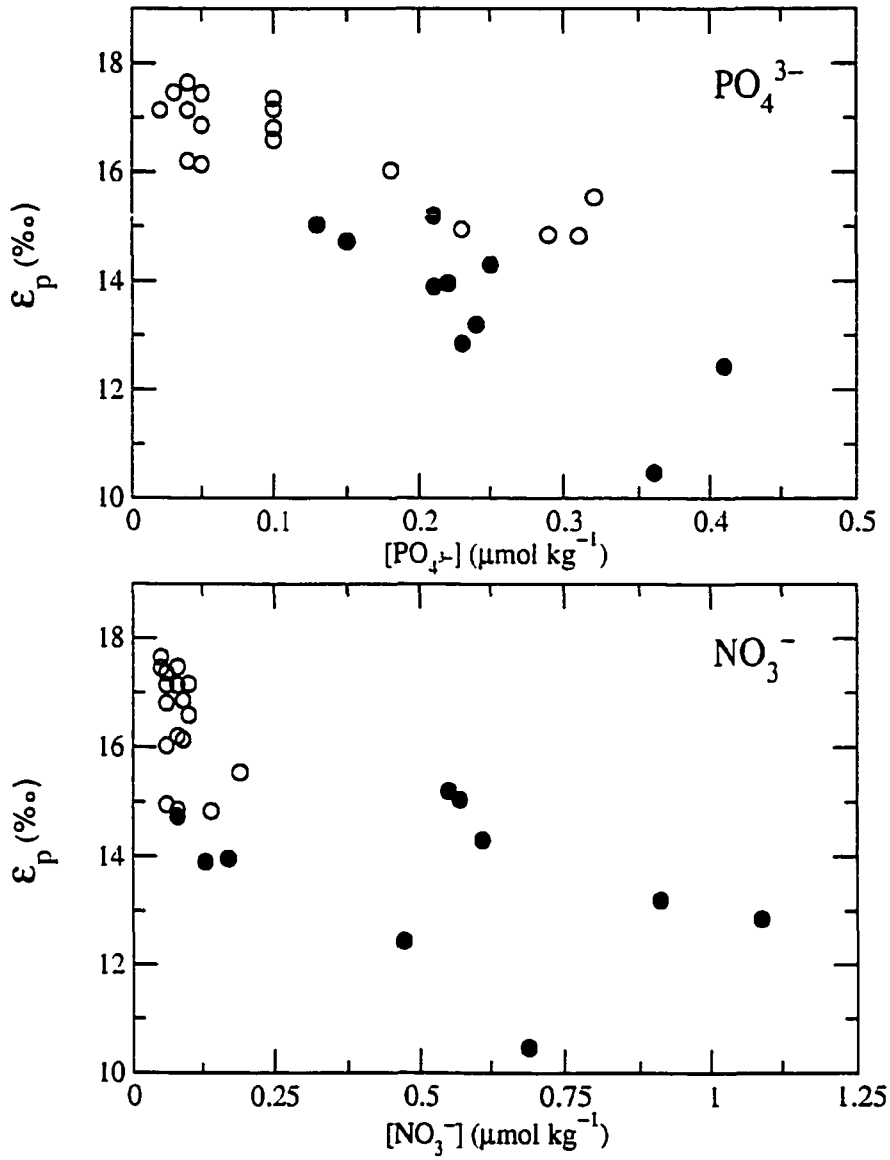

Figure 6.13: Concentration of nitrate (bottom panel) and phosphate (top panel) vs ε_p. Sub-arctic samples: filled circles, sub-tropical samples: open circles.

the samples with the highest fractionation have the lowest phosphate concentration (i.e. low growth rate and an imbalanced calcification-photosynthesis ratio). In the sub-tropical region the parameters that showed no relationship with ε_p in the sub-arctic, i.e. both dissolved CO_2 and temperature displayed a weak linear correlation. However, this may be a consequence of covariance with phosphate as shown in Fig. 6.14. Nitrate on the other hand did not seem to be correlated with ε_p in this region, however the range of nitrate concentration in the sub-tropical region was very narrow and the "resolution" of a ε_p-$[NO_3^-]$ relationship is therefore poor.

Therefore, it is possible that phosphate controls carbon isotope fractionation in both the sub-arctic and the sub-tropical region. This is confirmed by the negative relationship between phosphate concentration and ε_p along the cruise track (Fig. 6.15, *note that the scale for phosphate concentration is reversed*). This relationship can be caused by either a lowered growth rate with decreasing nutrient concentration resulting in an increased fractionation (Laws *et al.* 1995). However, nitrate, not phosphate, is generally considered to be the limiting nutrient in marine systems (Falkowski 1997). Nitrate concentration also shows a general agreement with ε_p but does not appear to follow the fractionation as closely as phosphate (Fig 6.16,*note that the scale for nitrate concentration is reversed*).

An alternative explanation to growth rate controlling ε_p is an imbalance in the calcification to photosynthesis ratio causing the pH in the cytosol to shift. Both nutrients can enhance calcification (Van Bleijswijk *et al.* 1994; Paasche and Brubak 1994; Anning *et al.* 1996; Paasche 1998) and it is therefore possible that the relationship seen between the nutrients and ε_p is a consequence of enhanced calcification. That phosphate appears to dominate is in agreement with observations showing a more dramatic increase in calcification under P-limitation than under N-limitation (Paasche 1998). McConnaughey and Whelan, (1997) suggested that calcification in calcifying algae serves as a mechanism to generate protons for nutrient uptake. The increased

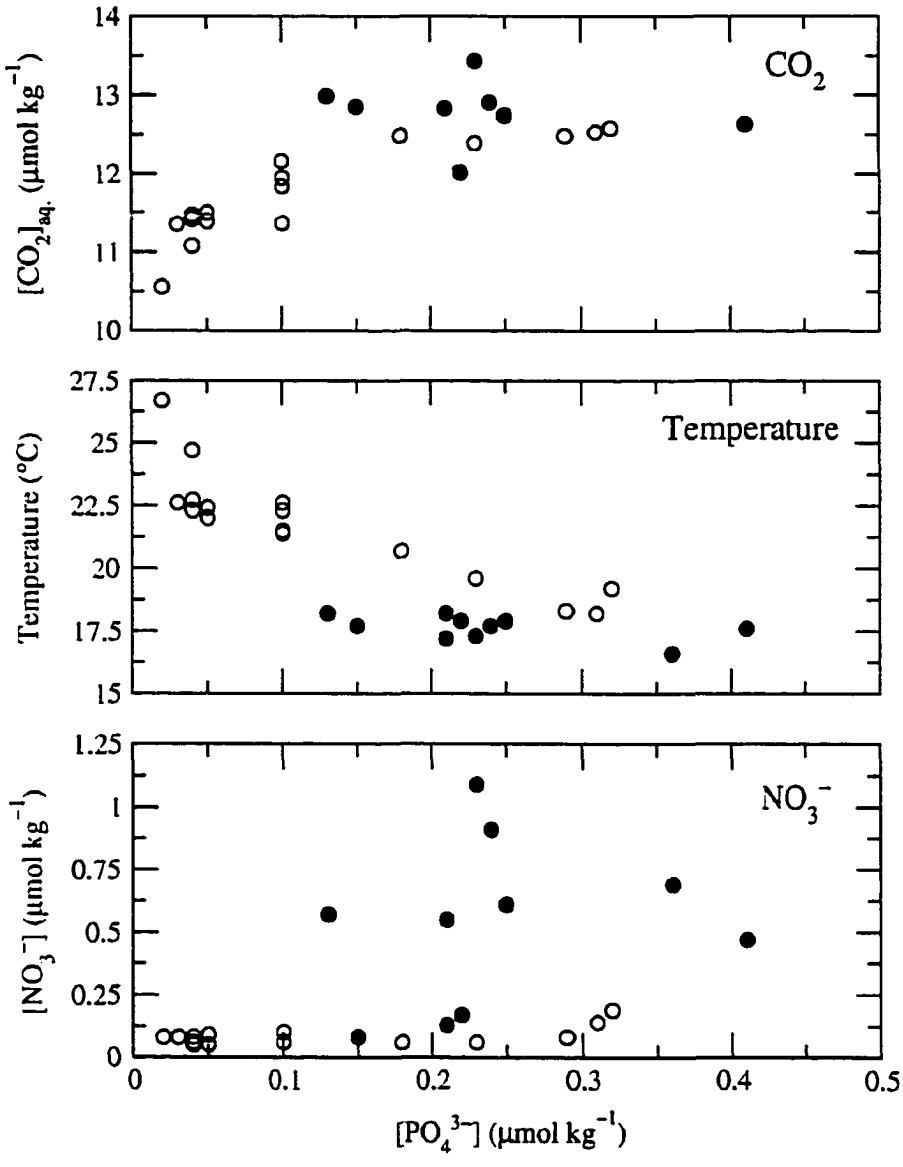

Figure 6.14: Dissolved CO_2, temperature and nitrate vs. phosphate. Sub-arctic samples: filled circles, sub-tropical samples: open circles.

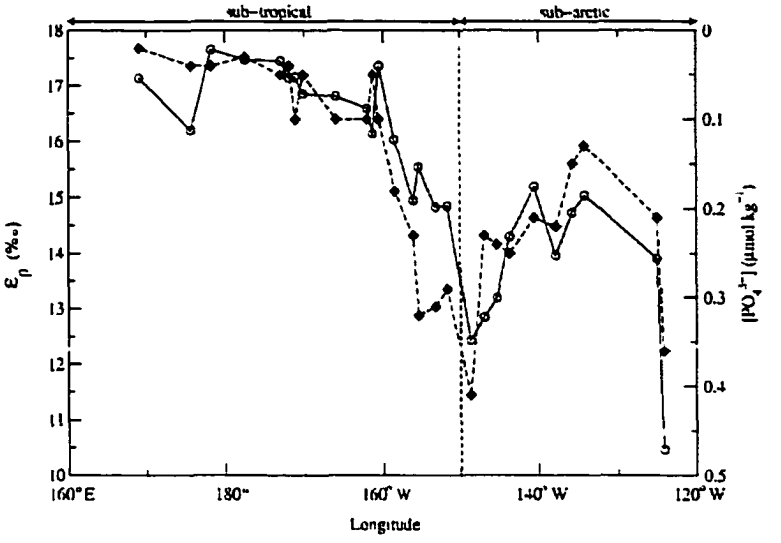

Figure 6.15: Carbon isotope fractionation and phosphate concentration along the transect. Note that the scale for the phosphate concentration is reversed. Sub-arctic samples: filled circles, sub-tropical samples: open circles.

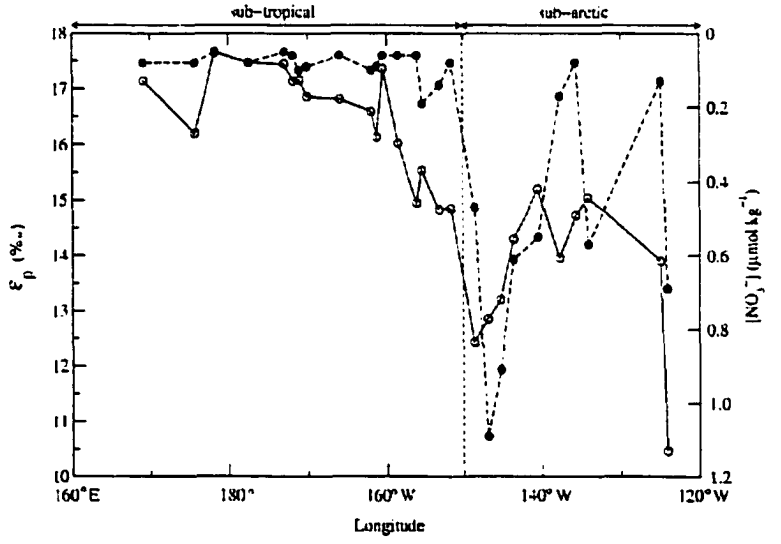

Figure 6.16: Carbon isotope fractionation and nitrate concentration along the transect. Note that the scale for the nitrate concentration is reversed. Sub-arctic samples: filled circles, sub-tropical samples: open circles.

calcification could therefore be a response to decreasing nutrient supply in order to enhance nutrient uptake. When calcification is enhanced relative to photosynthesis there will be an excess of protons from the formation of carbonate ions causing the cytosol to become more acidic. This will increase the internal CO_2 concentration and thus steepen the concentration gradient leading to a increased flux of CO_2 out of the cell. An increased leakage will lead to an increase of carbon isotope fractionation as discussed in Chapter 2.

6.5 Conclusions

First, these results may be an consequence of the consistently low levels of both nitrate and phosphate and the results should therefore be interpreted as applicable to a low nutrient environment. In an environment with more diverse nutrient conditions, other factors that affect the isotope fractionation will be superimposed on the nutrient effect seen here.

The data presented here show little or no influence of dissolved CO_2 on the magnitude of carbon isotope fractionation in alkenone producing phytoplankton. The weak relationship seen in the data contradicts the common notion of increased abundance of dissolved CO_2 should lead to increased isotope fractionation. Instead ε_p appears to be controlled by the availability of nutrients, and especially phosphate concentration. This is in agreement with the hypothesis previously presented earlier in this thesis of nutrient deficiency causing an imbalance in the calcification to photosynthesis ratio. This imbalance leads to an over-production of protons in the coccolith vesicle with acidification of the cytosol as a consequence. At a lower pH, the equilibrium concentration of dissolved CO_2 in the cytosol will increase and the concentration gradient over the cell membrane will become steeper. This change in concentration gradient

causes the diffusion of CO_2 out of the cell to increase and the ratio of carbon transported into the cell to the carbon diffusing out of the cell will approach unity, i.e. the leakage, L, is increasing (Eq. 2.19). As L increases the carbon isotope fractionation will become larger. The weak inverse relationship with dissolved CO_2 could also be explained with this theory, in that external dissolved CO_2 affects the diffusion gradient. High levels of external CO_2 will decrease the extent of leakage by limiting the diffusion out of the cell and thereby causing the carbon isotope fractionation to decrease.

Chapter 7

Implications for paleo-PCO_2 barometry

7.1 Carbon transport

The basic premise for paleo-PCO_2 barometry is the variation in the magnitude of the isotope effect associated with carbon assimilation in marine phytoplankton. The degree to which this isotope effect is expressed - the isotope fractionation - is dependent on the concentration of CO_2 surrounding the carbon fixing enzyme, Rubisco. This relationship between the concentration of CO_2 inside the cell and carbon isotope fractionation provides the gauge for the paleo-PCO_2 recorder. It should be noted here that this gauge represents the internal CO_2 concentration. Hence for phytoplankton to function as paleo-PCO_2 recorders the concentration of CO_2 inside the cell must be a known function of the concentration of CO_2 in the water surrounding the cell, i.e. $C_i = f(C_e)$. For this criteria to be fulfilled the phytoplankton must acquire carbon via passive diffusion, i.e. any mechanism to actively transport carbon into the cell will decouple carbon isotope fractionation from the external CO_2 concentration and the recorded isotope fractionation will not reflect the oceanic CO_2 concentration. Thus, organisms utilizing active carbon transport may not be suited for paleo-PCO_2 proxies. The mode of carbon uptake must therefore be carefully investigated before evaluating the potential of an phytoplankton as a paleo-PCO_2

recorder.

Plant physiological studies referenced in this thesis indicate that carbon assimilation in *Emiliania huxleyi* utilizes a complicated mechanism in which carbon for photosynthesis is supplied by the active transport of HCO_3^- associated with the production of coccoliths. Carbon uptake in this alga is therefore a complex interaction between calcification and photosynthesis, both responding individually to environmental conditions that produce a cellular carbon status which is the product of both processes.

This rather unique mechanism causes the carbon isotope fractionation to be decoupled from the external CO_2 concentration when the nutrient concentrations are low. As a consequence, the resulting a value of ε_p is decoupled from external CO_2, thus the paleo-PCO_2 barometer based on $C_{37:2}$-alkenone will for these oceanic conditions give an incorrect estimate of paleo-PCO_2.

7.2 Implications of Changing Oceanic Conditions

The general equation by which paleo-PCO_2 barometry relates to CO_2 dissolved in surface water is written as (Jasper *et al.* 1994):

$$\varepsilon_p = a - \frac{b}{C_e} \tag{7.1}$$

where a is the intercept at which the isotope effect associated with the enzyme Rubisco is fully expressed. The factor b, or the slope of the curve, can be a function of auxiliary

factors influencing ε_p, i.e. $b = f(nutrients, irradiance)$.

In this thesis, I have confirmed previous observations (Fluegge 1994; Thompson and Calvert 1995; Bidigare *et al.* 1997; Eek *et al.* 1999), that the carbon isotope fractionation in natural populations of Prymnesiophyte algae are affected by the concentration of nutrients and the availability of light. My work also shows that at oligotrophic conditions the carbon isotope fractionation is independent of external CO_2 concentration and that light limitation affects carbon isotope fractionation for cells growing close to the compensation point. Below is a discussion of the possible implications this environmental influence will have for paleo-PCO_2 barometry.

Results reported in the previous chapters from both the North east Pacific and from the Pacific Transect shows the effect of varying nutrient concentrations on carbon isotope fractionation. The availability of dissolved phosphate demonstrates a profound influence, especially in oligotrophic waters, which has been summarized in Fig. 7.1. The linear regression of ε_p vs. $[PO_4^{3-}]/C_e$ can be expressed in an equation similar to the general equation used in paleo-PCO_2 barometry.

$$\varepsilon_p = 21.8 - 151.7 \cdot \frac{[PO_4^{3-}]}{C_e} \tag{7.2}$$

The constants are the intercept and slope respectively, from the regression line in Fig. 7.1. In order to evaluate the influence of phosphate on the estimates of PCO_2 resulting from paleo-PCO_2 barometry, fixed concentrations of phosphate can be multiplied with the slope value in Eq. 7.2 producing an equation where the factor

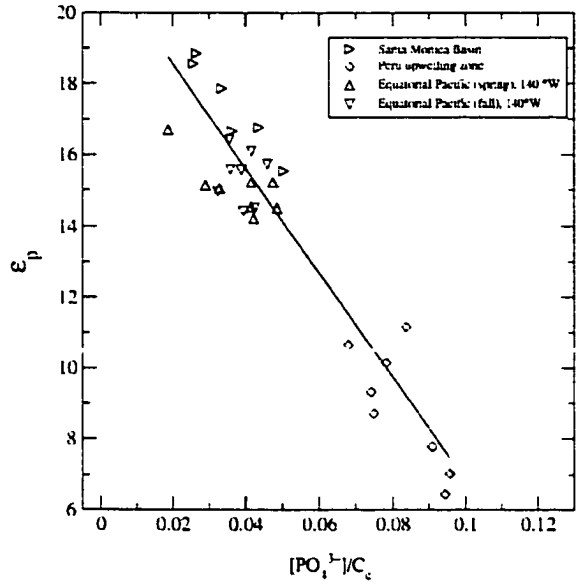

Figure 7.1: ε_p vs $[PO_4^{3-}]/C_e$ relationship Data from Bidigare et al., (1997). The line shows the linear regression of the data (r^2=0.93, $P \leq$ 0.01).

b is a function of phosphate. In Figure 7.2 the three solid lines represents Eq. 7.2 for phosphate concentrations of 0.1, 0.5 and 1.0 μM respectively. As illustrated by the example in the figure, ε_p is almost decoupled from the external CO_2 concentration when the phosphate concentration is 0.1 μM. An uncertainty in ε_p corresponding to the precision of the isotope measurements of $\pm$ 0.6 $^\circ/_{oo}$ results in an error in the estimated PCO_2 value of $\pm$ 126.5 μatm, which is more than half the atmospheric CO_2 concentration during glacial periods. If the phosphate concentration is increased to 1.0 μM, the slope becomes steeper indicating a stronger coupling of CO_2 with ε_p and the error in the PCO_2 estimate decreases to $\pm$ 10.5 μatm.

The shift from ε_p being nearly decoupled from CO_2 at low concentrations of

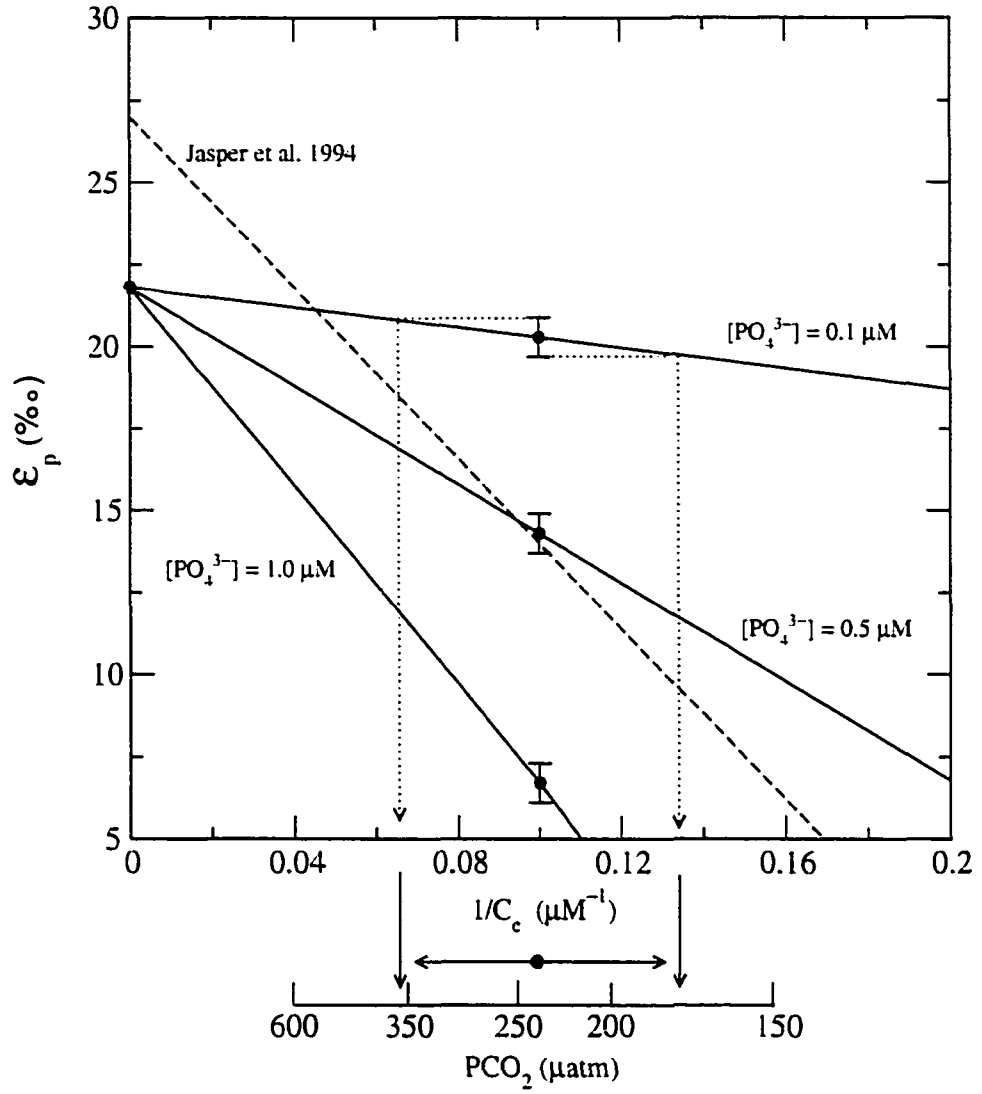

Figure 7.2: Evaluation of different phosphate concentrations on paleo-PCO_2 estimates. The solid lines represents the linear regression of Fig. 5.21 for different concentrations of phosphate. An example of the estimation of PCO_2 from ε_p is shown as a dotted line, where the error bars corresponds to a precision of ε_p of ± 0.6 °/₀₀. The PCO_2 scale is calculated with Henry's law using a salinity of 34 °/₀₀ and a temperature of 12 °C. The calibration curve from Jasper et al. 1994 is shown for comparison (dashed).

phosphate to a correlation between the two at phosphate concentrations above 0.5 μM could be a consequence of photosynthesis assimilating carbon at a rate faster than can be provided via the HCO_3^- pump and the auxiliary carbon is entering the cell via diffusion. An alternative explanation could be that photosynthesis is fast enough to reduce the internal CO_2 concentration to a value close to the external concentration, thus the flux of CO_2 out of the cell will be affected by the external concentration of CO_2.

In addition to the influence of nutrient concentrations at low levels, complete depletion of nitrate has shown to cause carbon isotope fractionation to decrease to values lower than predicted based on phosphate concentration. This drop in ε_p can be several permil. However, since nitrate and phosphate tend to covary, the phosphate concentration is generally very low when all nitrate is depleted and the carbon isotope fractionation is already decoupled from CO_2, making the effect of nitrate depletion less relevant in the evaluation of PCO_2.

It is interesting to note in Figure 7.2 the apparent maximal isotope fractionation indicated by the intercept of the ε_p vs. $[PO_4^{3-}]/C_e$ relationship. It is lower (21.8 $^\circ/_{oo}$) than the maximal isotope effect measured for Rubisco alone (27-30 $^\circ/_{oo}$). This may be caused by transport limitations, or it may be the result of an alternative enzyme (PEPC) operating in concert with Rubisco. A limitation of the apparent maximal fractionation has implications for paleo-PCO_2 barometry by modulating

the slope of the calibration curve, and thereby the errors in the estimated PCO_2 due to uncertainty in the determination of ε_p. For the calibration curve by Jasper et al. (1994), it was assumed that the maximal fractionation was the same as the maximal isotope effect of Rubisco. By using the maximal isotope fractionation from the ε_p vs. $[PO_4^{3-}]/C_e$ relationship instead leads to a calibration curve similar to that of the $[PO_4^{3-}] = 0.5\mu$M curve in Fig. 7.2. This is close to the estimate of $[PO_4^{3-}] = 0.4\mu$M by Fluegge (1994) for the samples used in the Jasper et al. (1994) calibration. The fact that the "apparent fractionation" is lower than the maximal isotope effect of Rubisco tend to lower the precision of the PCO_2 estimates.

In conclusion, *Emiliania huxleyi* is not well suited for paleo-PCO_2 estimations. In spite of producing the ideal biomarker, *E. huxleyi* does not fulfill the criteria for a paleo-PCO_2 proxy because it does not exclusively utilize passive carbon uptake.

The results presented in this thesis are consistent with a mechanism of carbon uptake which causes a decoupling between internal and external CO_2 concentrations at low nutrient concentrations. As a consequence, ε_p is independent of the concentration of dissolved CO_2 in oligotrophic waters.

References

Abelson, P. H., and T. C. Hoering, Carbon isotope fractionation in formation of amino acids by photosynthetic organisms, *Proceedings of the National Academy of Sciences*, *47*(5), 623–632, 1961.

Anderson, G. C., Subsurface chlorophyll maximum in the northeast pacific ocean, *Limnology and Oceanography*, 1969.

Anning, T., N. Nimer, M. J. Merrett, and C. Brownlee, Costs and benefits of calcification in coccolithophorids, *Journal of Marine Systems*, *9*, 45–56, 1996.

Aprin, N., W. A. Svec, and S. Liaaen-Jensen, New fucoxantin-related carotenoids from *Coccolithus huxleyi*, *Phytochemistry*, *15*, 529–532, 1976.

Arnelle, D. R., and M. H. O'Leary, Binding of carbon dioxide to phopsphoenolpyruvate carboxykinase deduced from carbon kinetic isotope effects, *Biochemistry*, *31*, 4363–4368, 1992.

Badger, M. R., T. J. Andrews, S. M. Whitney, M. Ludwig, D. C. Yellowlees, W. Leggat, and G. D. Price, The diversity and coevolution of Rubisco, plastids, pyrenoids, and chloroplast-based CO_2-concentrating mechanisms in algae, *Canadian Journal of Botany*, *76*, 1052–1071, 1998.

Balch, W. M., J. Fritz, and E. Fernandez, Decoupling of calcification and photosynthesis in the coccolithophore *Emiliania huxleyi* under steady-state light-limited growth, *meps*, *142*, 87–97, 1996.

Balch, W. M., P. M. Holligan, and K. A. Kilpatrick, Calcification, photosynthesis and growt of the bloom-forming coccolithophore *Emiliania huxleyi*, *Continental Shelf Research*, *12*, 1353–1374, 1992.

Barwell-Clarke, J., and F. Whitney, Institute of ocean sciences nutrient methods and analysis., *Tech. Rep. 182*, , Canadian Technical Reports in Hydrography and Ocean Sciences., 1996.

Baumann, F. G., I. H. D., and J. Gennaro, The inverse relationship between nutrient nitrogen concentration and coccolithcalcification in cultures of the coccolithophorid *Hymenomonas* sp., *Journal of Protozoology*, *23*, 253–256, 1978.

Beardall, J., Photosynthesis and photorespiration in marine phytoplankton, *Aquatic Botany*, *89*, 51–60, 1989.

Bell, M. V., and D. Pond, Lipid composition during growth of motile and coccolith forms of *Emiliania huxleyi*, *Phytochemistry*, *41*(2), 465–471, 1996.

Bentaleb, I., M. Fontugne, C. Descolas-Gros, C. Girardin, A. Mariotti, C. Pierre, and A. Brunet, C. nad Poisson, Organic carbon isotopic composition of phytoplankton and sea-surface pCO_2reconstructions in the Southern Indian Ocean during the last 50,000 yr, *Organic Geochemistry*, *24*(4), 399–410, 1996.

Bidigare, R. R., A. Fluegge, K. H. Freeman, K. L. Hanson, J. M. Hayes, D. Hollander, J. P. Jasper, L. L. King, E. A. Laws, J. Milder, F. J. Millero, R. Pancost, B. N. Popp, P. A. Steinberg, and S. G. Wakeham, Consistent fractionation of ^{13}C in nature and in the laboratory: Growth-rate effects in some haptophyte algae, *Global Biogeochemical Cycles*, *11*(2), 279–292, 1997.

Bishop, J. K. B., S. Calvert, and M. Soon, Spatial and temporal variability of POC in the Northeast Subarctic Pacific, *Deep-Sea Research 2*, *46*(11-12), 2699–2733, 1999.

Bishop, J. K. B., D. Schupack, R. M. Sherrell, and M. Conte, Multiple Unit Large Volume in-situ Filtration System (MULVFS) for sampling oceanic particulate matter in mesoscale environments., in *Mapping Strategies in Chemical Oceanography*, vol. 209 of *Advances in Chemistry Series*, edited by A. Zirino, 155-175 pp., American Chemical Soceity, Washington D. C., 1985.

Black, M., The systematics of coccoliths in relation to the paleontological record., in *The Micropaleontology of the Oceans*, edited by B. N. Funnell, and W. R. Reidel, 611-624 pp., Cambridge University Press, 1971.

Boyd, P., and P. J. Harrison, Phytoplankton dynamics in the NE subarctic Pacific, *Deep Sea Research II*, *46*, 2405–2432, 1999.

Brand, L. E., Genetic variability and spatial patterns of genetic differentiation in the reproductive rates of the coccolithophores *Emiliania huxleyi* and *Gephyrocapsa oceanica*, *LaO*, *27*(2), 236–245, 1982.

Brand, L. E., Physiological ecology of marine coccolithophorides, in *Coccolithophores*, edited by A. Winter, and W. G. Siesser, 39-49 pp., Cambridge University Press, 1994.

Brand, W. A., High precision isotope ratio monitoring techniques in mass spectrometry, *Journal of Mass Spectrometry*, *31*, 225–235, 1996.

Brownlee, C., M. Davis, N. Nimer, L. F. Dong, and M. J. Merrett, Calcification, photosynthesis and intracellular regulation in *Emiliania huxleyi*, in *Biomineralization 93, 7th International Symposium on Biomineralization*, vol. 2-3, edited

by D. Allemand, and J.-P. Cuif, 19-36 pp., Musée oceanographique, Monaco, 1995.

Buitenhuis, E. T., H. J. W. de Baar, and M. J. W. Veldhuis, Photosynthesis and calcification by *Emiliania huxleyi* (prymnesiophyceae) as a function of inorganic carbon species., *Journal of Phycology*, *35*, 949–959, 1999.

Bukry, D., Coccoliths as paleosalinity indicators - evidence from the Black Sea., in *The Black Sea - Geology, Chemistry and Biology.*, vol. Memoir 20, edited by E. T. Degens, and D. A. Ross, 353-633 pp., Amer. Asssn. Petrol. Geol., 1974.

Cadée, G. C., Macroaggregates of *Emiliania huxleyi* in sediment traps, *meps*, *24*, 193–196, 1985.

Christensen, T., Alger, in *Botanik II. Systematisk Botanik*, edited by T. W. Bocher, M. Lange, and T. Sorensen, Munksgaard, Copenhagen, 1962.

Conte, M. H., A. Thompson, D. Lesley, and R. P. Harris, Genetic and physiological influences on the alkenone/alkenoate versus growth temperature relationship in *Emiliania huxleyi* and *Gephyrocapsa oceanica*, *geocomics*, *62*(1), 51–68, 1998.

Crawford, D. W., and D. A. Purdie, Increase of pCO_2 during blooms of *Emiliania huxleyi*: Theoretical conciderations on the asymmetry between acuisition of HCO_3^- and respiration of free CO_2, *Limnology and Oceanography*, *42*(2), 365–372, 1997.

Davies, D. D., Control of and by ph, *Symp. Soc. Exp. Biol.*, *27*, 513–530, 1973*a*.

Davies, D. D., Metabolic control in higher plants, in *Biosynthesis and its Control in Plants*, edited by B. V. Milborrow, 1-20 pp., Academic, London, 1973.

Davies, D. D., The central role of phosphoenolpyruvate in plant metabolism, *Annual Reviews of Plant Physiology*, *30*, 131–158, 1979.

Descolas-Gros, C., and L. Oriol, Variations in carboxylase activity in marine phytoplankton cultures. β-carboxylation in carbon flux studies, *Marine Ecological Progress Series*, *85*, 163–169, 1992.

Dixon, G. K., C. Brownlee, and M. J. Merrett, Measurements of internal ph in the coccolithophore *Emiliania huxleyi* using 2',7'-bis-(2-carboxethyl)-5 (and -6)carboxyfluorescein acetoxymethylester and digital imaging microscopy, *Planta*, *178*, 443–449, 1989.

Dixon, G. K., and M. J. Merrett, Bicarbonate utilization by the marine diatom *Phaeodactylum tricornutum* Bohlin., *New Phytologist*, *109*, 47–51, 1987.

Dong, L. F., N. A. Nimer, E. Okus, and M. J. Merrett, Dissolved inorganic carbon utilization in relation to calcite production in *Emiliania huxleyi* (Lohmann) Kamptner, *New Phytologist*, *123*, 679–684, 1993.

Eek, M. K., M. J. Whiticar, J. K. B. Bishop, and C. S. Wong, Influence of nutrients on carbon isotope fractionation by natural populations of Prymnesiophyte algae in NE Pacific, *Deep Sea Research II*, *46*(11-12), 2863–2876, 1999.

Eppley, R. W., J. N. Rogers, and M. J. J., Half-saturation constants for uptake of nitrate and ammonium by marine phytoplankton., *LaO*, *14*, 912–920, 1969.

Epstein, B. L., S. D'Hondt, J. G. Quinn, J. Zhang, and P. E. Hargraves, An effect of dissoved nutrient concentrations on alkenone-based temperature estimates, *Paleoceanography*, *13*(2), 122–126, 1998.

Fairbanks, R. G., M. Sverdlove, R. Free, P. H. Wiebe, and A. W. H. Be, Vertical distribution and isotopic fractionation of living planktonic foramnifera from the Panama Basin, *Nature*, *298*, 841–844, 1982.

Falkowski, P. G., Species variability in the fractionation of ^{13}c and ^{12}c by marine phytoplankton, *Journal of Plankton Research*, *13*, *supplement*, 21–28, 1991.

Falkowski, P. G., Evolution of the nitrogen cycle and its influence on the biological sequestration of CO_2 in the ocean., *Nature*, *387*, 272–275, 1997.

Fluegge, A., Molecular-isotopic derivation of maps of sea-surface temperature and oceanic PCO_2 in the Eastern Equatorial Pacific, Master's thesis, Indiana University, 1994.

Francois, R., M. A. Altabet, R. Goericke, D. C. McCorkle, C. Brunet, and A. Poisson, Changes in the δ^{13}C of surface water particulate organic matter across the subtropical convergence in the S. W. Indian Ocean, *Global Biogeochemical Cycles*, *7*, 627–644, 1993.

Freeman, K. H., and J. M. Hayes, Fractionation of carbon isotopes by phytoplankton and estimates of ancient CO_2 levels, *Global Biogeochemical Cycles*, *6*(2), 185–198, 1992.

Fry, B., and E. B. Sherr, $\delta^{13}C$ measurements as indicators of carbon flow in marine and frash water ecosystems., *Contributions to Marine Science*, *27*, 13–47, 1984.

Glover, H. E., and I. Morris, Photosynthetic carboxylating enzymes in marine phytoplankton, *Limnology and Oceanography*, *24*(3), 510–519, 1979.

Goericke, R., and B. Fry, Variations of marine plankton $\delta^{13}C$ with latitude, temperature and dissolved CO_2 in the world ocean., *Global Biogeochemical Cycles*, *8*(1), 85–90, 1984.

Goericke, R., and B. Fry, Variations of marine plankton $\delta^{13}c$ with latitude, temperature and dissolved /coo in the world ocean, *Global Biogeochemical Cycles*, *8*(1), 85–90, 1994.

Goericke, R., and J. P. Montoya, Physiology of isotope fractionation in algae and cyanobacteria., in *Stable Isotopes in Ecology*, edited by K. Lajitha, and M. B., 187-221 pp., Blackwell Scientific, 1994.

Gostan, J., C. Lechuga-Deveze, and L. Lazzara, Does blue light affect the growth of *Chaetoceros protuberans* (bacillariophyceae)?, *Journal of Phycology*, *22*, 63–71, 1986.

Groom, S. B., and P. M. Holligan, Remote sensing of coccolithophore blooms., *Adv. Space Research*, *7*(2), 73–78, 1987.

Gutknecht, J., M. A. Bisson, and F. C. Tosteson, Effects of carbonic anhydrase, bicarbonate and unstirred layers, *The Journal of General Physiology*, *69*, 779–794, 1977.

Guy, R. D., G. C. Vanlerberghe, and D. H. Turpin, Significance of phosphophenolpyruvate carboxylase during ammonium assimilation: carbon isotope discrimination in photosynthesis and respiration by the n-limited green alga *Selenastrum minutum*, *Plant Physiology*, *89*, 1150–1157, 1989.

Haeckel, E., *Systematische Pylogenie der Protisten und Pflanzen*, Reimer, Berlin, 1894.

Haq, B. U., Calcareous nannoplankton, in *Introduction to Marine Micropaleontology*, edited by B. U. Haq, and A. Boersma, 79-107 pp., Elsevier, North Holland, 1978.

Harris, R. P., Zooplankton grazing on the coccolithophore *Emiliania huxleyi* and its role in inorganic carbon flux, *Marine Biology*, *119*, 431–439, 1994.

Harrison, P. J., R. E. Waters, and F. J. R. Taylor, A broad spectrum artificial seawater medium for coastal and open ocean phytoplankton, *Journal of Phycology*, *16*, 28–35, 1980.

Hayes, J. M., Factors controlling ^{13}c contents of sedimentary organic compounds: Principles and evidence, *Marine Geology*, *113*, 111–125, 1993.

Hellebust, J. A., and J. Terborgh, Effects of environmental conditions on the rate of photosynthesis and some photosynthetic enzymes in *Dunaliella tretiolecta*, *Limnology and Oceanography*, *12*(4), 559–567, 1967.

Hibberd, D. J., The ultrastructure and taxonmy of the Chrysophyceae and Prymnesiophyceae (Haptophyceae): a survey with some new observations on the ultra structure of the Chrysophyceae., *Bot. J. Linn. Soc.*, *72*, 55–80, 1976.

Hibberd, D. J., Prymnesiophytes (=Haptophytes), in *Phytoflagellates*, edited by E. R. Cox, 273-318 pp., Elsevier, North Holland, 1980.

Holligan, P. M., , and others., A biogeochemical study of the coccolithophore *Emiliania huxleyi*, in the North Atlantic., *Global Biogeochemical Cycles*, *7*(4), 879–900, 1993.

Holligan, P. M., T. Aarup, and S. B. Groom, The North Sea: Satellite colour atlas., *Continental Shelf Research*, *9*(8), 667–765, 1989.

Holligan, P. M., M. Viollier, D. S. Harbour, P. Camus, and M. Champagne-Philippe, Satellite and ship studies of coccolithophore production along a continental shelf edge., *Nature*, *304*, 339–342, 1983.

Jasper, J. P., and J. M. Hayes, A carbon isotope record of CO_2 levels during the late Quaternary, *Nature*, *347*, 462–464, 1990.

Jasper, J. P., J. M. Hayes, A. C. Mix, and F. G. Prahl, Photosynthetic fractionation of ^{13}c and concentrations of CO_2 in the eequatorial pacific during the last 255, 000 years, *Paleoceanography*, *9*, 781–798, 1994.

Jeffrey, S. W., and S. W. Wright, A new spectrally distinct component in preparations of chlorophyll *c* from preparations of *Emiliania huxleyi* (Prymnesiophysceae)., *Biochem. Biophys. Acta*, *894*, 180–188, 1987.

Katz, A., H. R. Kabach, and M. Avron, Na+/h$^+$ antiport in isolated plasma membrane vesicles from the halotolerant alga dunatinella salina, *Federation of European Biochemical Societies Letters*, *202*, 213–216, 1986.

Kirk, J. T. O., *Light and photosynthesis in aquatic ecosystems*, Cambridge University Press, second edition edition, 1994.

Klaveness, D., The flagellate cell, aberrant celltypes, vegetative propagation and life cycles, *British Phycology Journal*, *7*, 309–318, 1972.

Kroopnick, P. M., The distribution of ^{13}C in the world oceans, *Deep-Sea Research*, *32*, 57–84, 1985.

Laws, E. A., R. R. Bidigare, and B. N. Popp, Effect of growth rate and CO_2 on carbon isotopic fractionation by the marine diatom *Phaeodactylum tricornutum*, *LaO*, *42*(7), 1552–1560, 1997.

Laws, E. A., B. N. Popp, R. R. Bidigare, M. C. Kennicutt, and S. A. Macko, Dependence of phytoplankton carbon isotopic composition on growth rate and $[CO_2]_{aq}$.: Theoretical considerations and experimental results, *geocomics*, *59*(6), 1131–1138, 1995.

Leckrone, K. J., and J. M. Hayes, Efficiency and temperature dependence of water removal by membrane dryers, *Analytical Chemistry*, *69*, 911–918, 1997.

Leckrone, K. J., and J. M. Hayes, Water-induced errors in continous-flow carbon isotope ratio mass spectrometry, *Analytical Chemistry*, *70*, 2737–2744, 1998.

Lohmann, H., Die Coccolithophoridae, eine Monographie der Coccolithen bildenden Flagellaten, zugleich ein Betrag zur Kenntnis des Mittelmeerauftriebs., *Arch. Protistenk.*, *1*, 89–165, 1902.

MacCabe, B., The dynamics of ^{13}C in several New Zeeland lakes, Ph.D. thesis, University of Waikato, Hammilton, 1985.

MacIsaac, J. J., and R. C. Dugdale, The kinetics of nitrate and ammonia uptake by natural populations of marine phytoplankton., *Deep-Sea Research*, *16*, 45–57, 1969.

Marlowe, I. T., S. C. Brassell, G. Eglinton, and J. C. Green, Long-chain alkenones and alkyl alkeonates and the fossil coccolith record of marine sediments, *Chemical Geology*, *88*, 349–375, 1990.

Marshall, H. G., Observations of the vertical distribution of coccolithophores in the Northwestern Sargasso Sea., *Limnology and Oceanography*, *11*, 432–435, 1966.

McConnaughey, T. A., and J. F. Whelan, Calcification generates protons for nutrient and bicarbonate uptake, *Earth-Science Reviews*, *42*, 95–117, 1997.

McIntyre, A., and A. W. H. Bé, Modern coccolithophores in the Atlantic ocean - i. placolith and cyrtoliths., *Deep-Sea Research*, *14*, 561–597, 1967.

Merrett, M. J., L. F. Dong, and N. A. Nimer, Nitrate availability and calcite production in *Emiliania huxleyi* Lohmann., *European journal of Phycology*, *28*, 243–246, 1993.

Merritt, D. A., K. H. Freeman, M. P. Ricci, S. A. Studley, and J. M. Hayes, ?????, *Analytical Chemistry*, *67*, 2461–2473, 1995.

Morel, A., Available, usable and stored radiant energy in relation to marine photosynthesis, *Deep Sea Research*, *25*, 673–688, 1978.

Morel, A., L. Lazzara, and J. Gostan, Growth rate and quantum yield time response for a diatom to changing irradiances (energy and color), *Limnology and Oceanography*, *32*, 1066–1084, 1987.

Muggli, D. L., and P. J. Harrison, Effects of nitrogen source on the physiology and metal nutrition of *Emiliania huxleyi* grown under different iron and light conditions, *meps*, *130*, 255–267, 1996.

Nelson, J. R., and S. G. Wakeham, A phytol-substituted chlorophyll *c* from *Emiliania huxleyi*., *Journal of Phycology*, *25*, 761–766, 1989.

Nimer, M. A., G. K. Dixon, and M. J. Merrett, Utilization of inorganic carbon by the coccolithophorid *Emiliania huxleyi* Kamptner, *New phytologist*, *120*, 153–158, 1992.

Nimer, N., and M. J. Merrett, Calcification rate in *Emiliania huxleyi* Lohman in response to light, nitrate and inorganic carbon availability, *New Phytologist*, *123*, 673–677, 1993.

Nimer, N., and M. J. Merrett, Calcification rate in relation to carbon dioxide release, photosynthetic carbon fixation and oxygen evolution in *Emiliania huxleyi*, in *Biomineralization 93, 7th International Symposium on Biomineralization*, vol. 2-3, edited by D. Allemand, and J.-P. Cuif, 37-42 pp., Musée oceanographique, Monaco, 1995.

Nimer, N. A., C. Brownlee, and M. J. Merrett, Carbon dioxide availability, intracellular ph and growth rate of the coccolithophore *Emiliania huxleyi*, *Marine Ecology Progress Series*, *109*, 257–262, 1994*a*.

Nimer, N. A., L. F. Dong, Q. Guan, and M. J. Merrett, Calcification rate, dissolved inorganic carbon utilization and carbonic anhydrase activity in *Emiliania huxleyi*, in *Biomineralization 93, 7th International Symposium on Biomineralization*, vol. 2-3, edited by D. Allemand, and J.-P. Cuif, 43-49 pp., Musée oceanographique, Monaco, 1995.

Nimer, N. A., Q. Guan, and M. J. Merrett, Extra- and intra-cellular carbonic anhydrase in relation to culture age in a high-calcifying strain of *Emiliania huxleyi* lohmann, *New Phytologist*, *126*, 601–607, 1994*b*.

Nimer, N. A., and M. J. Merrett, Calcification and utilization of inorganic carbon by the coccolithophorid *Emiliania huxleyi*, *New Phytologist*, *121*, 173–177, 1992.

Nimer, N. A., and M. J. Merrett, The development of a CO_2-concentration mechanism in *Emiliania huxleyi*, *New Phytologist*, *133*(3), 383–389, 1996.

Ohkouchi, N., K. Kawamura, H. Kawahata, and H. Okada, Depth ranges of alkenone production in the central Pacific Ocean., *Global Biogeochemical Cycles*, *13*(2), 695–704, 1999.

Okada, H., and S. Honjo, The distribution of oceanic coccolithophores in the Pacific., *Deep-Sea Research*, *20*, 355–374, 1973.

Okada, H., and A. Mcintyre, Modern coccolithophores of the Pacific and North Atlantic Ocean, *Micropaleontology*, *23*, 1–55, 1977.

Okada, H., and A. McIntyre, Seasonal distribution of modern coccolithophores in the western North Atlantic Ocean., *Marine Biology*, *54*, 319–328, 1979.

Paasche, E., A tracer study of the inorganic carbon uptake during coccolith formation and photosynthesis in the coccolithophorid *Coccolithus huxleyi*, *Physiologia Plantarum Supplementum*, *3*, 1–82, 1964.

Paasche, E., Roles of nitrogen and phosphorus in coccolith formation in *Emiliania huxleyi* (prymnesiophyceae), *European Journal of Phycology*, *33*, 33–42, 1998.

Paasche, E., and S. Brubak, Enhanced calcification in the coccolithophorid *Emiliania huxleyi* (haptophyceae) under phosphorous limitation., *Phycologia*, *33*, 324–330, 1994.

Pappenfuss, G. F., Classification of the algae, in *A Century of progress in the Natural Sciences, 1853 -1953*, 115-224 pp., California Academy of Sciences: San Francisco, 1955.

Parke, M., and J. C. Green, Haptophyta, in *Check-list of British Marine Algae*, vol. 56, edited by M. Parke, and P. S. Dixon, 551-555 pp., J. mar. biol. Ass. U.K., 3d edition, 1976.

Pascher, A., Chrysomonaden aus dem Herschberger Grossteiche, *Monogr. Abh. Intern. Rev. Gesammt. Hydrobiol. Hydrogr.*, *1*, 1–66, 1910.

Perch-Nielsen, K., Cenozoic calcareous nannofossils, in *Plankton Stratigraphy*, vol. 1, edited by H. M. Bolli, J. B. Saunders, and K. Perch-Nielsen, 427-554 pp., Cambridge University Press, 1985.

Popp, B. N., F. Kenig, S. G. Wakeham, E. A. Laws, and R. R. Bidigare, Does growth rate affect ketone unsaturation and intracellular carbon isotopic variability in *Emiliania huxleyi*?, *Paleoceanography*, *13*(1), 35–41, 1998.

Popp, B. N., R. Takigiku, J. M. Hayes, J. W. Louda, and E. W. Baker, The post-paleozoic chronology and mechanism of ^{13}C depletion in primary marine organic matter, *American Journal of Science*, *289*, 436–454, 1989.

Prahl, F. G., G. J. de Lange, M. Lyle, and M. A. Sparrow, Post-depositional stability of long-chain alkenones under contrasting redox conditions, *Nature*, *341*, 434–437, 1989.

Purdie, D. A., and M. S. Finch, Impact of a coccolithophorid on dissolved carbon-dioxide in seawater enclosures in a Norwegian fjord., *Sarsia*, *79*, 379–387, 1994.

Quiroga, O., and E. Gonzalez, Carbonic anhydrase in the chloroplast of a coccolithophorid (prymnesiophyceae), *Journal of Phycology*, *29*, 321–324, 1993.

Rau, G. H., U. Riebesell, and D. Wolf-Gladrow, A model of photosynthetic ^{13}c fractionation by marine phytoplankton based on diffusive molecular CO_2 uptake., *Marine Ecological Progress Series*, *133*, 275–285, 1996.

Rau, G. H., U. Riebesell, and D. Wolf-Gladrow, CO_{2aq}-dependent photosynthetic ^{13}c fractionation in the ocean: A model versus measurement., *Global Biogeochemical Cycles*, *11*(2), 267–278, 1997.

Rau, G. H., T. Takahashi, and D. J. Des Marais, Latitudinal variations in plankton $\delta^{13}C$: Implications for CO_2 and productivity in past oceans., *Nature*, *341*, 516–518, 1989.

Rau, G. H., T. Takahashi, D. J. D. Des Marias, D. J. Repta, and J. Martin, The relationship between organic matter $\delta^{13}C$ and $[CO_{2(aq)}]$ in ocean surface water: Data from a JGOFS site in Northeast Atlantic Ocean and a model., *Geochimica et Cosmochimica Acta*, *56*, 1413–1419, 1992.

Raven, J. A., Carbon:a phycocentric view, in *Towards a model of ocean biogeochemical processes*, edited by G. T. Evans, and M. J. R. Fasham, 123-152 pp., Springer-Verlag, Berlin, 1993.

Raven, J. A., and A. M. Johnston, Mechanisms of inorganic-carbon aquisition in marine phytoplankton and their implications for the use of other resources, *Limnology and Oceanography*, *36*(8), 1701–1714, 1991.

Rechka, J. A., and J. R. Maxwell, Unusual long chain ketones of algal origin, *Tetrahedron Letters*, *29*, 2599–2600, 1988.

Rees, T. A. V., Sodium dependent photosynthetic oxygen evolution in a marine diatom., *Journal of Experimental Botany*, *35*, 332–337, 1984.

Riebesell, U., D. A. Wolf-Gladrow, and V. Smetacek, Carbon dioxide limitation of marine phytoplankton growth, *Nature*, *361*, 249–251, 1993.

Rivkin, R. B., Influence of irradiance and spectral quality on the carbon metabolism of phytoplankton. i Photosynthesis, chemical composition and growth, *Marine Ecological Progress Series*, *55*, 291–304, 1989.

Robertson, J. E., , and others., The impact of a coccolithophore bloom on the oceanic carbon uptake in the northeast Atlantic during summer 1991, *Deep-Sea Research*, *41*, 297 314.

Round, F. E., *The biology of the algae*, Edward Arnold, London, 2nd edition, 1973.

Rowland, S. J., and J. K. Volkman, Biogenic pollutant aliphatic hydrocarbons in *Mylitus edulis* from the North Sea, *Marine Environmental Research*, *7*, 117–130, 1982.

Roy, R. N., L. N. Roy, K. M. Vogel, C. Porter-Moore, T. Pearson, C. E. Good, F. J. Millero, and D. M. Campbell, The dissociation constants of carbonic acid in seawater at salinities 5 to 45 and temperatures 0 45 °c, *Marine Chemistry*, *44*, 249–267, 1993.

Sikes, C. S., R. D. Roer, and K. M. Wilbur, Photosynthesis and coccolith formation: Inorganic carbon sources and net inorganic reaction of deposition, *Limnology and Oceanography*, *25*(2), 248–261, 1980.

Steeman-Nielsen, E., The uptake of free CO_2 and HCO_3^- during photosynthesis of planktonic algae with special reference to the coccolithophorid *Coccolithus huxleyi*, *Physiologia plantarum*, *19*, 232–240, 1966.

Tabata, S., Annual and interannual variability of baroclinic transports across line p in the northeast pacific ocean, *Deep-Sea Research*, *38*, *Suppl. 1*, S221–S245, 1991.

Tappan, H., *The Paleontology of Plant Protists*, Freeman, W. H. and Co., San Francisco, 1980.

Tchen, T. T., and B. Vennesland, Enzymatic carbon dioxide fixation into oxaloacetate in wheatgerm., *Journal of Biological Chemistry*, *213*, 533–546, 1955.

Thibault, D., S. Roy, C. S. Wong, and J. K. B. Bishop, The downward flux of biogenic material in the NE subarctic Pacific: importance of algal sinking and mezozooplankton herbivory, *Deep Sea Research II*, *46*(11-12), 2669–2698, 1999.

Thierstein, H. R., K. R. Geitzenauer, B. Molfino, and N. J. Shackelton, Global synchroneity of late Quarternary coccolith datum levels: validation by oxygen isotopes., *Geology*, *5*, 400–404, 1977.

Thompson, P. A., and S. E. Calvert, Carbon isotope fractionation by *Emiliania huxleyi*, *Limnology and Oceanography*, *40*(4), 673–679, 1995.

Townsend, D. W., M. D. Keller, P. M. Holligan, S. G. Ackleson, and W. M. Balch, Blooms of the coccolithophore *Emiliania huxleyi* with respect to hydrography in the Gulf of Maine, *Continental Shelf Research*, *14*, 979–1000, 1994.

Truper, H. G., and C. S. Yentsch, Use of glass fiber filters for the rapid preparation of *in vivo* absorption spectra of photosynthetic bacteria, *Journal of Bacteriology*, *94*, 1255-1256, 1967.

Tyrell, T., and A. H. Taylor, A modelling study of *Emiliania huxleyi* in the NE Atlantic, *Journal of Marine System*, *9*, 83–112, 1996.

Uriarte, I., A. S. Farias, A. W. Hawkins, and B. L. Bayne, Cell charachteristics and biochemical copmposition of *Dunaliella primolecta* butcher conditioned at different concentrations of dissolved nitrogen, *Journal of Applied Phycology*, *5*, 447–453, 1993.

Van Bleijswijk, J. D. L., M. J. Veldhuis, and P. Westbroek, Cell and growth characteristics of types a and b of *Emiliania huxley* (prymnesiophyceae) as determined by flow cytometry and chemical analyses., *Journal of Phycology*, *30*, 230–241, 1994.

Van Der Wal, P., J. D. L. van Bleijswijk, and J. K. Egge, Primary productivity and calcification rate in blooms of the coccolithophorid *Emiliania huxleyi* (lohmann) hay et mohler developing mesocosms., *Sarsia*, *79*, 401–408, 1994.

Vargaftik, N. B., Y. K. Vinogradov, and V. S. Yargin, *Handbook of physical properties of liquids and gases*, New York: Begell House, 3rd edition, 1996.

Volkman, J. K., S. M. Barrett, S. I. Blackburn, and E. L. Sikes, Alkenones in *Gephyrocapsa oceanica*: Implications for studies of paleoclimate, *geocomics*, *59*(3), 513–520, 1995.

Weiss, R. F., Carbon dioxide in water and seawater: The solubility of a non-ideal gas, *Marine Chemistry*, *2*, 203–215, 1974.

Whiticar, M. J., and M. K. Eek, Challenges of $^{13}c/^{12}c$ measurements byCF-IRMS of biogeochemical samples at sub-nanomolar levels, *IAEA TECDOC, in press*, 1999.

Wilbur, K. M., and N. Watabe, Experimental studies on the calcification in mulluscs and the alga *Coccolithus huxleyi*, *Annals of the New York Academy of Sciences*, *109*, 82–112, 1963.

Winter, A., Z. Reiss, and B. Luz, Distrubution of living coccolithophore assemblages in the Gulf of Eilat ('Aqaba), *Marine Microplaleontology*, *4*, 197–223, 1979.

Wolf-Gladrow, D., and U. Riebesell, Diffusion and reactions in the vicinity of plankton: A refined model for inorganic carbon transport, *Marine Chemistry*, *59*, 17–34, 1997.

Wong, C. S., and Y. H. Chan, Temporal variations in the partial pressure and flux of CO_2at ocean station P in the subarctic northeast Pacific Ocean, *Tellus*, *00B*, 1–18, 1991.

Wong, K. F., and D. D. Davies, Regulation of pep carboxylase of *Zea mays* by metabolites, *Biochemistry Journal*, *131*, 451–58, 1973.